3D Regional Geological Modelling in Structurally Complex Environments

Gaining geological insight for the northern Labrador Trough

Rebecca Montsion

A thesis submitted to the

Faculty of Graduate and Postdoctoral Studies

In partial fulfillment of the requirements for the

Master of Science Degree in Earth Sciences

Department of Earth and Environmental Science

Faculty of Science

University of Ottawa

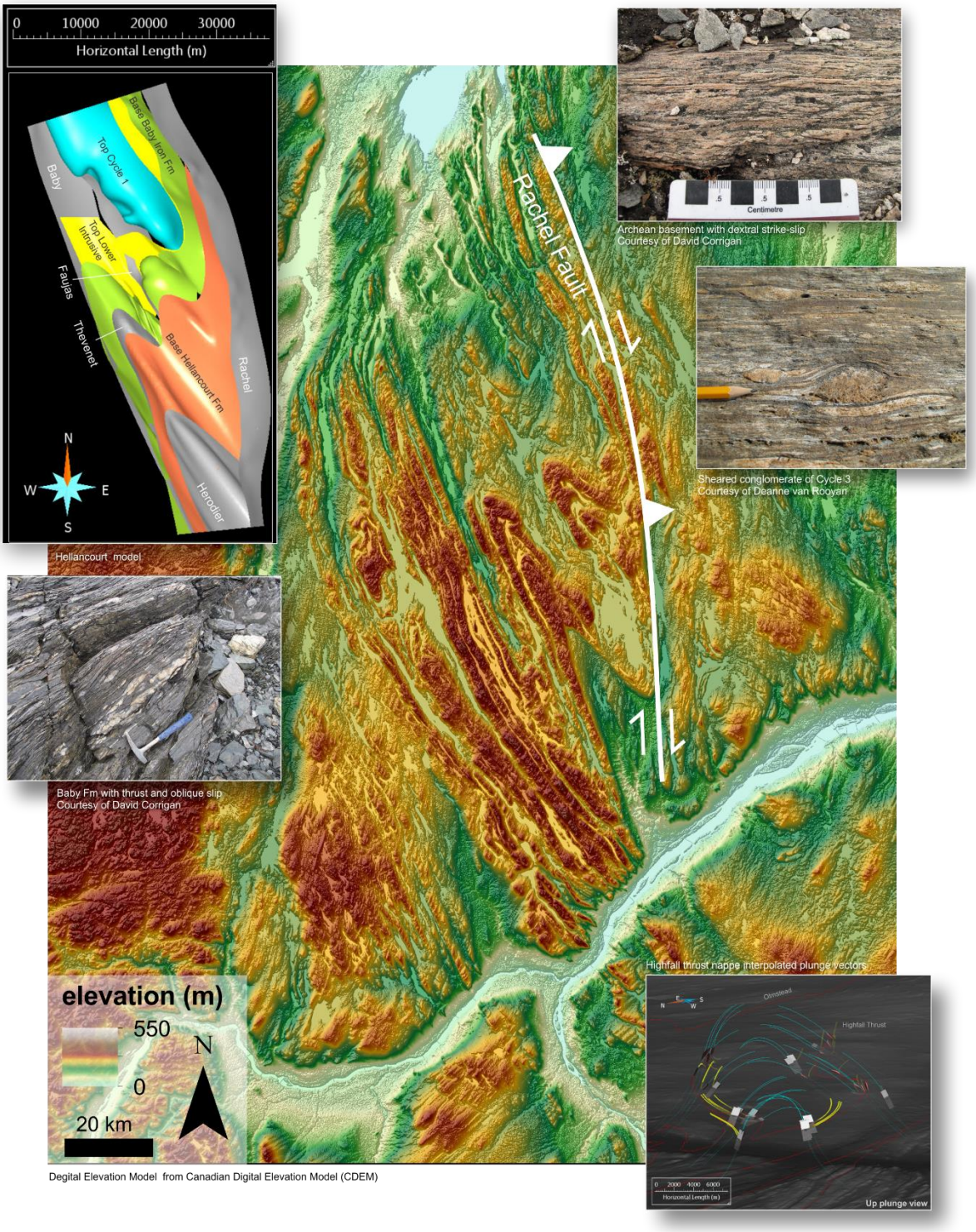

Composite image of Digital Elevation Model, field photos from highly strained and deformed outcrops, 3D characterization of field data as interpolated plunge vectors, and horizon surface model of the Hellancourt Sub-Region.

Abstract

3D geological modelling is becoming an effective tool for communication and development of geological understanding. This is due to increased computer performance and availability of improved geological modelling software. 3D geological modelling technology has reached the stage where it can be implemented in regionally extensive and geologically complex settings, with the ability to achieve geological insight beyond what could otherwise have been gained through 2D investigations alone. Insight includes better constrained fault and horizon topologies, refined fold geometries, improved understanding of tectonic processes, and characterization of deformational events. By integrating field observations, aeromagnetic maps, and 3D modelling techniques in the northern Labrador Trough, a regionally extensive and structurally complex geological environment, regional faults geometries and topological relationships were refined. Additionally, a new fault, the Ujaralialuk Fault, and two shear zones were interpreted. During modelling, several challenges were identified, including higher computational costs for regionally extensive models, sparse 3D constraints, algorithmic limitations related to complex geometries, and the large investment of time and effort required to produce a single model solution. A benefit of this investigation is that new insight was also gained for a greenfields region which may assist future exploration efforts. Developing 3D models in challenging environments allows for better definition of future workflow requirements, algorithm enhancements, and knowledge integration. These are needed to achieve a geologically reasonable modelling standard and gain insight for poorly constrained geological settings.

Acknowledgements

It is with deep gratitude that I thank Eric de Kemp for his tireless guidance and support throughout my research. His enthusiasm and passion for 3D modelling has inspired me to become a better researcher and to appreciate developing technologies. I am very thankful for the countless hours and many impromptu help sessions, as well as the pep-talks regarding software frustrations. Eric has been an amazing supervisor and I am very grateful to have worked with him.

I would also like to thank my faculty supervisor, David Schneider, for his support, sending me to conferences, and suggesting excellent field courses. His guidance and advice has been very much appreciated.

Additionally, I thank Michael Hillier for building and troubleshooting SURFE as well as the countless mini chats about modelling and related subjects. It has been a great experience assisting with SURFE's development and I look forward to it becoming a staple in 3D modelling.

I would like to thank the Geological Survey of Canada and Canada 3D for the opportunity to apply my newly minted skills to a project that adds value to the Canadian public. I am very proud to be a member of the team and look forward to the great work that will be done in the future. I am also grateful for the financial support the project has provided which allowed me to conduct this research.

I also appreciate the ongoing collaboration between Mira Geoscience and the Geological Survey of Canada. Academic software was provided through the RING (Research for Integrative Numerical Geology) research consortia, by Paradigm and Mira Geoscience Ltd.

Finally, I must express my very profound gratitude to my husband and to my peers for providing me with unfailing support and continuous encouragement throughout my years of study and all that entailed. This accomplishment would not have been possible without them and is their triumph as much as my own. Thank you.

Table of Contents

List of Tables

List of Figures

1.0.0 Introduction

Recent increased computational power and development of improved geological software has allowed the geoscientific community to add 3D modelling as a tool for advancing geologic practice. The modelling process and the resultant products are useful for generating new insight into geological histories, as support for mineral exploration, and for identifying geological knowledge gaps. 3D modelling has matured in recent years, having been implemented at the mine or camp scale to guide mine development and extraction strategies (Dag and Ozdemir, 2013; Kaufmann and Martin, 2009; Koivisto et al., 2015; Montsion et al., 2015; Schetselaar, 2013). With these advances, the geoscientific community is attempting to apply technologies, workflows, and lessons-learned to more regional scale scenarios with more complex geology (de Kemp et al., 2016; Lindsay et al., 2013; Maxelon et al., 2009; Philippon et al., 2015).

The new 3D modelling environments present several challenges that are not addressed by local scale studies which need to be resolved for successful application in frontier or greenfields regions. In contrast to mine scale models, regional models are limited by the computational cost of working with non-standard 2D datasets and large model spaces. The amount of data included and the number of cells in the model exponentially increase as the study area expands. This can be mitigated to some extent with increased computational power and/or applying a divide and conquer approach by partitioning a model space into many individual regional studies (Laurent et al., 2015). In further contrast to mine scale models, regional studies often suffer from limited 3D data such as geophysical surveys or drill core, thus making them poorly constrained at depth compared to data-rich models in mining camps. While sub-surface 3D datasets are available for mine scale work, they are prohibitively expensive to gather for large areas and they may not sample deep, crustal scale features. Therefore, interpolation, interpretation, and extrapolation techniques are used in regional studies to fill in gaps and to extend knowledge beyond available data. Additionally, regional models often span several tectonic domains with unique structural styles and histories. To create a model that reflects this variable geology, new modelling strategies will have to be implemented, including dividing regions into tectonic domains and modelling each domain independently, developing tools which capitalize on geological knowledge such as deformation histories, and classification tools.

The geoscientific community is also seeking to model increasingly complex geological terranes where resource mineralization occurs. New and improved geological software and modelling algorithms

are now providing the necessary tools for such endeavours. The technologies and workflows used to model complex regions build upon hydrocarbon exploration standards, which were designed to deal with simpler structures in relatively un-deformed basin settings. While these tools provide foundation for software development, some refinement is still needed to fully capture the complexity that characterizes these mineralized terranes.

The northern Labrador Trough represents a regionally extensive and structurally complex area with a range of geological structures, thus making it useful to evaluate current technology and practices. The study area contains variable fold structures ranging from simple, upright folds in the western foreland to complex interference patterns and sheath folds in the eastern hinterland. The northern Labrador Trough also benefits from extensive field observation datasets produced by Ministère de l'Energie et des Ressources Naturelles (MERN) and the Geological Survey of Canada (GSC) as well as by significant mineral exploration. Appendix A describes some of the industry-led and survey-led studies conducted in the area. Resources currently being explored are iron, copper, nickel, platinum group elements (PGE), zinc, gold, and cobalt (Appendix B).

The aim of developing regionally extensive, structurally complex geological models is to characterise the crustal scale geometry of critical geological features and thereby gain insight into tectono-stratigraphic and mineralization processes. In creating the model, geoscientists are able to better investigate data relationships, are confronted with discrepancies between data and geological theories, and are guided through defining topological relationships in the model. Additionally, these models can serve as communication tools, making geology accessible to all stakeholders.

1.1.0 Geologic Context

The northern Labrador Trough is the foreland of a west-vergent Paleoproterozoic fold and thrust belt made up of early thin-skinned imbricate thrusts and later out-of-sequence thrusts, which divide the major lithotectonic blocks of the orogen (Clark and Wares, 2006) (Figure **1**). The Labrador Trough, has been the subject of much study since its discovery in the 1800s and has historically included all the metasedimentary and meta-volcanic units found between the Superior Province and the Core Zone. This includes the shelf-sequence Kaniapiskau Supergroup and backarc basin-sequence Rachel-Laporte Supergroup. To the west of the Labrador Trough the Superior Craton, the basement of the Tran Hudson Orogen, is exposed. To the east is the Core Zone, which is interpreted to be a raft of the Superior Craton that separated during rifting that preceded deposition of the Labrador Trough's Paleoproterozoic sediments.

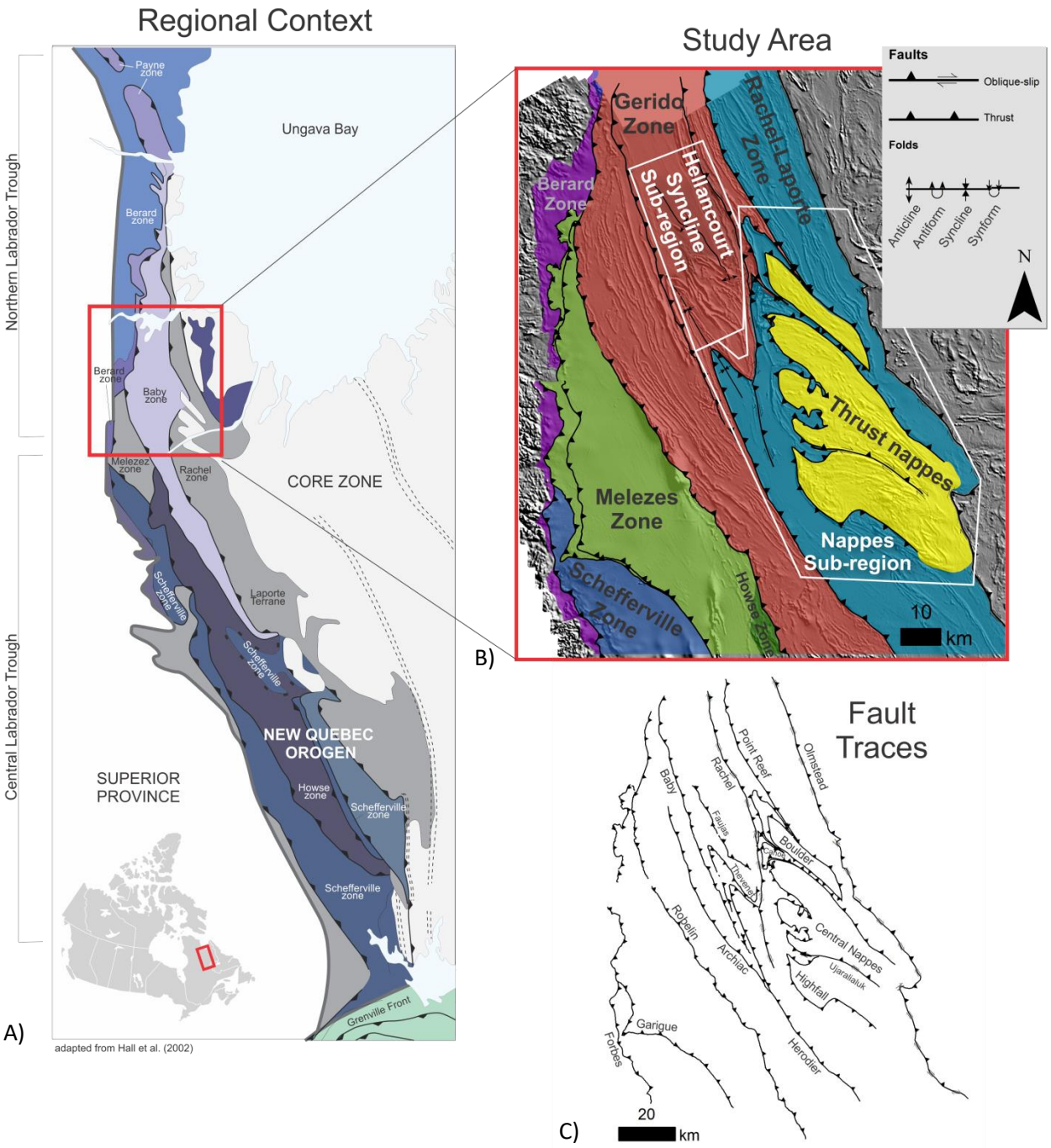

Figure 1. A) Simplified litho-tectonic map showing regional context of the Labrador Trough (adapted from Hall et al. (2002) and litho-tectonic blocks (coloured zones) in the study area. B) Generalized litho-tectonic map of study area (coloured zones) superimposed on hillshade of first vertical derivative of total magnetic field map (hillshaded using 45° azimuth and 45° elevation; 75 m x 75 m cell size grid from magnetic survey with 300 m line spacing). Sub-region model extents outlined in white. C) Fault traces map for the study area.

Stratigraphy

The majority of work done in the area has focused on the Kaniapiskau Supergroup; however, its regional stratigraphy has been established based on limited geochronological work (Chandler, 1980; Clark and Wares, 2006; Houlé et al., 2016; Rohon et al., 1993; Wardle and Bailey, 1981; Weber et al., 1990). Two cycles of deposition during separate stages of rifting as well as a synorogenic sedimentation cycle have been defined in Figure 2 (Clark, 1988; Clark and Wares, 2006; Dimroth, 1981). Sedimentation began with Cycle 1, which corresponds to 2.2 Ga intracratonic rift basin sequence which records a transition from the Seward Group's immature continental rift sequence of sandstones and conglomerates, which lay discordantly over the Superior Craton's Ashuanipi complex, to the passive margin sediments of the Dolly Formation (Clark and Wares, 2006; Wardle et al., 2002). This was followed by Cycle 2, which consists of stable passive margin sedimentary rock, including banded iron formations, and MORB-type, axial mafic volcanic rocks at 2.17 – 2.14 Ga (Clark and Wares, 2006). Both Cycle 1 and 2 sequences were intruded by the mafic and ultramafic Montagnais sills from 2.169 to 1.875 Ga (Clark and Wares, 2006; Houlé et al., 2016). Following intrusion, an erosional surface developed and Cycle 3 molasse sediments were deposited during late-stage orogenesis (Clark and Wares, 2006).

There has been limited published work for the Rachel-Laporte Supergroup; however, recent field campaigns by the MERN and GSC are underway. From these investigations it is generally thought that the Rachel-Laporte Supergroup represents distal backarc basin sediments that are likely chronostratigraphic equivalents of the Kaniapiskau Supergroup (Corrigan, 2016; Corrigan et al., 2015).

Structural and tectonic setting

In the Labrador Trough, three phases of deformation recorded collision between the Nain and Superior Cratons. These collisions occurred during the Trans-Hudson Orogeny and resulted in roughly 50% shortening across the Labrador Trough as well as crustal-scale fold, which are presented in Figure 3 (Dimroth, 1981). Details related to each deformation event are outlined in Table 1 and Figure 4 illustrates a hypothesized reconstruction of the Trans-Hudson Orogen formation.

D_1 was dominated by east-west convergence as an east-west collision between the Nain and Superior cratons began (1.845-1.82 Ga panel in Figure 4). The initial collision produced NNW-trending thrust faults, a décollement, a bedding-parallel foliation consistent with east-west shortening (Moorhead, 1989; Poirier, 1989; Poirier et al., 1990). The expression of these structures is not uniform across the orogen. Instead, they are preserved in the west where later deformation events have not overprinted structures as strongly; however, the S_1 schistosity is more strongly developed in the

hinterland (Moorhead, 1989). Moving eastward, D1 structures become obscured by increasingly intense deformation associated with the Lac Tudor shear zone and nappe structures.

D_2 was also dominated by intensified east-west convergence, and produced large-scale folds and thrust faults consistent with east-west shortening. In the west, the D_2 phase is expressed by outcrop to regional scale, tight, upright to recumbent folds with axial planes trending to the NE. An associated S_2 foliation is rare and generally only observed in metapelitic units (Poirier et al., 1990). Additionally, Moorhead (1989) reports E to NE trending, shallowly plunging open folds that deform the basement and cover rocks in the Labrador Trough into large-scale folds. These observations suggest that the nappes along the eastern margin of the Labrador Trough may have developed during this phase of deformation. This interpretation is supported by Moorhead (1989)'s field observations that D_1 and nappes fold morphologies greatly differ, that S_1 is deformed by the nappes, and the presence of interference patterns between F_1 folds in the interior of the nappes. In the west, the D_2 phase is expressed by outcrop to regional scale, tight, upright to recumbent folds with axial planes trending to the NE. An associated S_2 foliation is rare and generally only observed in metapelitic units (Poirier et al., 1990). Additionally, Moorhead (1989) reports E to NE trending, shallowly plunging open folds that deform the basement and cover rocks in the Labrador Trough into large-scale folds. These observations suggest that the nappes along the eastern margin of the Labrador Trough may have developed during this phase of deformation. This interpretation is supported by Moorhead (1989)'s field observations that D_1 and nappes fold morphologies greatly differ, that S_1 is deformed by the nappes, and the presence of interference patterns between F_1 folds in the interior of the nappes.

D_3 was dominated by transcurrent and transpressional regimes that produced folds with a strong axial planar cleavage, creating interference patterns with F_1 and F_2 folds and the local transposition of bedding. Across the Labrador Trough, D_3 is expressed by numerous outcrop- to regional-scale folds and an associated crenulation cleavage (S_3). Fold geometry and orientation is variable at the regional scale. In the northern region of the study area, folds have steep, upright axial planes and plunge to the NE. In the south, folds are overturned and axial planes trend SE (Poirier et al., 1990). This is further complicated by interference with the competent, basement-cored thrust nappes in the east of the study area. Figure 3 demonstrates interpreted fold geometries and fault topology that resulted from these deformational events within the Kaniapiskau Supergroup.

Table 1 Timing and notable observations of deformation events in the northern Labrador Trough

Event	Timing (Ga)	Dominant Strain	Characteristics and field observations
D_1	1.86 to 1.85	East-west convergence	• Strong, bedding-parallel foliation and schistosity (S_1) (Moorhead, 1989) • NNW trending thrust faults with listric geometry • Development of décollement (Moorhead, 1989; Poirier et al., 1990) • Rare, outcrop-scale, west-verging folds associated with faults (Boone, 1987; Goulet, 1987, 1986; Wares et al., 1988) • Fault-associated stretching lineation (L_1)(Hoffman, 1988)
D_2	1.845 to 1.82	East-west convergence	• Outcrop to regional scale, tight, upright to recumbent folds with axial planes trending NE (Moorhead, 1989; Poirier et al., 1990) • East-dipping thrust faults • Rare thrust fault associated S_2 (Moorhead, 1989; Poirier et al., 1990) • Strong L_2 stretching lineation parallel to fold axes near major fold closures (Moorhead, 1989; Poirier et al., 1990) • Development of imbricate thrust nappes (Moorhead and Hynes, 1990)*
D_3	1.8 to 1.74	Dominantly dextral shear and continued east-west convergence	• Fold orientations, geometries and intensity is typical for a fold and thrust belt and are a function of location in the orogen (Dimroth, 1981; Moorhead and Hynes, 1990; Poblet and Lisle, 2011) • Interference between F_2 and F_3 in the eastern allochthonous zone has caused local reversals in fold plunges and several types of interference patterns (Moorhead, 1989) • A strong axial planar cleavage developed in association with folds and acted as a plane for bedding transposition (Hynes, 1978)

* There has been some disagreement about the nappes' age; however, they deform the S_1 schistosity and T_1 thrust faults, and show evidence of dextral deformation after they were emplaced, indicating that their age must be after D_1 and before D_3 (Moorhead and Hynes, 1990).

Metamorphism

The timing of regional metamorphism varies across the orogen. In the east, granulite facies metamorphism was coeval with D_1 and occurred before 1845 Ma (Machado et al., 1997). In the western Core Zone, peak metamorphic conditions reached upper amphibolite facies at 1.83 Ga and is generally coeval with D_3 (Hynes, 1978; Perreault and Hynes, 1990).

For an expanded presentation of the northern Labrador Trough's geological context, see Appendix C – Expanded Geological Context.

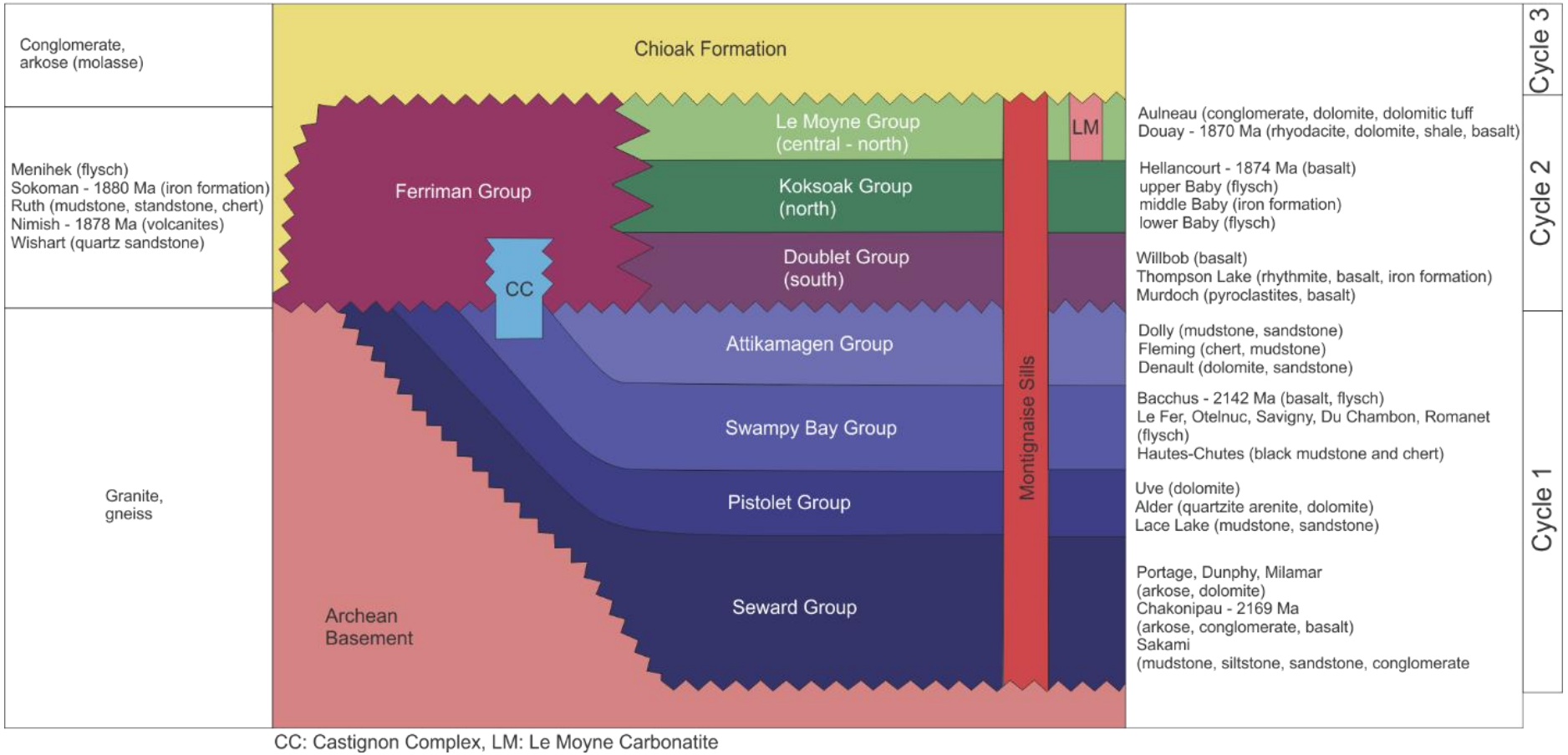

Figure 2. Kaniapiskau Supergroup, of the Labrador Trough, simplified stratigraphy after Clark and Wares (2006).

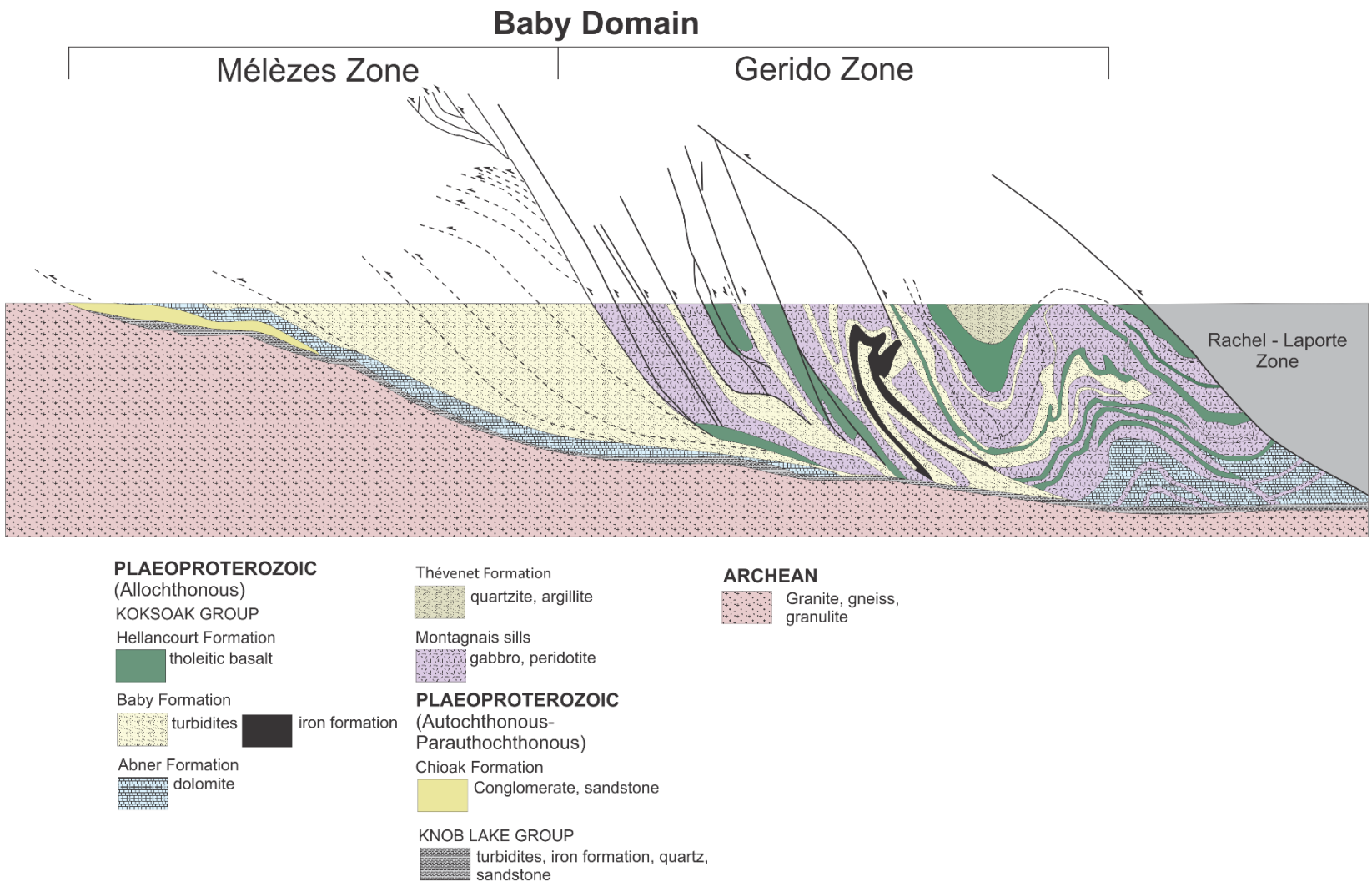

Figure 3 Unbalanced west to east cross section of the Kaniapiskau Supergroup. After Wares and Goutier (1990)

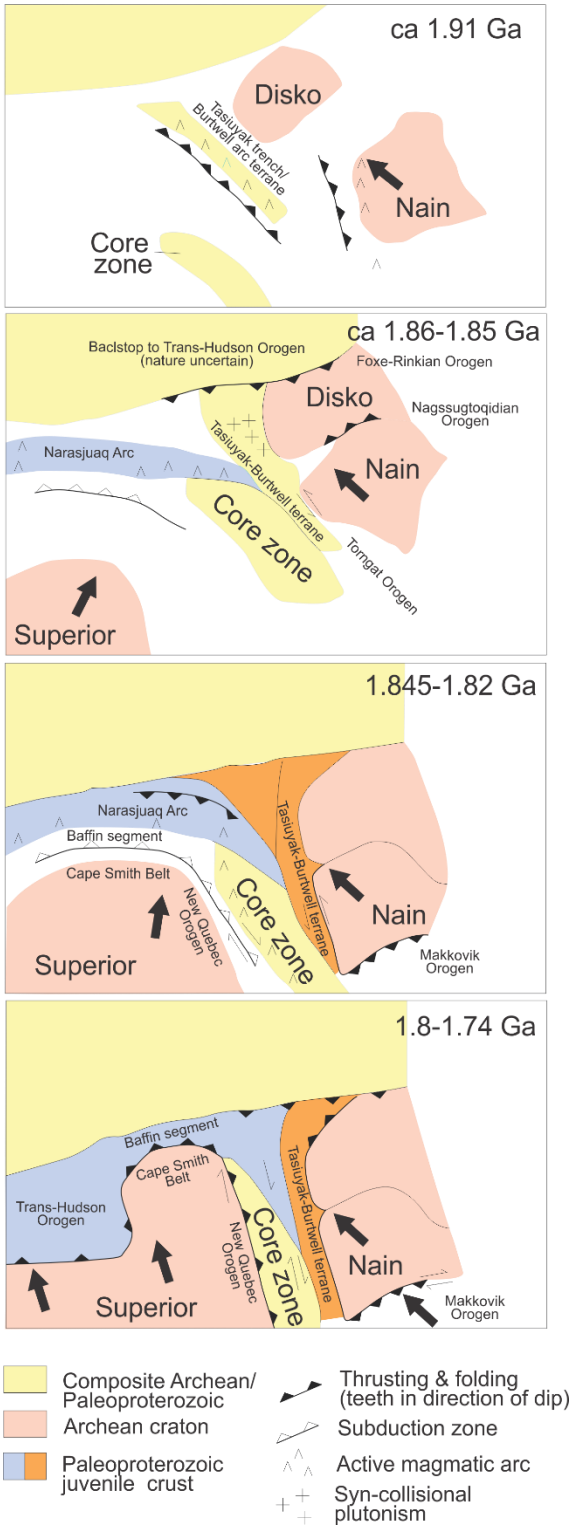

Figure 4. Schematic maps of the Paleoproterozoic evolution of northeastern Laurentia and deformation of the northern Labrador Trough. D1 likely began in second frame (1.86-1.85 Ga) and progressed to D3 in the third frame (1.8-1.75 Ga). (after Clowes et al (1999)). See Table 1 for further details on deformation events.

1.2.0 Model Constraints

To a construct a 3D model, interpolation and extension algorithms are guided by input constraints. These are points or lines where geological information has been observed or interpreted. Therefore, constraints fall into two categories: Observational or derived. Observational constraints are considered "data" and are observed, either in the field (outcrop or drill core observations) or through geophysical methods (seismic, gravity, magnetics, electric logs etc.). Sources of data used here include the Système D'Information Géominière (SIGEOM) database (*Système d'information géominière du Québec*, 2016), scanned legacy maps (See Appendix D) and airborne magnetic surveys (D'Amours and Intissar, 2013, 2012a, 2012b). Derived constraints may arise from interpretation or interpolation of observational data. Examples of derived constraints are cross sections, interpolated structural points from stereonets, and map traces. These points are useful to constrain models when observational data is absent or sparse. For this model, they were compiled from the SIGEOM database (*Système d'information géominière du Québec*, 2016), journal articles (Moorhead and Hynes, 1990), reports (Lafrance et al., 2014; Simard et al., 2013), summary papers (Clark and Wares, 2006), cross sections (Boone and Hynes, 1990; Clark and Wares, 2006; Goulet, 1987; Goutier and Wares, 1991; Lafrance et al., 2014; Moorhead and Hynes, 1990; Simard et al., 2013; Wares and Goutier, 1990), and maps (see Appendix D).

Since 1892, field observations have been gathered from abundant and well exposed outcrops across the Labrador Trough, especially in areas of economic interest (Figure 5). The economic focus of field campaigns has led to clustering in prospective areas and sparse data elsewhere. This affects modelling capabilities and confidence in interpretations because clustered data must be generalized or up-scaled to be relevant to the regional model. Figure 6 illustrates this clustering and presents an estimate of confidence related to data quality. This point density map was constructed using the normalized sum of a normalized point density map of structural observations that were assigned to a structural generation and a normalized point density map of observations that had younging directions. Both sets of points indicate areas where the geology is understood and have a high confidence.

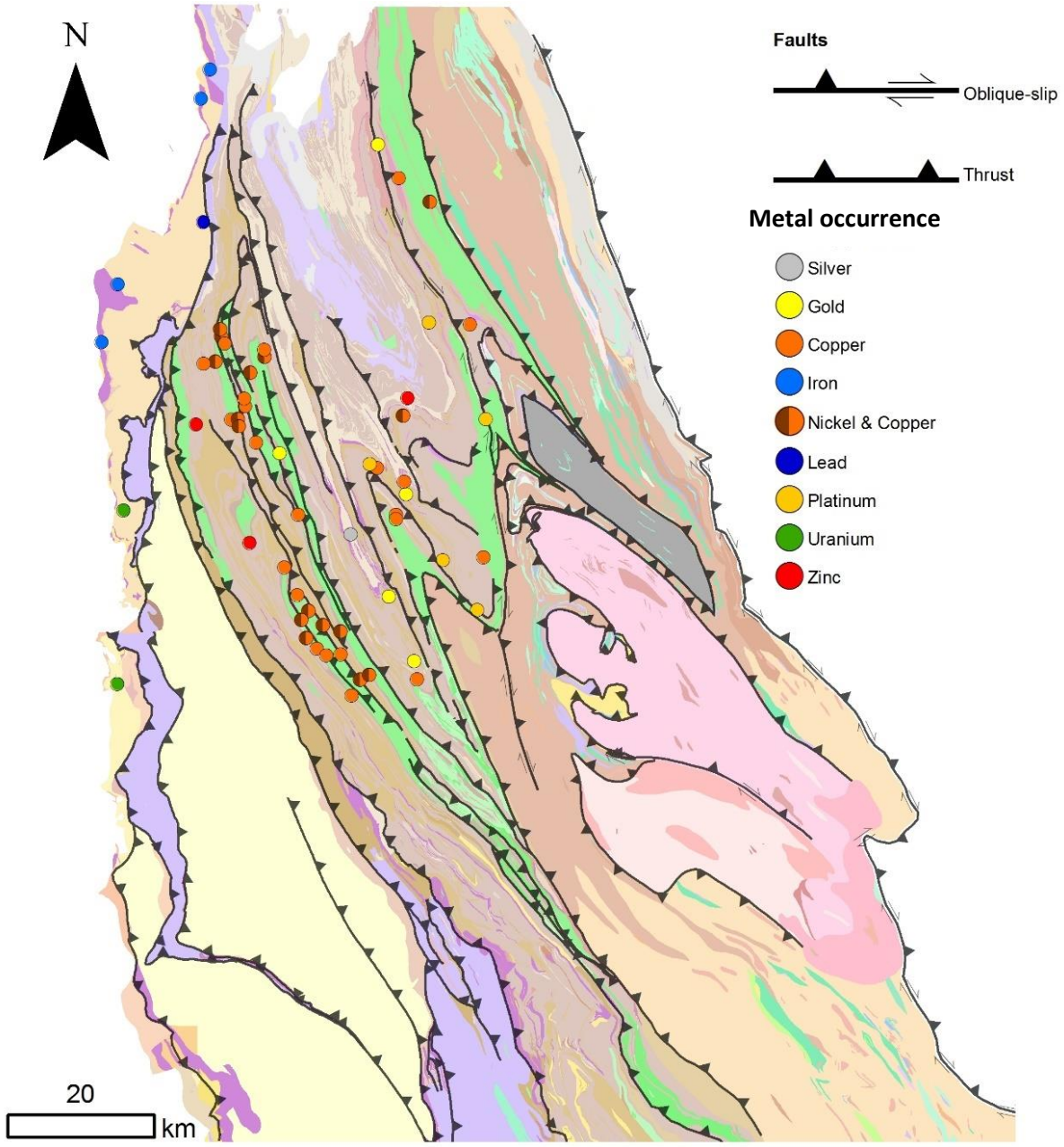

Figure 5. Coloured mineral occurrence points superimposed on bedrock geology map of the northern Labrador Trough. Metal occurrence present in the area are represented in the legend to the right. Highlights areas of economic significance. Many mineralized zones along contact of gabbro (green) and Kaniapiskau sedimentary units (Mineral occurrence points and geological units from SIGEOM geodatabase(Système d'information géominière du Québec, 2016)).

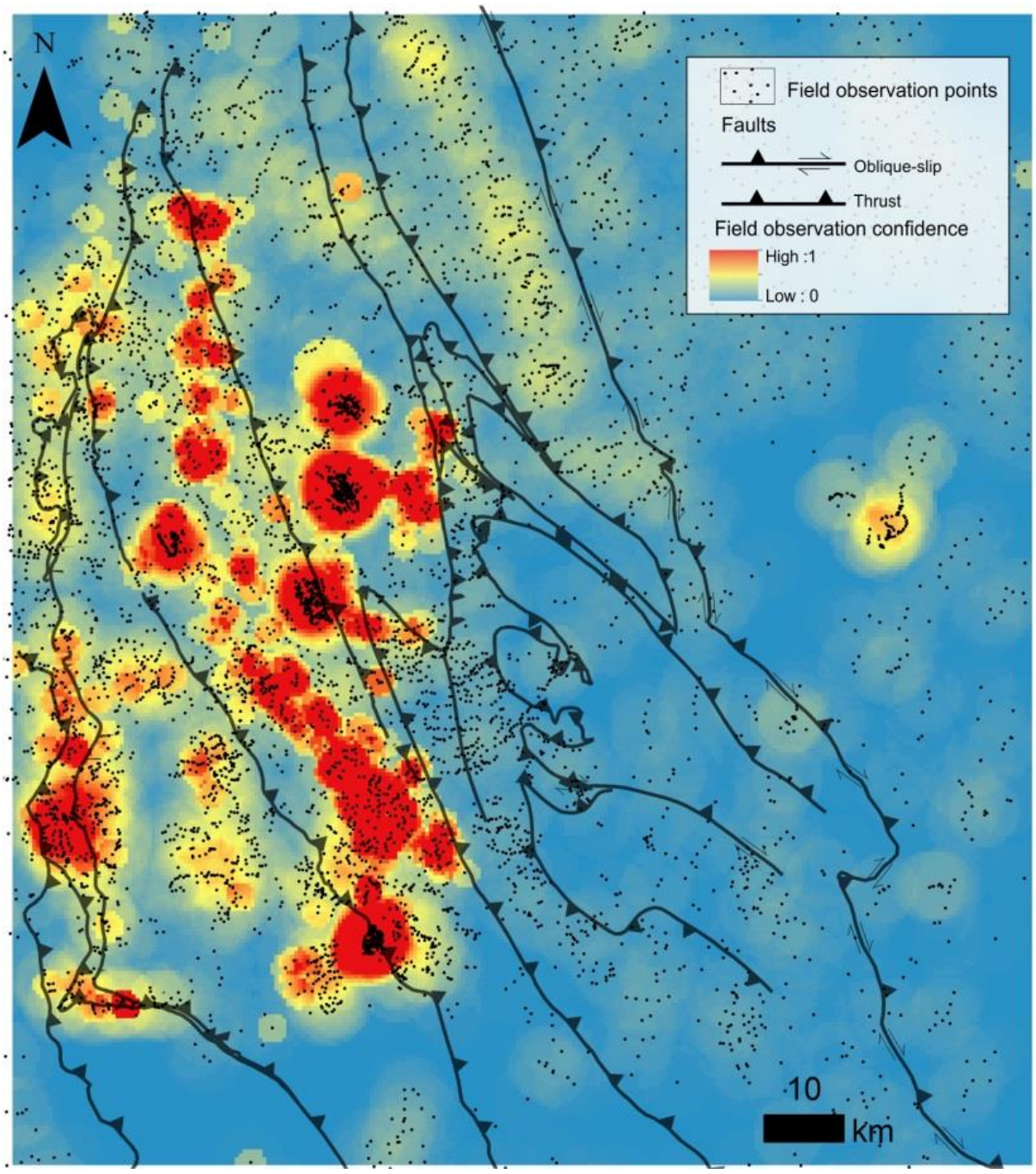

Figure 6. Normalized point density map of structural field observations showing confidence distribution of data. Map was developed by combining normalized point density maps for all field observation points with deformation event classification and those points with top indicators. These two maps were added together and the result was normalized. High confidence areas can be used as a low uncertainty indicator and low confidence for high apriori uncertainty. See Figure 1 for names of fault traces (black lines).

2.0.0 3D Interpretation and modelling

The interpretation approach used in this study follows from the best practice of 2D map interpretation and is seen as an extension of 2D methods (Fossen, 2016; Passchier et al., 2011; Rowland et al., 2007; Twiss and Moores, 2007). Building on these techniques, computers have been able to facilitate virtual interpretive environments in which more complex geometric relationships and forms can be reconciled. As with 2D mapping, the possibility of subjective bias is large; however, the models presented in this study are a step beyond being unsupported 3D concepts in that they are spatially linked to a model space where observational data and interpretations can be jointly viewed and managed. In this study, several tools were used to perform estimation calculations. These include Mira Geoscience's Structural Field Interpolator (SFI)(Hillier et al., 2013), a software tool for calculating form lines using 3D structural data, and SPARSE for manual 3D creation and editing of complex forms (de Kemp and Sprague, 2003; Sprague and de Kemp, 2005)(Hillier et al., 2013). The study uses the Hillier et al. (2014)'s SURFace Estimator (SURFE) to automatically calculate volumetric structural fields and surfaces from contact and gradient constraints as well as Paradigm's Subsurface Knowledge Unified Approach (SKUA) to build 3D volumetric grids of fault blocks and stratigraphic units using contact constrains, seismic cubes, and drill logs.

2.1.0 Introduction to 3D modelling

When working in any area of geology, some element of subjective bias is introduced as geoscientists seek to explain and represent features that are obscured from direct view. Even analysing features exposed at surface outcrops provides a limited view of reality since these represent a small selective sample of the underlying phenomena, are fortuitously provided, and are biased by recent natural erosive processes, uplift history and accessibility. It is, therefore, necessary to apply geological knowledge to fill in gaps with meaningful interpretations. However, working at the regional scale accentuates the problem where observation density is much lower than, for example, at the mine scale.

Sources of bias for this modelling process range from bias in up-scaling localized field observations to a regional context, selecting relevant data as constraints in the models, and assigning uncertainty estimates to values. Ideally, data and knowledge based methods would be integrated in a streamlined and automated way; however, these tools are still in development. To create reliable models, a balance between the various end member approaches must be found as there are often gaps in observations. When working in an under constrained science like geology, a geoscientist should understand this issue and be able to work along the data-knowledge spectrum.

In many areas of geoscience, integrating data and knowledge based methods is a common practise for map making (Fossen, 2016; Passchier et al., 2011; Rowland et al., 2007; Twiss and Moores, 2007). For example, structural geologists use field observations and interpretation techniques to generate 2D maps and cross sections. They plot structural measurements and outcrop maps and essentially connect the dots (between points) using their knowledge and experience. Additionally, they extend these connections beyond known points using similar methods to make interpretations. 3D modelling has the same philosophical basis as 2D mapping and could be considered as both an art and a science (Brodaric et al., 2004). To construct geologic models (2D and 3D), a geoscientist must integrate observations with interpretations while being influenced by theory, data, individuality and specific situations. Despite having a similar foundation, 3D modelling differs from 2D mapping in several aspects. It adds a third dimension, giving it an extra degree of freedom to fit the data. It applies more data-driven techniques, such as modelling algorithms and uncertainty analysis, to produce a solution, compared to traditional mapping techniques where a geoscientist interprets a 3D model and produces a 2D slice, in the form of a cross section, of that model. By utilizing 3D surface and volume building algorithms that are constrained by data, the process is made more rigorous and repeatable.

However, modelling techniques which respect sparse constraints may not produce geologically valid models. Often, modelling algorithms seek to fit a smooth, best fit function to produce a surface, regardless of geological context (de Kemp, 2015). As a work-around, geological knowledge can influence algorithms to produce more geologically meaningful results by the manual insertion of interpreted constraints. This issue is accentuated when working in intensely metamorphosed or deformed terranes and was applied while developing the 3D models of the northern Labrador Trough.

2.2.0 The Workflow

3D modelling consists of many stages of interconnected and iterative processes. Since these processes and their interactions are often convoluted, it is important to keep the flow of knowledge and data focused using a defined workflow. Without such a workflow, modelling becomes unfocused, leading to corrupted data, unrealistic models and a significant decrease in efficiency (de Kemp et al., 2016). There are benefits to building 3D geologic models with regional-scale, poly-deformed, mid-crustal settings. These include better understanding of complex deformation histories in orogenic belts, targeting of prospective mineralized zones, and understanding of crustal scale processes (de Kemp et al., 2016; Lindsay et al., 2013; Maxelon et al., 2009; Philippon et al., 2015).

These studies show that a standardized 3D modelling workflow is still in its infancy. This current study undertakes to create a 3D model of the northern Labrador Trough, using available technologies and methods, to further define requirements for the workflow, while at the same time attempting to gain geological insight for a regionally extensive and structurally complex terrane.

In general, the 3D modelling workflow is a simple loop where data is gathered and applied to generate geological understanding and a model (Figure 7). The process is a loop because it can be updated with new data or interpretations as they become available. Within the global loop are smaller loops which represent smaller scale feedbacks between data and interpretation. Iterations through the feedback loops refine individual components of the model so that they become more geologically "reasonable" (spinning wheel at the center of Figure 7). Geologic reasonableness refers to models where the solution fits all the constraints as well as geological knowledge of the area and geological processes (de Kemp, 2015).

This workflow employs elements of implicit and explicit modelling techniques. Explicit methods of modelling, which use more Computer Aided Design (CAD), or manual interaction, were common in early 3D geological modelling workflows (de Kemp and Sprague, 2001, 2003; Sprague and de Kemp, 2005; Putz et al., 2006). Explicit methods can be considered a knowledge-driven and hands-on approach to modelling that gives geoscientists freedom to shape surfaces according to their interpretation. In 3D explicit modelling, a geological interface is defined by a set of on-contact points where the feature is known or interpreted to exist. A surface is then interpolated between the nodes to produce a 3D mesh. While this modelling method is heavily influenced by user bias, it allows geoscientists to visualize surfaces in regions with sparse or minimal constraint data and can generate new interpreted constraints to support later implicit modelling.

The emergence of faster and more efficient computers has allowed computationally expensive algorithms to be used more extensively in the geological modelling process. One family of these currently popular algorithms falls under the umbrella of implicit methods. Implicit modelling is a data-driven and more automated approach that seeks to solve for a function within a volume rather than just a single surface. The advantage of this method is that it capitalizes on many data types, such as on- and off-contact constraints, and efficiently solves for several surfaces within the scalar field at once (Hillier et al., 2014; Lindsay et al., 2013; Philippon et al., 2015). In a general sense, this method minimizes human bias as it is data-driven and allows for the efficient calculation of complex surfaces while respecting topology

and surface polarity (Hillier et al., 2014); however, interpretive points and dip estimations are often included into the input set in order to produce a geologically reasonable result. Implicit or explicit modelling may also employ Eigen analysis used for characterizing structural fabric anisotropy (Woodcock, 1977). In the workflow presented here, a hybrid approach of explicit and implicit methods is used to construct a 3D model of the northern Labrador Trough. The following sections will describe this workflow (Figure 7).

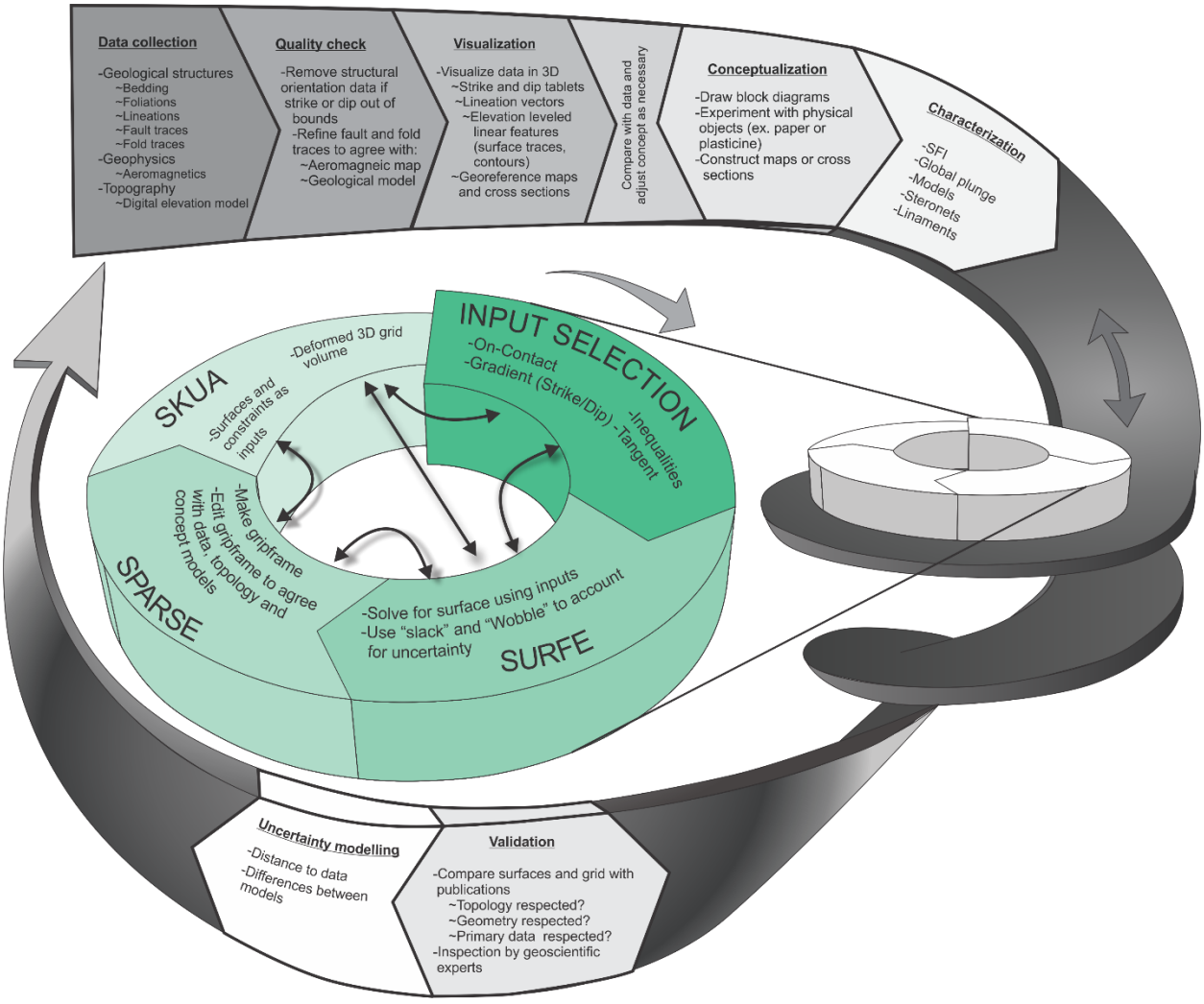

Figure 7. 3D modelling workflow diagram. Pre-processing stages across the top panel symbolize data collection, integration and visualization. Spinning wheel at center represents the convoluted and iterative flow of modelling with explicit and implicit modelling tools and techniques. Each vertical level in the spiral represents a geologic event and each turn of the wheel represents modelling a single surface. Post-processing stages of the workflow are symbolized along the bottom.

2.2.1 Pre-modelling

Data preparation accounts for a significant portion of time invested in the 3D modelling workflow which was beneficial in improving model quality and streamlined later activities in the workflow. Extracting relevant information from the various contributions, and combining them, required that data structure be clear and organized. Due to the diversity of data types and sources, rigorous organization and documentation was required to ensure that it was clean and useable. Information was then integrated and harmonized, using Microsoft Access and ArcMap, and compiled in a geospatial database. In order to keep track of significant data sources, a code system (Appendix J) was developed.

Following harmonization, the data passed through quality control measures and preconditioning so that it is useful for later modelling. Incomplete entries and those that were unreasonable were removed from the population (for example all planar observations had to be in the range of 0° > dip > 90° and 0° > strike >360°). Some integration of the various datasets was also needed as each source used a unique coding system to capture field observations and interpretations. A new, harmonized structural feature code system was used to identify general structure characteristics and classification (Appendix K).

Once constraints were integrated and harmonized, they were visualized in a 3D framework using Mira Geoscience's SPARSE structural graphics utility and elevation correction in GOCAD. SPARSE is a parametric graphics interpretation plug-in that visualizes and models geological data. The structural graphics utility constructs 3D symbols or glyphs (tablets, washers, etc.) for each structural point. In the case of planar observations, it uses the strike, dip, and overturned property. By viewing structural points as tablets, it was possible to better visualize the spatial continuity within structural domains and across the study area. This is quite useful as data density was insufficient for variogram analysis of specific structural features like faults. Through visual inspection, with varying view directions and scales, of these 3D structural graphic symbols, the tectonic domains, folds and faults that were proposed in the literature were validated. If discrepancies were found between data and published interpretations as well as geological features such as structural domains, breaks, areas of continuity, and folds were updated in the map pattern.

Through 3D visualization of the data, georeferenced interpretations such as cross sections, and applying geological expertise, a geological concept model was developed in the form of network diagrams (Figure 8), adjacency matrices (Figure 9), block diagrams (Figure 10) and maps. In the northern Labrador Trough, the regional map pattern is established in published works (Clark and Wares, 2006);

however, there is disagreement around the nappe structures along the eastern margin. To develop a geologic concept model efficiently, the differences and similarities between map patterns needed to be presented clearly. Although not in common practice, methods have been proposed to communicate these relationships as encoded geological topology information (Burns, 1975; Thiele et al., 2016). In areas with complex deformation histories, it is difficult to discern key relationships in the map pattern. In this study, simplified network diagrams communicate cross-cutting and truncation relationships. These were used to compare characteristics of various proposed map patterns and models in a way that is easy to understand (Figure 8).

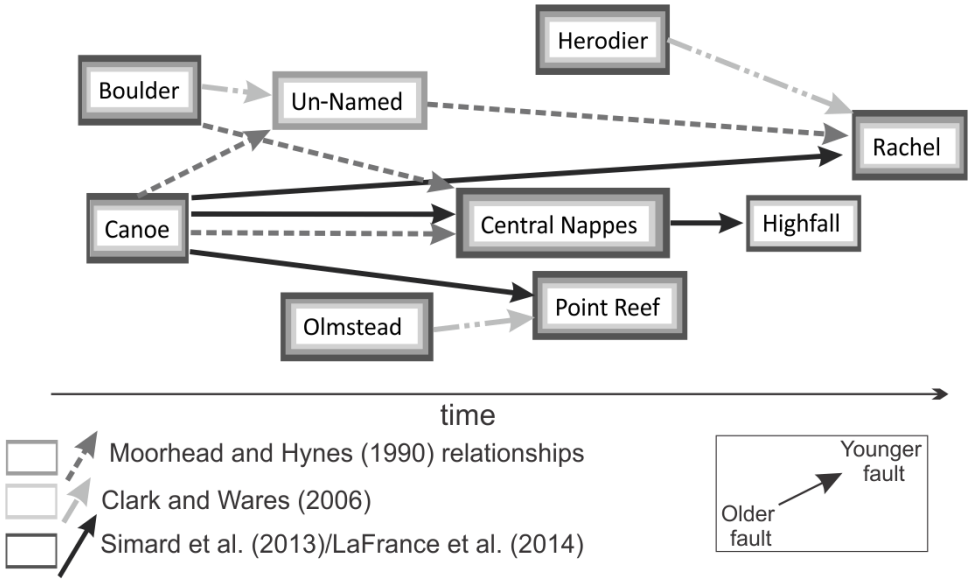

Figure 8. Fault network diagram for nappes structures of the northern Labrador trough. Shows cross cutting relationships and generations of faulting in the study area for faults that appear in the Nappes Sub-Region model. Relationships from Clark and Wares (2006), Moorhead and Hynes (1990), Simard et al. (2013), and LaFrance et al. (2014). Older faults (at origin of arrow) are cut by younger faults (end of arrow). Arrows point from faults that are cut to faults the faults that cut them.

A)

Younger Faults \ Older Faults	Olmstead	Point Reef	Boulder	Rachel	Canoe	Central Nappes	Hérodier	Un-named thrust
Olmstead		0	0	0	0	0	0	0
Point Reef	0		0	0	0	0	0	0
Boulder	0	1		0	0	0	0	0
Rachel	0	0	0		0	0	0	1
Canoe	0	0	0	0		0	0	0
Central Nappes	0	0	0	0	1		0	0
Hérodier	0	0	0	0	0	0		0
Un-named thrust	0	0	0	0	1	0	0	

B)

Younger Faults \ Older faults	Olmstead	Point Reef	Boulder	Rachel	Canoe	Central Nappes	Highfall	Hérodier	Un named thrust
Olmstead		0	0	0	0	0	0	0	0
Point Reef	1		0	0	0	0	0	0	1
Boulder	0	0		0	0	0	0	0	1
Rachel	0	0	0		0	0	0	1	1
Canoe	0	0	0	0		0	0	0	0
Central Nappes	0	0	0	0	0		0	0	0
Highfall	0	0	0	0	0	0		0	0
Hérodier	0	0	0	0	0	0	0		0
Un-named thrust	0	0	0	0	0	0	0	0	

C)

Younger Faults \ Older faults	Olmstead	Point Reef/ Hérodier	Boulder	Rachel	Canoe	Central Nappes	Highfall
Olmstead		0	0	0	0	0	0
Point Reef/ Hérodier	0		0	1	1	0	0
Boulder	0	0		0	0	0	0
Rachel	0	0	0		0	0	0
Canoe	0	0	0	0		0	0
Central Nappes	0	0	0	0	1		0
Highfall	0	0	0	0	0	1	

Figure 9. Fault adjacency matrices from topology in map patterns of published maps and Figure 8. Represents cross cutting relationships and generations of faulting in the study area for faults that appear in the Nappes Sub-Region model. Relationships from A) Moorhead and Hynes (1990) B) Clark and Wares (2006) C) Simard et al. (2013)/LaFrance et al. (2014) (0 = no relationship, 1 = Truncation relationship, 2 = cross cutting).

Similar to network diagrams, adjacency matrices (Figure 9) can be useful to track most relative timing relationships between geological features including faults, horizons, unconformities, fabrics, intrusions, and alterations (Burns, 1975). In creating these for 3D modelling, the goal was to highlight differences in relationships and relative ages; however, quantitative methods of comparison would also be beneficial for future work. For this study only the fault to fault adjacency relations were tabulated.

Block diagrams were used during pre-modelling as they facilitated geometrical and topological theory development without the investment of significant effort or time. Since the investment is low, several theories and models may be tested and updated. Figure 10 presents the evolution of block diagrams for the eastern thrust nappes from simple surface design to complete block diagrams. Throughout the design phase, 3D geometries of key surfaces were tested by hand using silicone baking sheets (Figure 11) and paper. Results from these simple tests were then captured in a series of block diagrams (Figure 10).

During the initial stages of 3D modelling, 3D data were visualized spatially as 3D symbols and as derived 3D form lines using the interpolation tool from Mira Geoscience called the Structural Field Interpolator (SFI). Stereonet analysis was also undertaken to define structural domains and individual structural features (See Appendix G). Graphical objects produced with these tools could then be used as secondary ‘interpreted’ or ‘estimated’ constraints where observational data were not directly available.

SFI was used to interpolate down dip vectors to characterize underlying geology based on the notion that field observations have structural relevance to the surface being modelled. It uses an anisotropic inverse distance weighting scheme, derived from Eigen analysis of poles to structural points' strike, dip and overturned properties, to calculate plunge models and 3D form lines (de Kemp, 2000; Hillier et al., 2013). These outputs can be used to characterise folding style, estimate depth of folds and can be set as inputs for later modelling algorithms. The form lines in Figure 12 show how SFI was used to characterize the Highfall antiformal thrust surface and Figure 13 shows how this technique can be applied regionally to estimate fold hinges.

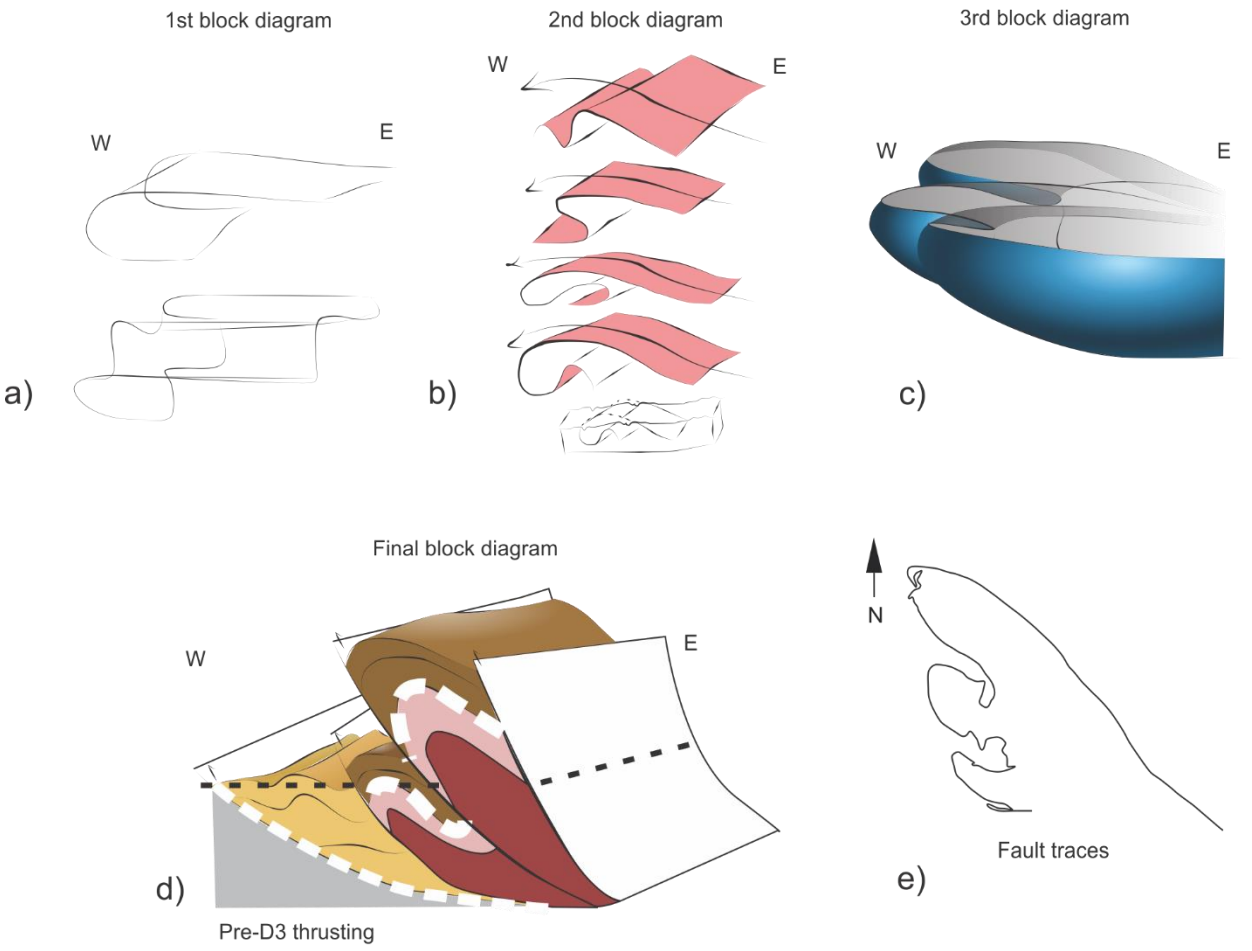

Figure 10. Progression of nappes conceptualization through sketches and block diagrams. Simplistic, wire-frame sketches (a) evolve into more complex and complete block diagrams (b, c, d) as data trends are investigated and surface geometry is tested in the 3D workflow. E) shows the surface trace of the central nappes block from the map pattern.

Figure 11 Example of folded surface nappes using silicone banking sheet.

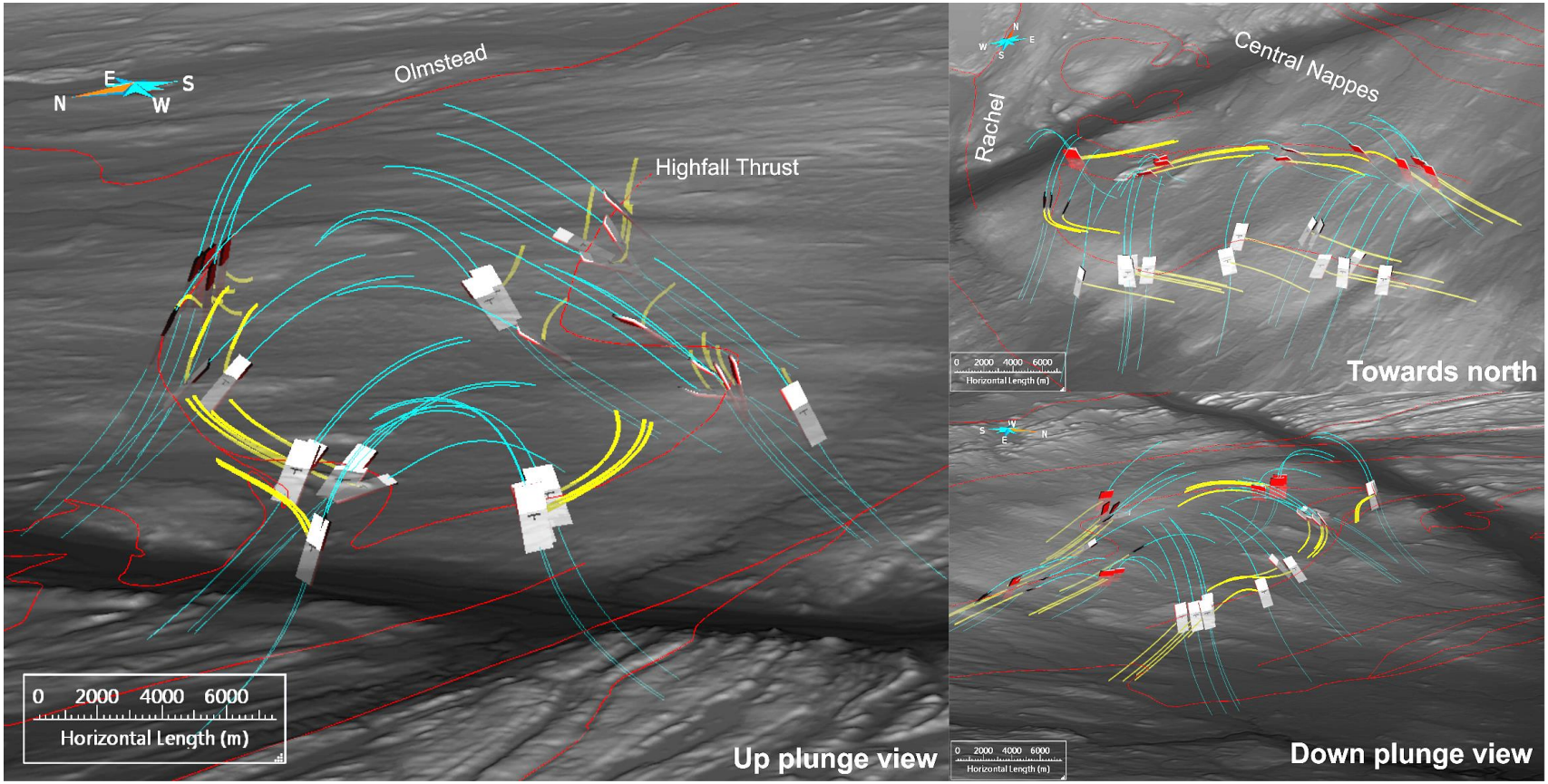

Figure 12. 3D visualization using SPARSE's Structural Field Interpolator (SFI) to visualize antiformal behaviour of the Archean-Paleoproterozoic contact of the Highfall nappe. Yellow = Interpolated strike vectors (principal eigen vector direction E2), Teal = Interpolated structural vectors, red = fault traces, and white/red tablets represent 2-sided, 3D structural field measurements used in the interpolation. Grey surface represents the digital elevation model (DEM).

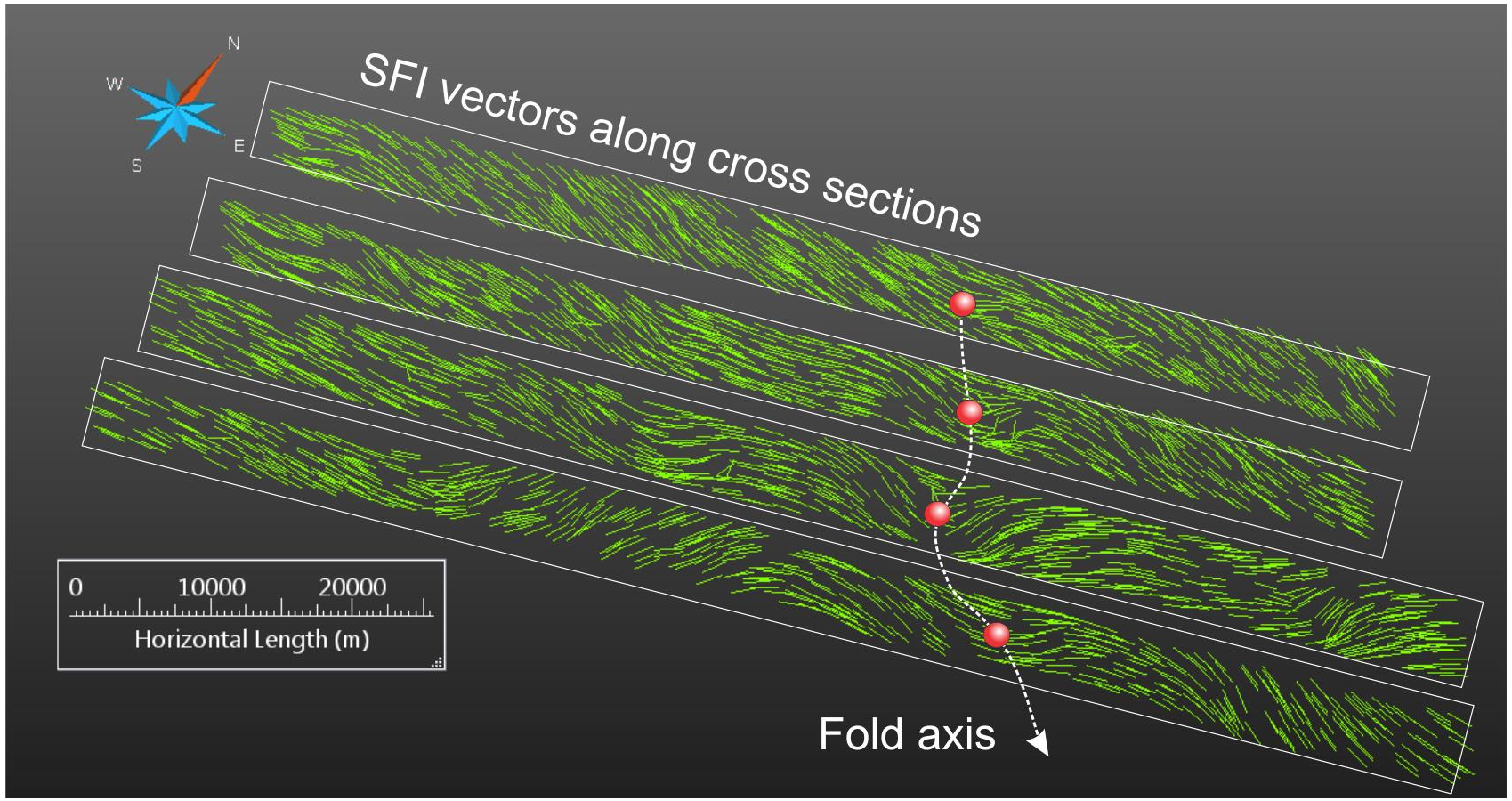

Figure 13. Structural Field Interpolator (SFI) 3D form lines along cross sectional surfaces spanning the study area. Created using bedding orientations across the study area and cut into four cross sectional views. Useful for visualizing large scale folds and tracking hinge lines in 3D.

2.2.2 Modelling loop

After visualization, classification, and structural analysis was completed, representative field observation points and derived constraints (form lines, axis, map and cross section feature traces) were used to generate surfaces and volumes using explicit and implicit modelling techniques in a GOCAD environment. Young, undeformed surfaces were modelled first, followed by increasingly older and more complex surfaces. To create these surfaces, input selection and modelling algorithms were applied in an iterative fashion to construct the most cohesive and geologically reasonable model.

During input selection, points were selected to constrain modelling of each surface based on their appropriateness for the feature being modelled. Appropriateness was determined using knowledge of local geology and 3D fit within the model. Points were selected when they were parallel to the feature and when they were assigned to the correct structural generation. For example, S_0 and S_1 are bedding parallel planar features. Whenever the points from those generations were parallel to the surface trace of a horizon, they were included in the selected set. Those points that were not parallel were set aside. This concept is demonstrated in Figure 14 where in Figure 14a shows an ideal case where S_0 bedding measurements are parallel to the interpreted trace of a banded iron formation, as well as an anomaly in the aeromagnetic map. However, data is often not ideal and the selection criteria must be broadened to include points which are more oblique to the feature being modelled or from another structural generation. This includes points which have not been assigned to a generation. Figure 14B demonstrates a case where data belonging to the relevant structural generation were too sparse and required an expanded selection set. In this case, many points were displayed and only those that were subparallel to the trace of the antiformal surface were manually selected and included in the model. In the northern Labrador Trough, bedding and the S_1 foliation were used to approximate early thrust fault geometry. Later faults are often associated with a late foliations or fabrics and can be constrained using S_2 or S_3. Selected points were chosen when they were subparallel to the strike of the feature and were assigned to the appropriate generation of deformation.

Since many regional scale faults are not directly measured in the field, interpretations, calculations, and approximations are sometimes used to constrain models. In such cases, or where observational points are sparse, new points were calculated on stereonets, non-traditional modelling constraints were used, interpolated vectors from Sparse's Structural Field Interpolator (SFI) were used, or interpreted points were created. Non-traditional modelling constraints include lineations and inequalities.

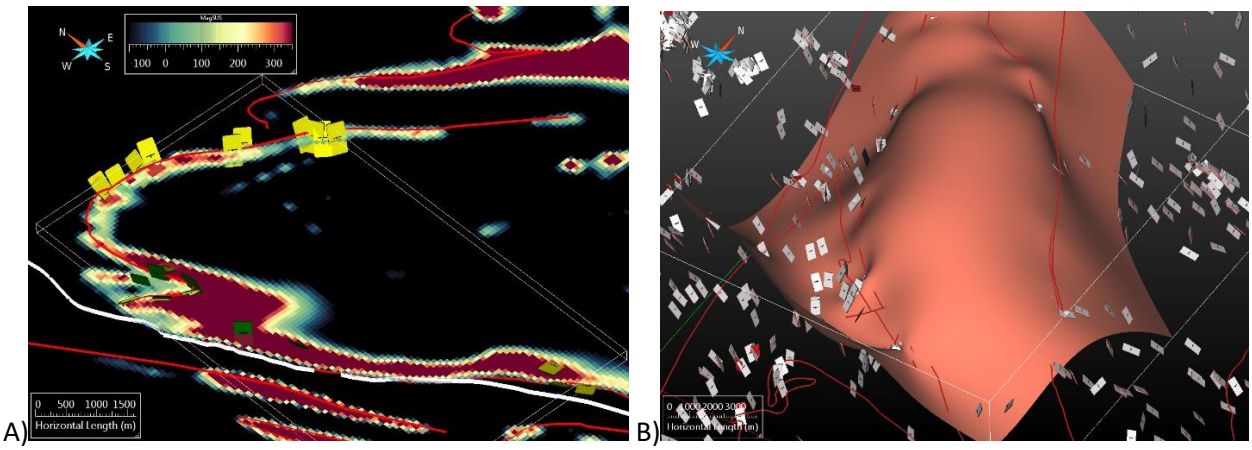

Figure 14 Demonstration of data and the selection process A) In some cases, the observed structural points are all generally parallel to a horizon's surface trace (red line) and anomalies on the aeromagnetic map (gradient coloured surface). The white line represents an east dipping thrust fault. B) Relevant structural points (white tablets) are selected from the global population of points when strike is subparallel to a fault's surface trace (red lines). In this figure, many structural observations have been collected and some do not reflect the geometry of the antiformal feature (pink surface).

Data were also clustered such that outcrop-scale features were over-represented compared to sparsely sampled, uneconomic areas. To obtain a more geologically valid result, data were subjectively selected based on relevance to the model scale and to the feature of interest. While up-scaling and input selection can be done using quantitative methods (Carmichael and Ailleres, 2016), oversampled local structures in clustered data muted the influence of regional points. It was, therefore, necessary to supervise input selection methods by manually selecting only those points that were interpreted as "regionally representative" (Kaufmann and Martin, 2009). If the resulting surface was geologically invalid, or did not fit with other aspects of the model, a refined set of constraints were selected and the modelling process began again.

Geologic feature surface estimation was undertaken using an implicit calculation algorithm developed at the Geological Survey of Canada called SURFE (SURFace Estimator, Hillier et al. 2014). Following data input selection, SURFE was extensively used to model fault and contact surfaces. This plug-in for GOCAD, fits a scalar function *f(x),* where x is equal to X, Y, and Z location of the input locations and the combined weighted constraints, to input constraints such as on-contact, gradient (strike/dip), tangents (lineations) and inequality points (Figure 15A). To solve for a scalar function, SURFE employs the GREEDY (Carr et al., 2001) and Restricted Range (Beatson et al., 2004) methods, both of which are efficient at finding solutions for high resolution grids (Figure 15C and D). Once a solution is found, the function is then evaluated throughout a volume of interest, producing a 3D scalar field where $f(x) = 0$ represents the geological surface, $f(x) < 0$ represents the volume below the surface, and $f(x) > 0$

represents the volume above the surface (Figure 15B) (Hillier et al., 2014). The final stage is a marching cube algorithm (Lorensen and Cline, 1987) which is used to extract an interpolated surface from the scalar field wherever *f(x)* = 0.

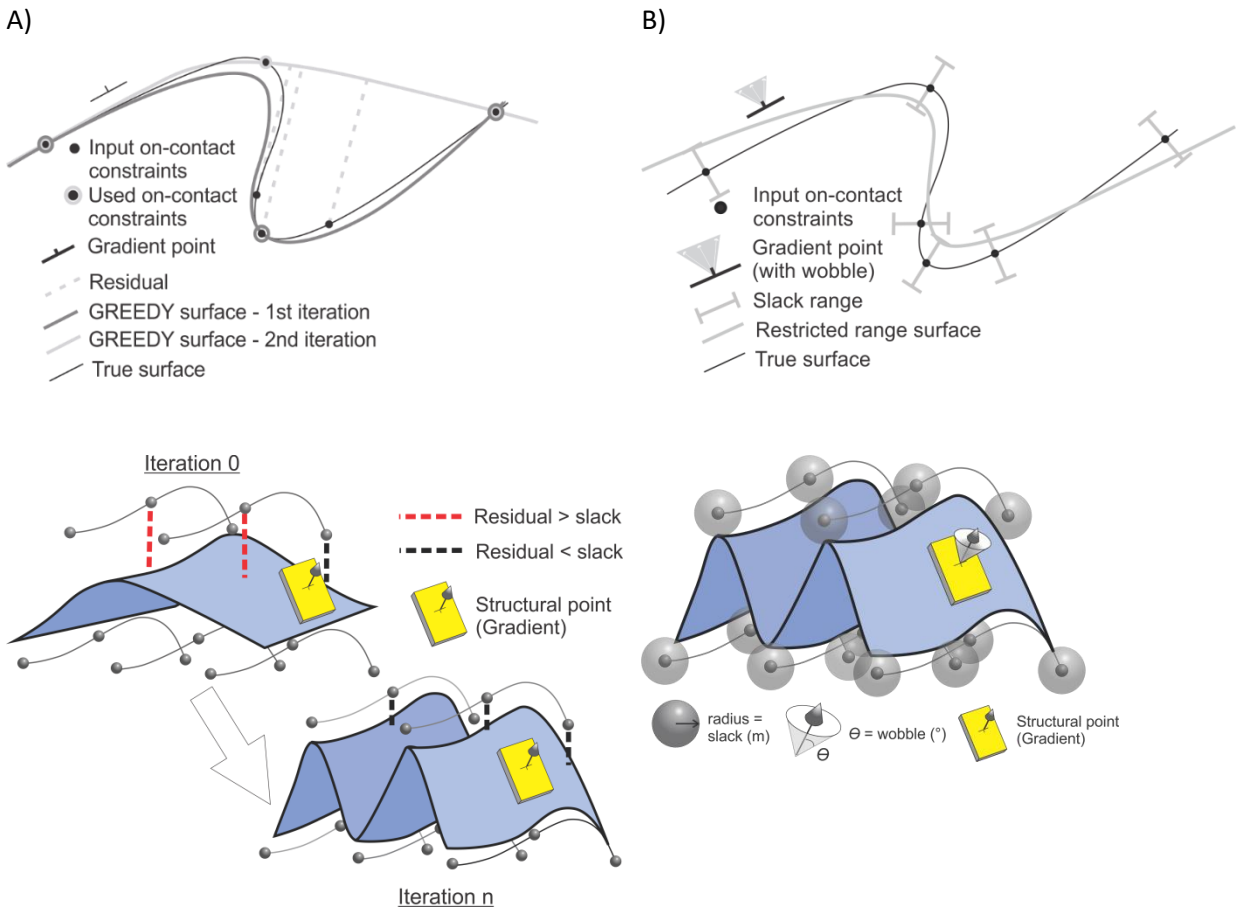

Figure 15. A) Examples of 2D and 3D GREEDY method solutions. B) Examples of 2D and3D Restricted Range solutions. On-contact points represented by black points or grey spheres, Fault sticks connect the on-contact points. Purple surface represents where the scalar function = 0 and the geological surface exists.

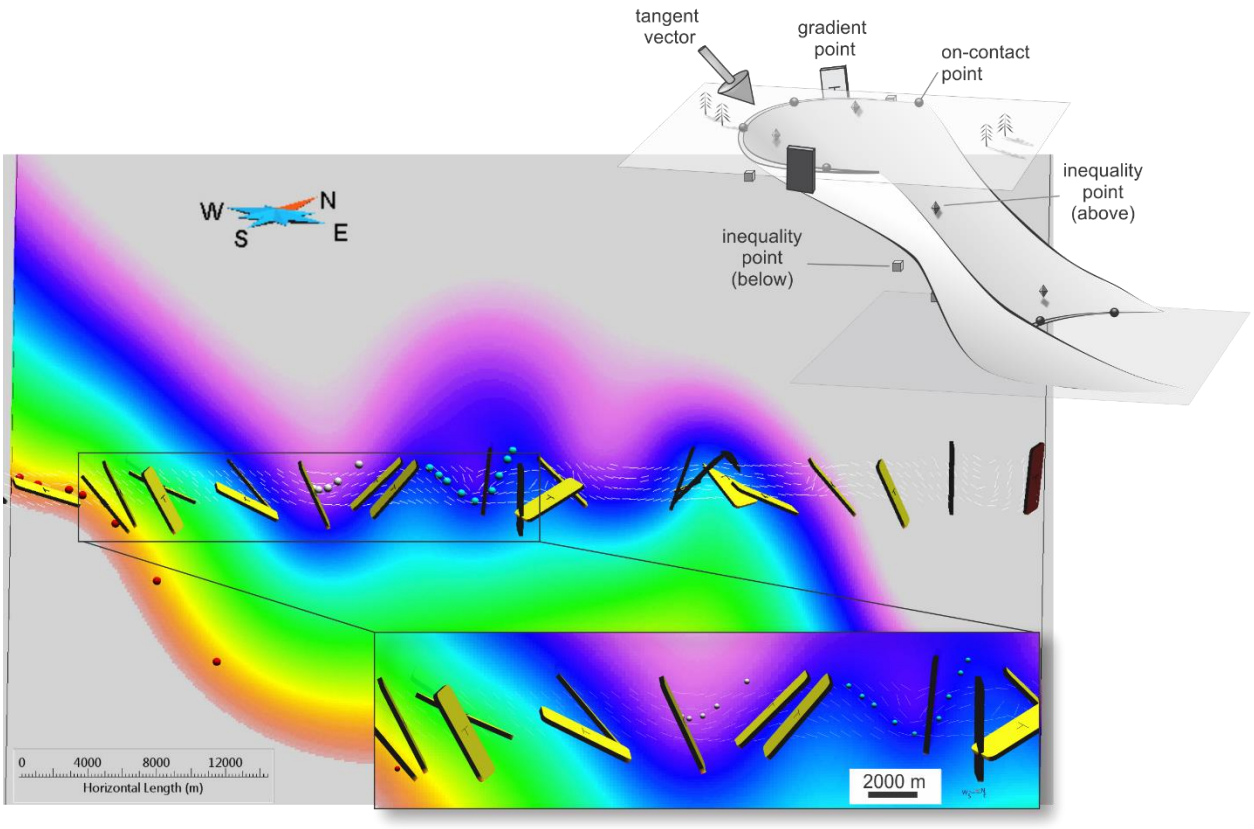

Figure 16. Profile view of an example of a multi-level (several parallel horizon surfaces) scalar field calculated by the SURFace Estimator (SURFE). Inset of idealized examples of inputs that SURFE can utilize. (yellow tablets = gradient with polarity, coloured spheres = three successive stratigraphic horizons (levels), and coloured gradient symbolized for scalar values of stratigraphic horizons).

SURFE is ideal for creating surfaces using sparse 3D data as it utilizes most types of field observation data, which are demonstrated in Figure 16. SURFE also efficiently up-scales data, by varying the scalar grid size and extracts regional trends from convoluted data while respecting input constraints using a specified fitting tolerance.

Additionally, SURFE can incorporate uncertainty by providing slack and wobble tolerance applied to constraints through the GREEDY (Figure 15A) and Restricted Range (Figure 15B) methods. Two types of values are subjectively determined for each surface based on input variability and confidence: 1) slack, which refers to a distance value, in meters, or acceptable residual values that the surface can be from a point, and 2) wobble, which refers to the allowable variation in the normal vector of gradient and tangent points (Figure 15). The slack and wobble settings were applied globally to the

selected set. In future studies, an attribute of slack or wobble for each point in the dataset would reflect knowledge and confidence more accurately.

Once a preliminary surface was constructed with SURFE, SPARSE was used for smoothing or generalizing; it was also used to generate interpreted constraints in areas of sparse data. Creating and applying interpreted points in this way is important as it allows under-constrained surfaces to be modelled by applying geological knowledge when data is sparse.

SPARSE is a knowledge-driven tool that interpolates Bézier and Non-Uniform Rational Basis Spline (NURBS) curves or surfaces using interactive grip frame points. These control points were dynamically adjusted in the 3D scene to interpret a given structural form. Bézier surfaces use a set of control nodes to construct a polynomial curve using a polynomial degree of one less than the number of control nodes. While putting this in practise is unreasonable for a large set of nodes, partitioning the nodes into smaller, low-polynomial-ordered, localized Bézier curves and linking them as B-splines allow simple interpolation between any number of data points (de Kemp and Sprague, 2003). The nodes of the B-splines are then tied across several partitioned curves, based on node occurrence order, to create a 3D surface.

Similar to Bézier curves and surfaces, a NURBS surface uses control nodes; however, NURBS surfaces fit data points exactly using tension and knot sequencing (Figure 17A)(Sprague and de Kemp, 2005). Knot sequencing refers to the method of indexing and weighting nodes based on order rather than spatial characteristics. This may cause issues if nodes do not occur in a logical order (i.e. nodes were digitized all over the map pattern). To construct surfaces, this study used on-contract points such as map traces, cross section contacts, and interpreted points as control nodes to constrain the Bézier and NURBS surfaces to represent fault and stratigraphic horizon geometry.

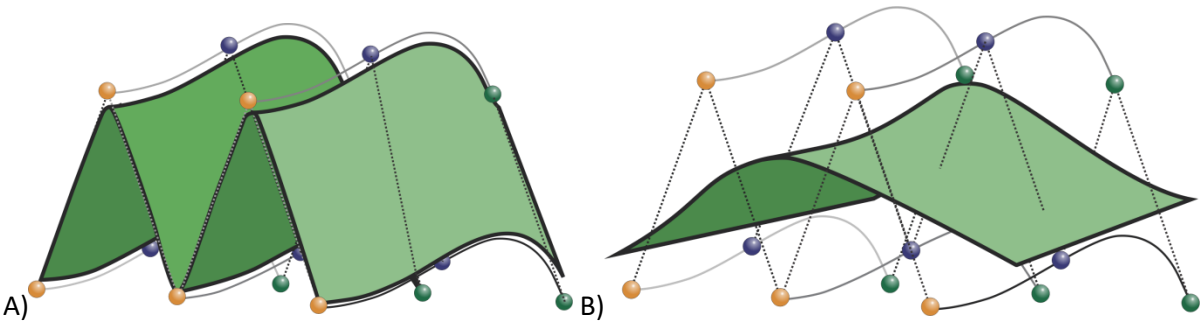

Figure 17. A) Example of idealized NURBS surface B) Example of idealized Bézier Surface. On-contact control nodes represented by coloured spheres. Colours indicate which points are connected between dotted lines. Grip frames are represented by the solid and dotted lines connecting control nodes. Surface solution is green.

Subsequent to surface construction, the Subsurface Knowledge Unified Approach (SKUA)'s Structure and Stratigraphy Workflow in GOCAD was used to create a 3D volumetric model of fault-displaced and deformed lithological units using a curvilinear grid (Mallet, 2002). Curvilinear grids have been useful is modelling mine-scale geology. One example of this is Schetselaar (2013). SKUA's method of interpolating a surface, the Discrete Smooth Interpolator (DSI) method, primarily uses on-contact constraints such as surface traces, cross lection contacts, and nodes from SURFE or SPARSE surfaces.

DSI, which is interpolation technique, was used to solve for surface node locations while trying to minimize a weighted sum of surface roughness and constraint misfit (Caumon et al., 2009; Mallet, 2002). Using surfaces, SKUA builds sealed fault blocks and lithological units within each block based on surface geometry. This resulting grid uses a UVT coordinate transformation that respects deformation within lithological units, making it useful for geophysical inversions (Mallet, 2002). The UVT transform is especially useful as it maps pre-deformational geometries to a horizontal Cartesian grid while respecting stratigraphic correlations across fault blocks.

2.2.3 Post modelling

Following the modelling process, the model solution should be evaluated for accuracy and geologic reasonableness using validation and uncertainty estimation techniques. Due to time restrictions, this thesis was not able to conduct this evaluation. Instead, individual components were validated throughout the modelling process using expert knowledge of those active in the study area and those familiar with similar terrains, as well as comparisons to published interpretations from the northern Labrador Trough.

Without several models to compare and dense datasets, rigorous quantitative validation processes that evaluate the performance of modelling algorithms are challenging to implement and will naturally be associated with very high uncertainty. Instead, regional scale 3D models use subjective validation by geological experts who evaluate models based on geological 'reasonableness.' During evaluation, the geoscientist will apply their experiences and knowledge of how geology formed and deformed given the study area's tectonic setting. Bond et al. (2012) has shown that incorporating formational processes such as these into model development increases accuracy and reliability. In addition to mental exercises, model/cross-sectional balancing can be used to evaluate accuracy. However, in the northern Labrador Trough, several factors prevented balancing, including a lack of thickness constraints in stratigraphy throughout the model space, the diversity of folding mechanisms, protracted histories and a lack of kinematic constraints. In the absence of balancing, ground-truthing the model by conducting targeted field work and collecting new observations is warranted.

After passing subjective and qualitative validation tests, the accuracy of the model can be measured quantitatively using uncertainty estimation techniques. Uncertainty estimation is an area of 3D modelling that is currently in development; however, it is limited by complexity in the 3D modelling workflow. When constructing 3D models, it is difficult to quantify uncertainty as the model incorporates observational and derived constraints which have unique biases and errors associated with them from acquisition and processing (Lindsay et al., 2013).

In addition to input uncertainty, conceptual uncertainty as defined by Bond et al. (2007) is an area of concern. When developing a model, a geoscientist uses their experience and training to select relevant theories and concepts that give meaning to data. The selection and application of relevant concepts are biased by the individual, resulting in conceptual uncertainty and a wide range of model products.

Some uncertainty estimation techniques that are currently available include quantitatively comparing several model solutions using geodiversity metrics and entropy property estimation (Lindsay et al., 2013; Wellmann and Regenauer-Lieb, 2012), comparing the various generations of the model, distance to data, and distance from the topographic surface (de Kemp et al., 2016). The limited at-depth data used to develop interpretive models as well as the use of knowledge assisted approaches embeds non-uniform uncertainty across the model. It is sometimes beneficial to consider confidence estimates for regions where data were used to construct any given model (Figure 6).

3.0.0 Results

While creating a 3D geologic model of the northern Labrador Trough, new geologic insight was gained and challenges related to the 3D modelling workflow were highlighted. The geological map pattern of several faults was updated through better 3D inspection of planar and linear observations. A cryptic early thrust, the Canoe Fault, was re-interpreted to close at a shallower (~10 km) level than previous (~20 km) (Moorhead and Hynes, 1990). The Ujaralialuk Fault was proposed as a solution to the unexplained juxtaposition of two thrust nappes as well as two new shear zones were proposed to the north and south of the Boulder Antiform. A single geological model concept was developed which integrates elements from three conflicting map patterns around the thrust nappes. The new map pattern and concept model have implications for timing of nappe development and relative ages of the Hérodier, Point Reef, and Rachel faults. Finally, areas of future geologic investigation are proposed to collect better constraints for displacement history, kinematics, tectonic models, and basement cover relations.

During model development, issues related to working in regionally extensive and structurally complex settings were highlighted. To improve the modelling workflow, new techniques that integrate data with expert knowledge are required. Additionally, the large investment of time and effort to create a single model solution inhibits geological theory development and uncertainty analysis. A streamlined workflow or simulation based method may assist with this issue. Finally, current modelling algorithms struggle with certain aspects of structural complexity, such as intense folding. Further development is required for these algorithms.

3.1.0 Geological insights

While the Labrador Trough experienced at least two phases of rifting during its early geologic history (Clark and Wares, 2006), the subsequent formation of the Trans-Hudson Orogen and collision between the Nain and Superior cratons reactivated normal faults into thrusts and oblique-dextral faults. While collisional deformation has obscured the normal displacements, some early normal faults are likely preserved in the hinges of folds, such as the Canoe Fault. A detailed geochronological study across fold hinges and the Canoe Fault would detect repeated stratigraphy, constrain the location of obscured faults, provide insight for the early tectonic history of the Labrador Trough, and may assist with kinematic calculations.

Early normal faults may include the Canoe Fault and Thévenet Fault. The presence of thrust faulting in the northern Labrador Trough is evident by the presence of older over younger stratigraphy at fault contacts such as the Robelin, Garigue and Forbes faults. Thrust fault geometry is also supported by repeated stratigraphy in the map pattern, specifically in the Kaniapiskau Supergroup, and is accompanied with right lateral offsets in stratigraphy such as the Hellancourt Basalts along the eastern boundary of the Kaniapiskau Supergroup block.

The first sub-region, the Hellancourt Syncline sub-region, is located in the central part of the study area and contains intensely folded and mineralized Kaniapiskau units (Clark and Wares, 2006). The model represents a complexly deformed region with several generations of faulting and intense folding (Clark and Wares, 2006; Corrigan, 2016). High resolution field data in the area and tilted beds provide good constraints for modelling.

The second model is the Nappes sub-region. This model contains complexly deformed faults, a unique view of basement-cover contact faults and nappe geometry (Moorhead, 1989; Moorhead and Hynes, 1990). Field data is sparse and there are few published cross sections, thus allowing a hybrid implicit-explicit modelling method to be tested.

Table 2 Description of fault surfaces present in the regional model, Nappes model, and Hellancourt model

Fault	Deformation event	Details
Robelin Thrust	D_1	East dipping thrust fault that cuts or over-rides the Forbes and Garigue fault in the north of the study area. Marks the boundary between the allochthonous and autochthnonous blocks. Geometry only affected by minor folding from late stage deformation. Interpreted to be generally parallel to bedding and S1.
Garigue Thrust	D_1	East dipping thrust fault that cuts or over-rides the Forbes fault. Likely a spay off of the Robelin Fault. Interpreted to be generally parallel to bedding and S1.
Forbes Thrust	D_1	East dipping thrust fault. Fault is the furthest west and may represent the orogenic front. Likely a spay off of the Garigue Fault. Interpreted to be generally parallel to bedding and S1.
Archaic Thrust	D_1	East dipping thrust fault that is parallel to the Robelin fault and is cut by the Hérodier fault in the south. Interpreted to be generally parallel to bedding and S1.
Canoe Thrust	D_1	Early thrust that cuts Rachel-Laporte Sueprgroup units. Deformed around the Rénia Synform. Interpreted to be generally parallel to bedding and S1.
Hérodier Thrust	D_1 or D_2	Marks major tectonic boundary, acting as the major slip plane which transports the Rachel-Laporte Supergroup onto the parathochthonous

		Kaniapiskau Supergroup. Fault is folded by D_3 transpression and is east dipping.
Boulder Fault	D_2	Contact between the Archean gneiss of the Boulder Antiform and the Rachel-Laporte Supergroup. Geometry is generally that of a sheath fold and extends roughly 6 km below the surface. See Appendix G for stereonet plots which characterize structural orientation
CentralNappes Fault	D_2	Contact between the Archean gneiss of the central block of thrust nappes and the Rachel-Laporte Supergroup. Must be younger than Canoe Fault as the Canoe fault deforms around it. Geometry is a complex sheath fold which developed prior to D_3 transpression. See Appendix G for stereonet plots which characterize structural orientation.
Highfall fault	D_2	Contact between the Archean gneiss of the Highfall Antiform and the Rachel-Laporte Supergroup. Sheath fold geometry is similar to the Boulder antiform, however, D_3 transpression has sinistrally offset the F2 fold axis. See Appendix G for stereonet plots which characterize structural orientation
Point Reef Thrust	D_2 or D_3	Tightly folded and poly-deformed fault. Likely the northern extension of the Hérodier fault. Has been sheared around the Boulder Antiform. Marks the contact between the Kaniapiskau Supergroup in the west and the Rachel-Laporte Supergroup in the east. Fault is east dipping
Lac Olmstead Thrust	D_2 or D_3	Fairly undeformed, east dipping oblique thrust fault with dextral offset. It is a major tectonic break and marks the boundary between the Core Zone and Labrador Trough.
Lac Ujaralialuk Thrust	D_3	Late stage, north-dipping fault which juxtaposes the central block of thrust nappes and the Highfall Antiform
Lac Rachel Thrust	Post D_3	Late stage oblique slip fault. 15 km right-lateral offset and 10 km vertical offset (Simard et al., 2013)

3.1.1 Regional model

The northern Labrador Trough is an area of complex geology ranging from simple foreland structures in the west to intensely deformed, metamorphosed hinterland rocks in the east. This complexity, coupled with incomplete lithological information and the geographic extent of the model space, limits what can be reasonably done with 3D modelling. A 3D grid could not be built because of insufficient control on horizon surfaces. Alternatively, a fault network, represented by a series of triangulated mesh surfaces, was constructed (Figure 18). During modelling, several fault topological schemes (Clark and Wares, 2006; Lafrance et al., 2014; Simard et al., 2013) were tested and a final fault network diagram was produced to demonstrate 2D topological relationships observed or interpreted at the surface (Figure 18). A description of each fault can be found in Appendix E.

The model in Figure 18 reflects topological relationships. It integrates the interpreted geometry published by Boone and Hynes (1990), Moorhead and Hynes (1990), Wares and Goutier (1990), Clark

and Wares (2006), and the SIGEOM geodatabase (*Système d'information géominière du Québec*, 2016). Respected geometries include dip direction, surfaces traces, and topological relationships. In general, faults have a northwest or north strike, are east dipping, have reverse displacement, and listric geometry, which was reliced from early normal fault displacement. Exceptions include the Hérodier, Point Reef, and Archiac faults which are folded such that their fold axis are southeast plunging. Plunge directions was constrained using the L2 stretching lineation, bedding, and S_1 observations. Additional exceptions are the imbricate thrust nappes (purple surfaces in Figure 18) in the Rachel-Laporte Zone which formed early sheath folds and were further deformed during D_3 transpression. One final exception is the Canoe Fault (yellow surface in Figure 18) which is a polydeformed D_1 thrust within the Rachel-Laporte zone. The fold preserves a complex interference pattern and is deformed around the Rénia Synform. The geometry of the fault is interpreted to resemble a bent canoe that plunges to the east and sits below the Central Nappes block.

Interpretations of regional faults among published maps generally agree; however, there was some ambiguity and disagreement related to fault topological relationships in some areas. Specifically, the relationships of the Forbes, Garigue, and Robelin faults was ambiguous in published cross sections. Also, the Hérodier, Point Reef, and Rachel faults were interpreted differently by Clark and Wares (2006) and the Système d'information géominière du Québec (2016). During model construction, topological relationships and interpretations were tested, resulting in a single fault topology scheme (Figure **1**), an estimate of occurrence order, and general descriptions (Table 2).

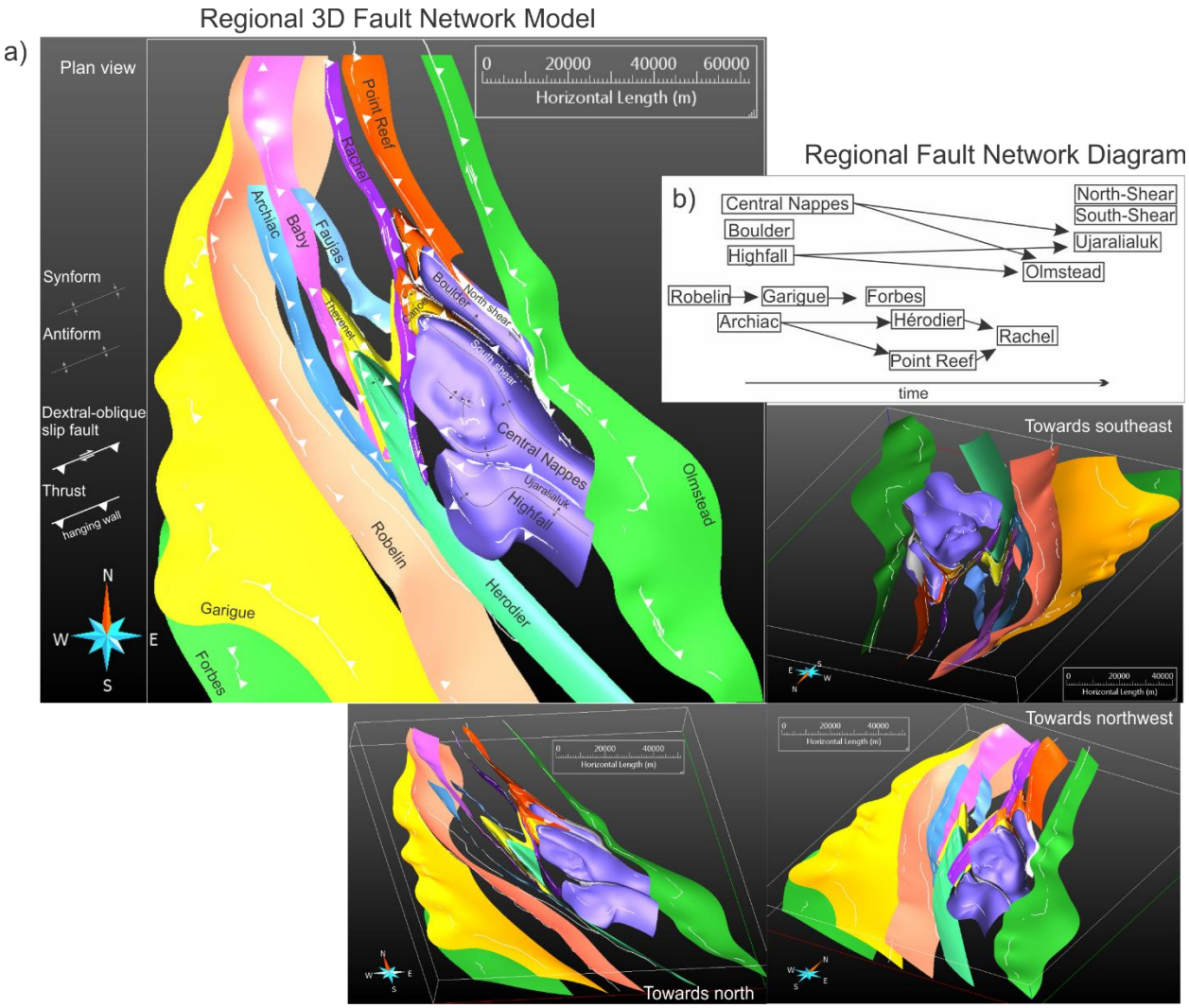

Figure 18. A) Regional 3D fault network model and fault network diagram with superimposed structures to indicate dipping direction. B) Fault network diagram showing cross cutting relationships and generations of faulting in the study area for faults that appear in the Regional fault network model. Oldest faults on left and youngest on right. Arrows point from faults that are cut (older faults) to faults that cut them (younger faults).

3.1.2 Hellancourt Syncline sub-area

The Hellancourt sub-area is a complexly deformed region with several generations of faults and intense folding. This model is supported by high resolution field observation data that allows for the creation of horizon surfaces and the creation of a volumetric geology model. It hosts several economically prospective areas which has resulted in data clusters and local scale interpretations around economically prospective areas. Therefore, model inputs required up-scaling to become useful for regional scale modelling.

Another benefit of choosing this model space is the exposure of tilted beds, which allowed unit thickness to be estimated providing greater control on model surfaces. This is in contrast to working in undeformed regions where beds are flat-lying. In such a case, only the uppermost unit is measured in the field, thus providing no insight into 3D geometries and unit thicknesses.

3D horizons and faults were constrained using several cross sections (Boone and Hynes, 1990; Clark and Wares, 2006; Goulet, 1987; Goutier and Wares, 1991; Moorhead and Hynes, 1990; Simard et al., 2013; Wares and Goutier, 1990), field data, the SEIGOM map pattern and aeromagnetic maps. Since there was intense deformation, numerous thin beds, and several generations of local faulting, it was difficult to construct a detailed 3D lithologic volumetric model. To overcome this issue, the stratigraphic column was simplified, while ensuring the general sub-regional structures were represented. Figure 19 shows the generalized stratigraphic column used in SKUA to build the 3D model. Generalized horizons were selected based on available data, SIGEOM mapping, and contacts that were traceable on the aeromagnetic map (i.e. iron formation and intrusive bodies). Figure 20 presents the 3D surfaces and volumetric model of the Hellancourt syncline sub-region. Generalized stratigraphic horizons and units are coloured and locally significant faults are grey. In the volumetric model, offsets of lithological units are obvious and an m-fold is apparent.

The Hellancourt Sub-Region is comprised of a sub-regional scale anticline-syncline pair, the Hellancourt Syncline and Faujas Anticline, which is bounded by two thrust faults, the Baby and Rachel faults. Stratigraphy generally youngs to the southeast and a complex fold relationship between Cycle 1 and the lower intrusive unit had been interpreted by the Système d'information géominière du Québec (2016) and Simard (2013); however, generalizations in the model surface smooth out the contact between these two units since modelling algorithms could not capture the complexity.

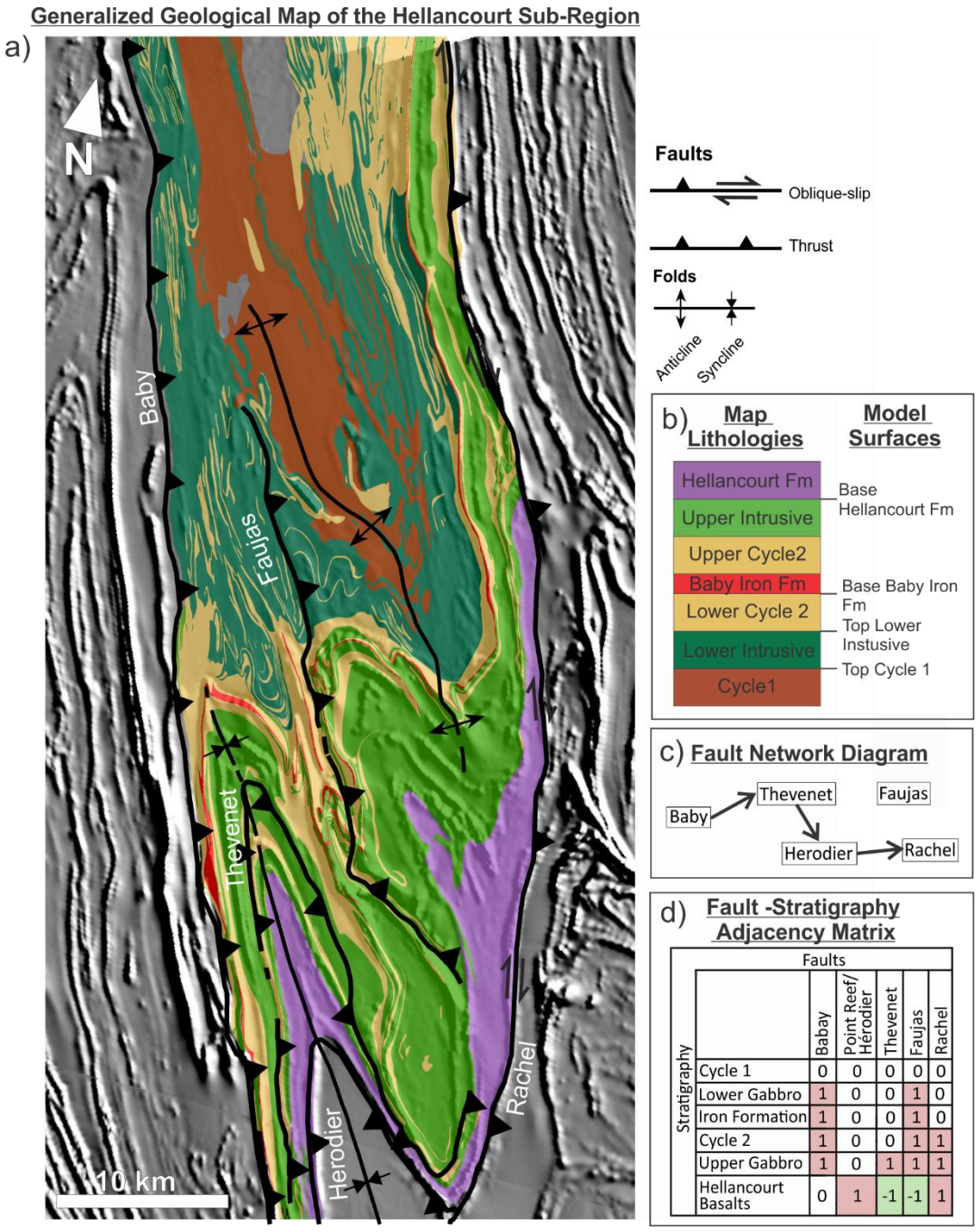

Figure 19. A) Generalized geologic map of Hellancourt sub-region fused with hillshaded aeromagnetic grid. Map units simplified to reflect units that were modelled in the Hellancourt Sub-Region model. B) Insets on right of simplified stratigraphy used in the model, c) fault network diagram, and d) adjacency matrix. Fault network diagram shows cross cutting relationships and generations of faulting in the model area. Oldest faults on left and youngest on right. Arrows point from faults that are cut (origin of arrow) to faults that cut them (end of arrow). Fault-stratigraphy adjacency matrix has red (value = 1) for cross cutting and green (value = -1) for intrusive relationships.

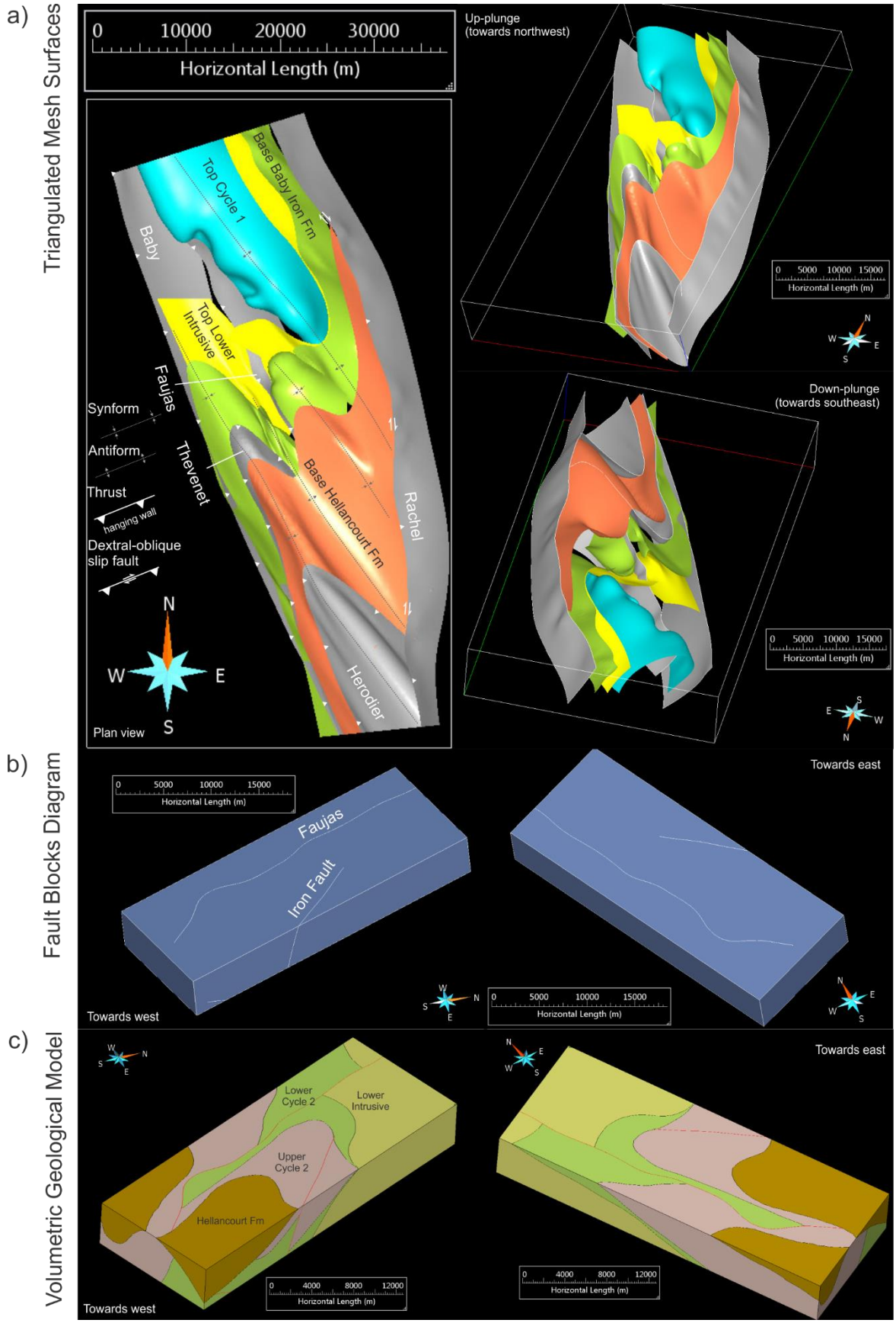
a)
Triangulated Mesh Surfaces
0 10000 20000 30000
Horizontal Length (m)
Base Baby Iron Fm
Top Cycle 1
Baby
Top Lower Intrusive
Faujas
Synform
Antiform
Thevenet
Thrust
hanging wall
Dextral-oblique slip fault
Base Hellancourt Fm
Rachel
Herodier
N
W
E
S
Plan view
Up-plunge (towards northwest)
0 5000 10000 15000
Horizontal Length (m)
Down-plunge (towards southeast)
b)
Fault Blocks Diagram
Faujas
Iron Fault
Towards west
Towards east
c)
Volumetric Geological Model
Lower Cycle 2
Lower Intrusive
Upper Cycle 2
Hellancourt Fm
0 4000 8000 12000
Horizontal Length (m)
Towards west
Towards east

Figure 20. Results of 3D modelling in the Hellancourt Sub-Region. A) Triangulated mesh surface with grey faults and generalized stratigraphic horizons with superimposed structures to indicate dipping direction. B) Fault block model from SKUA with fault edges (white lines). C) Volumetric geological model of generalized stratigraphy in Hellancourt Sub-Region. With contacts (black lines) and fault traces (red lines).

3.1.3 Nappes sub-region

The Nappes sub-region represents an area of intense deformation at the interface between high metamorphic grade Archean basement and Paleoproterozoic cover rocks. It provides a unique opportunity to test modelling capabilities with complex faults such as antiformal and synformal nappes, sheath folds, tight folds, surfaces with multiple folds, and shear zones.

While there has been limited research in this area beyond publications by Moorhead and Hynes (1990), Clark and Wares (2006), Simard et al. (2013) and Lafrance et al. (2014), the GSC is currently compiling and interpreting results from recent mapping programs and graduate studies. Publications of this work will follow the submission of this thesis and were not available for the 3D modelling presented here. Future modelling of the area will benefit from these publications once they are released. The lack of currently available data and interpretations has been restrictive to the 3D modelling workflow. Without sufficient lithostratigraphic constraints for this sub-region, it is not possible to construct a 3D geologic grid. Instead, a fault network and gridded fault blocks representing the volumetric fault compartments were modelled and the structural orientation of the nappes were characterized on stereonet plots in Appendix G (Figure 21).

Among the three published map patterns of the nappes, there are conflicts in fault topology and geometry. In order to create a 3D model, a single topological scheme and map pattern was developed. The new scheme and map integrated the most geologically reasonable elements from each interpretation. The map pattern (Figure 22) needed to respect observations such as trends in the aeromagnetic map and be geometrically plausible at depth.

The Nappes Sub-Region fault block model has several features of interest. First, the Canoe Fault which sits beneath the Central Nappes, is a complex surface with a chevron fold interference pattern and tight geometry. Because of these characteristics, the fault could not be modelled in SKUA given the coarse resolution of the regional grid. Similarly, the Boulder and Highfall nappe antiforms were removed from the fault block model because SKUA could not resolve their sheath fold geometry.

Additionally, one northwest trending fault surface has been identified using the aeromagnetic map and model development techniques. This study proposes the name Ujaralialuk Fault for this fault

(Figure 23). It is interpreted to be a steep, late-stage, north-dipping fault which divides the lower grade Highfall nappe from the central nappe block to the north. Fault trace extent was interpreted from the aeromagnetic map, dip direction was interpreted by Lafrance et al. (2014), and dip angle was estimated from foliation measurements which are located near and subparallel to the fault trace.

Two northwest trending shear surfaces where also identified using the aeromagnetic map and model development techniques (red in Figure 22) These surfaces are likely late stage, similar in age to the Ujaralialuk Fault, and may have acted as slip planes that allowed for the upward displacement of the Boulder Antiform during or after D_3.

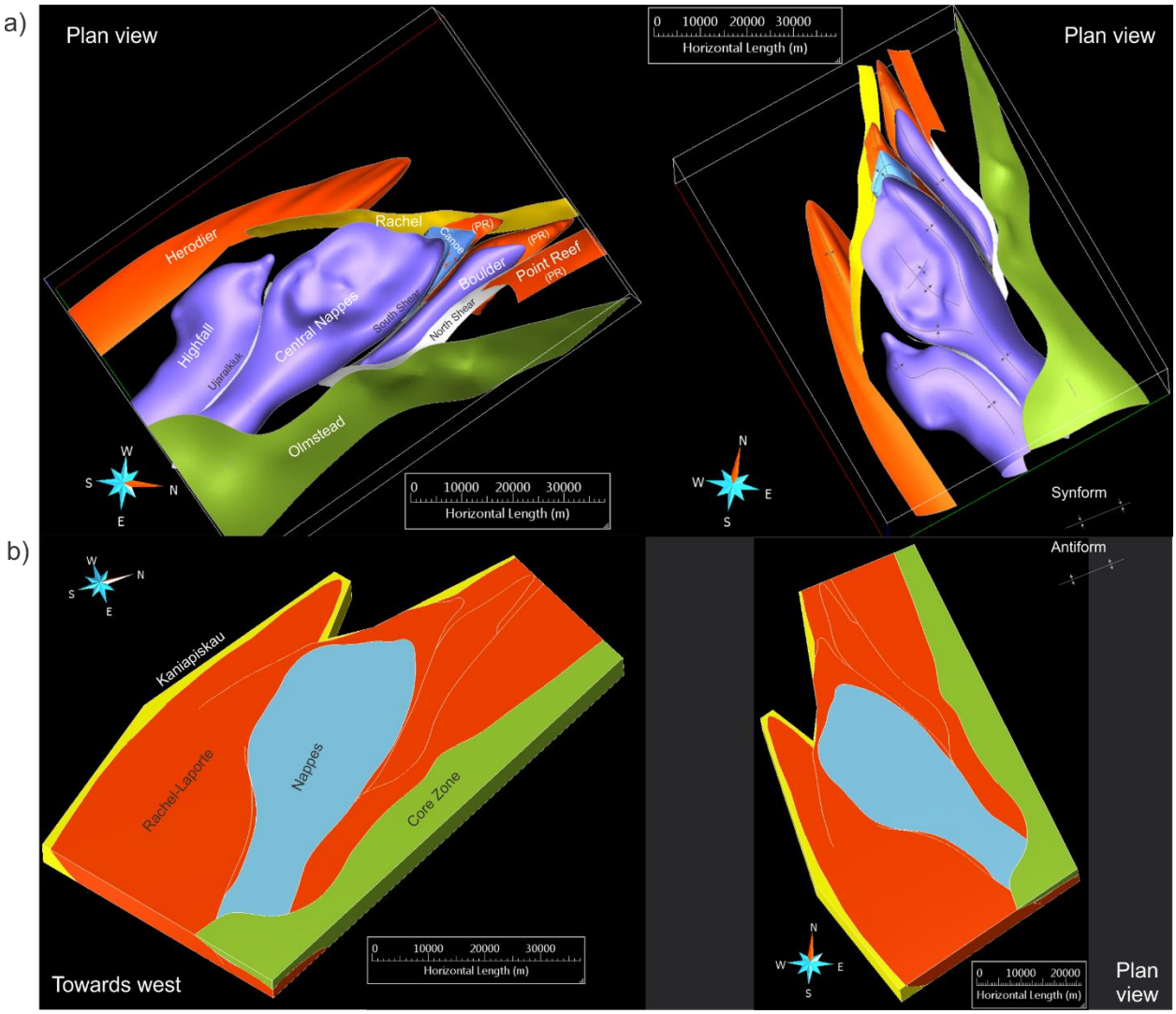

Figure 21. Results of 3D modelling the Nappes Sub-Region. A) Plan views of fault network surface model of the Nappes Sub-region with superimposed structures to indicate dipping direction. B) Irregularly shaped fault block model from SKUA with fault traces (white lines). PR = Point Reef Fault.

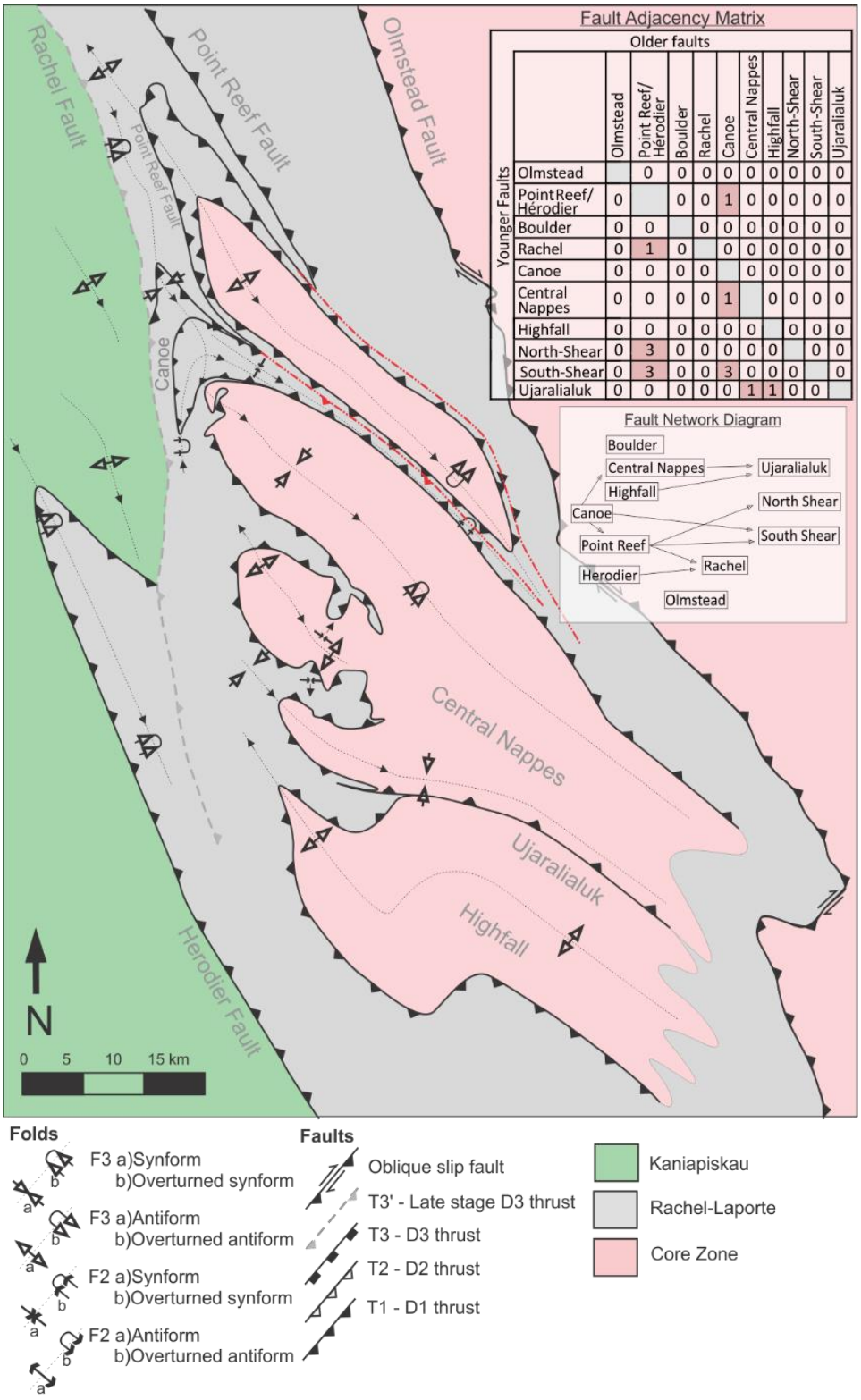

Figure 22. Proposed generalized geological map for Nappes Sub-Region. Insets of fault adjacency matrix and fault network diagram. Fault network diagram shows cross cutting relationships and generations of faulting in the model area. Oldest faults (origin of arrow) on left and youngest (arrow tip) on right.

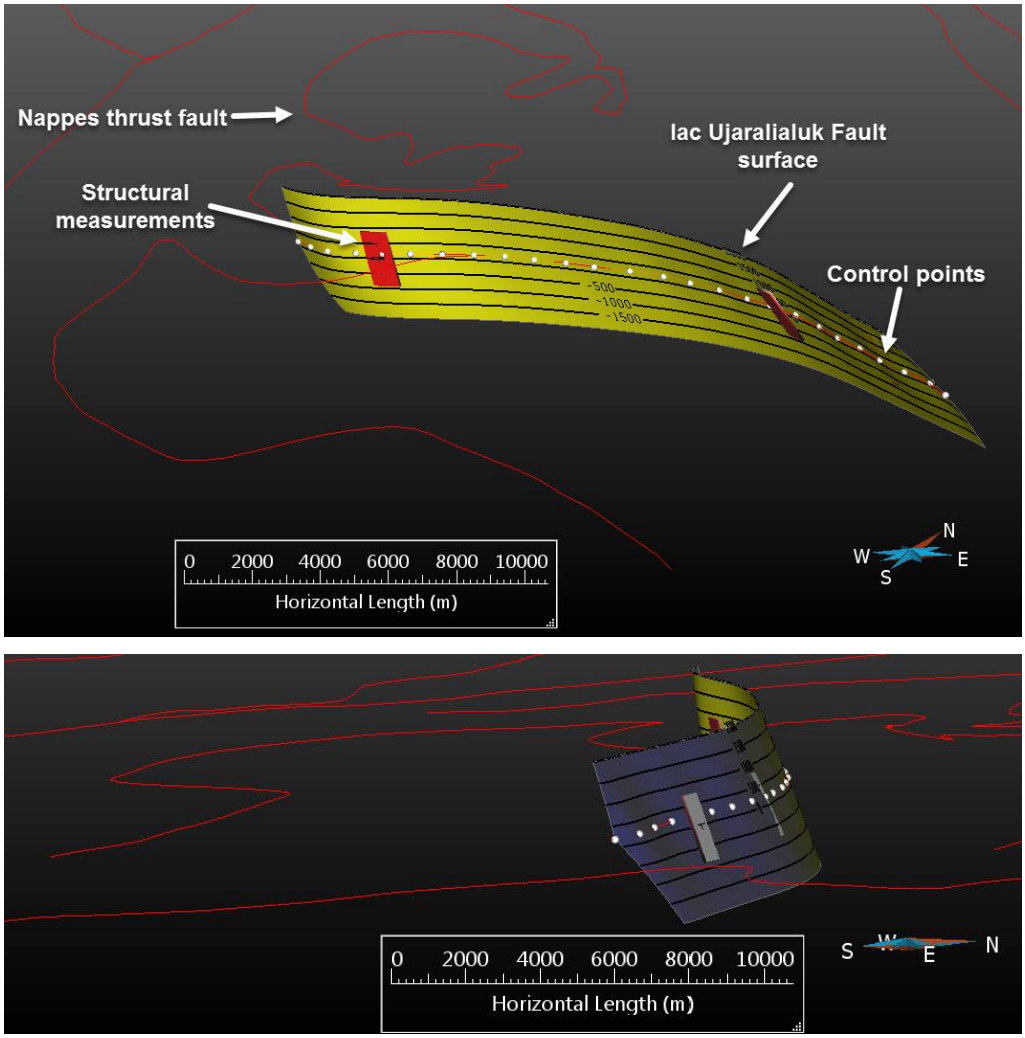

Figure 23. Proposed 3D geometry of Ujaralialuk Fault with fault traces (red lines), 3D structural point tablets (red/white tablets), on-contact constraint points (white spheres) and elevation contours (500 m spacing).

3.2.0 Modelling method results

In recent years, several 3D geologic models of regional-scale, poly-deformed, mid-crustal settings have been developed to test 3D modelling methods and gain geological insight (de Kemp et al., 2016; Lindsay et al., 2013; Maxelon et al., 2009; Philippon et al., 2015). From the modelling efforts of these studies several new tools have been developed to support model construction in these challenging terrains (SURFE (Hillier et al., 2015), SFI (Hillier et al., 2013), GIS3D plugins to Gocad (Mira Geoscience and Geological Survey of Canada), Leapfrog, GeoModeller, structural modelling from Caumon et al. (2013), and uncertainty modelling from Lindsay et al. (2012)); however, it is still the case that a standard 3D modelling workflow has not yet been realized for complex geology. Through creating

a 3D model of the northern Labrador Trough, we continue this process of identifying issues and benefits in the workflow. Besides simply not having regionally distributed, good quality at-depth data, challenges are generally related to the large extent of regional modelling and limitations of available software.

3.2.1 Regionally extensive model challenges

Through constructing a 3D model at the regional scale, two challenges have been identified. Firstly, the computational cost of modelling large areas with current grid based technology is prohibitive. As the model size increases, the computational cost increases exponentially. While computational power is increasing to meet the needs of 3D modelling, a balance between model resolution and scale must be found. Ideally, a model would use the lowest resolution that captures all the relevant features in a model. Finding this balance, however, is difficult and a more rigorous method of selecting the appropriate resolution is warranted.

Secondly, sparse 3D data requires knowledge-driven modelling methods to be developed. Constraint sources such as drill core and geophysical surveys are often prohibitively expensive to gather for large regions and those that are gathered may not sample relevant features. The northern Labrador Trough has benefited from many decades of study; however, until recently, research conducted in the area has not been coordinated and publications were focused on specific research questions rather than a consistent regional understanding. The challenge related to this issue is that integration is time consuming and extracting regional meaning from these locally focused studies is difficult. Currently, integration and data preparation accounts for the largest time and effort investment within the 3D modelling workflow (75-90%).

3.2.2 Geologically complex model challenges

The northern Labrador Trough is a structurally complex fold and thrust belt. Creating a 3D model in this sparse data setting has highlighted limitations of currently available software and modelling algorithms. The limitations include representing tight folds, interference folds, sheath folds, folds with overturned limbs, and surfaces with high frequency disharmonic folds. Additionally, interformational sills and dykes which may be volumetrically significant and may mask critical boundaries are indeed a challenge to model.

Tight folds

When constructing the SKUA fault block model of the Nappes Sub-Region, the tight fold geometry of the Point Reef Fault provided a unique challenge for the SKUA implicit algorithm to solve. To correctly represent the fault's tight geometry, a balance in 3D grid resolution and scale, as well as

distance of influence of other surfaces, was required. Discovery of the correct combination of resolution and influence settings was time consuming as many combinations were tested for each surface in the model. Figure 24 demonstrates this issue for the Point Reef Fault.

Similarly, SURFE's implicit modelling method also struggles to resolve tight to isoclinal folds and often joins limbs into one surface. When modelling tight folds, implicit algorithms such as SURFE and SKUA implicit calculations do not recognize point occurrence order or limb assignment. Instead, they respect the geographic location of constraints and join all on-contact constraints into the simplest surface. While this is useful for creating smooth surfaces, their method of joining limbs is not geologically valid for tight folds. Even with the use of inequality constraints SURFE and SKUA were not able to reasonably represent the Canoe Fault (Figure 25).

Surface with multiple folds (Interference folding)

When working at the regional scale and in areas with intense deformation, it is common to encounter surfaces with multiple folds. For example, the Point Reef Fault has been deformed around the eastern thrust nappes in the Labrador Trough and has two northward facing hinges. Surfaces such of these are a challenge for explicit modelling tools, such as SPARSE, to accurately represent. Often the large number of control points required to fully capture the surfaces fold geometries causes a creasing effect (Figure 26 and Figure 27) that likely does not reflect the geology. Conversely, the SURFE and SKUA modelling algorithms are able to satisfactorily represent surfaces with multiple folds.

Sheath folds

The SKUA implicit calculation was not able to resolve sheath folds such as the Boulder Antiform and Highfall Antiform in the regional model as well as the Nappes Sub-Regional model. When given a dense set of on-contact constraints, SKUA was not able to construct a geologically reasonable sheath fold (Figure 28). Instead, it tried to respect the points and create a single tilted surface. The other modelling methods, SURFE and SPARSE, were able to construct the desired geometry. In other cases, such as Passchier et al. (2011) and Wex et al. (2014), there has been success modelling, sheath folds using dense data. Improvement in the modelling practices and methods is needed if it is to be implemented in other structurally complex settings.

Folds with overturned limbs

The SKUA implicit calculation struggles to model folded surfaces with limbs that overturn. For example, the top of the Cycle 1 sedimentary sequence (Figure 29) was not resolved correctly and had to be removed from the Hellancourt Sub-Region model.

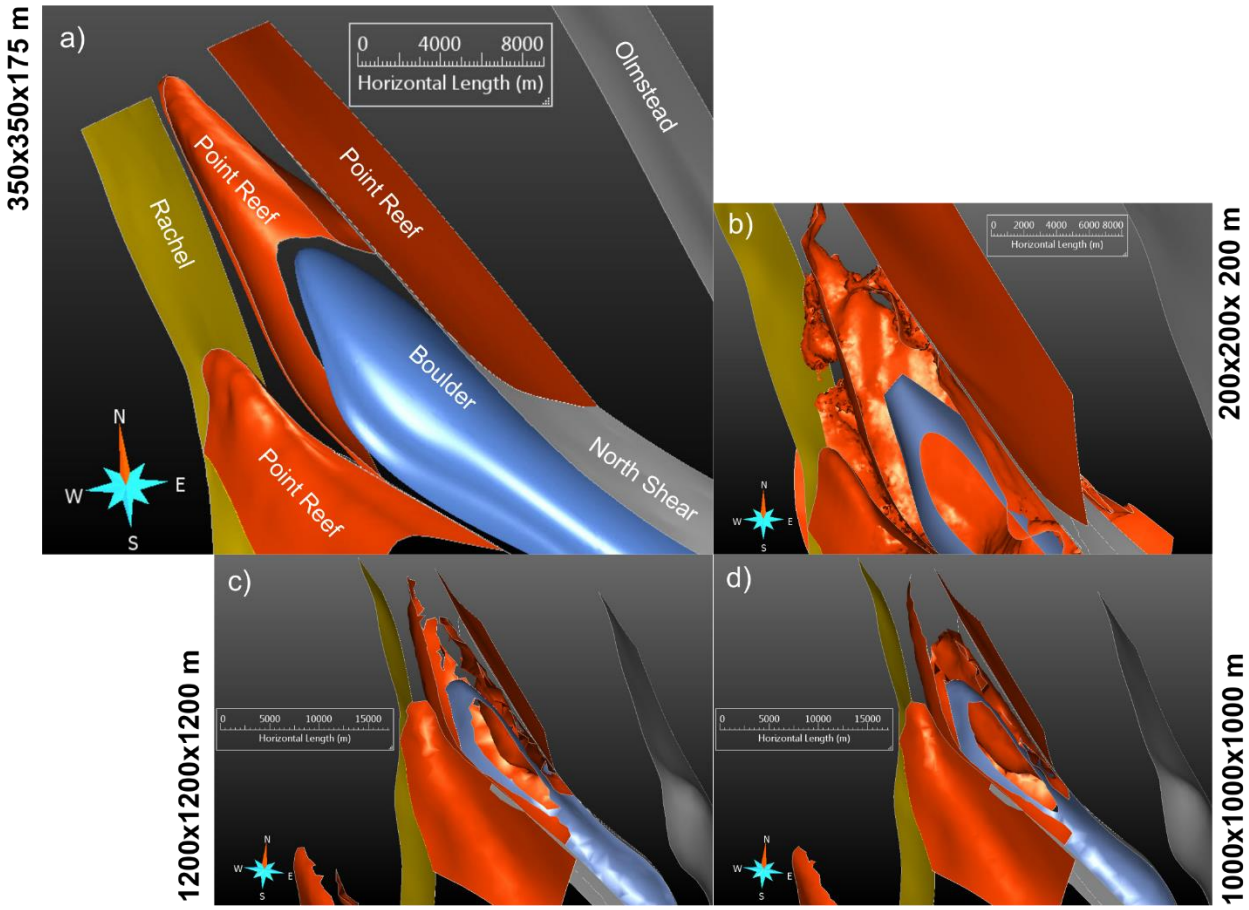

Figure 24. Example of surfaces created in SKUA using various 3D grid resolution settings to model the fault network in the Nappes Sub-Region model. Cell size of grids vary from a)350x350x175 m, b) 200x200x200 m, c) 1200x1200x1200 m, and d) 1000x1000x1000 m. Figures show progression from over sampling fine grids (200m) to under sampling (1200m). There is a balance where data were sampled correctly (350x350x175 m).

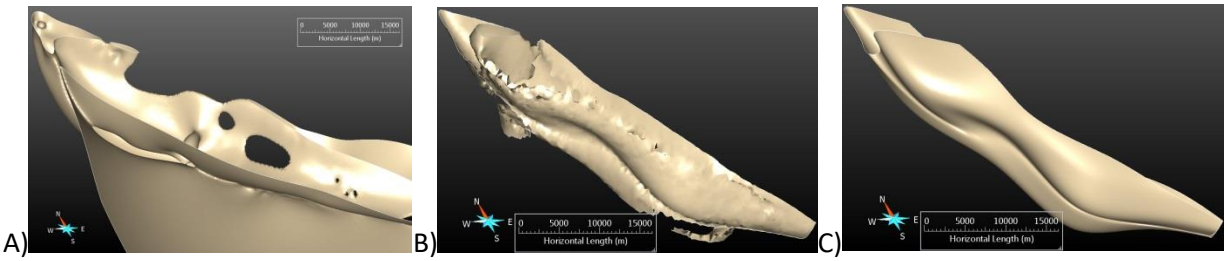

Figure 25. Examples of modelling algorithm solutions for tight folds. Surface solutions for the Canoe Fault using A) SURFE, B) SKUA and, C) SPARSE.

Complex surfaces and local anisotropy

In the Hellancourt Sub-Region model, complexly folded contacts required generalization and smooths as modelling algorithms were not able to fully capture fold complexity. To accurately model these surfaces, a high resolution grid which adequately sampled the small structures was required; however, such a grid was computationally expensive to create and store. Additionally, constructing such surfaces required a large investment of time and effort as each fold along the surface had to modelled

separately. This piecewise approach was necessary as SURFE could not resolve local anisotropy in fold orientations, SPARSE's complex grip frames were too complex, and SKUA smoothed out local scale folds.

3.2.3 Other observations for the 3D modelling workflow

The collection and creation of constraints for modelling is currently a difficult and cumbersome process because there are no software packages that fully integrate and organize both 2D and 3D objects. At the moment, tabular (field observations or geochemistry), 2D objects (fault traces, lithological maps, geophysical maps, etc.), and 3D objects (fault surfaces, horizon surfaces, models, etc.) are stored separately in folder trees and project files which cannot be queried or sufficiently organized. This unorganized and unintegrated system often cumbersome to use and often decreases modelling efficiency as data may be lost or forgotten. A new system which integrates all data types, allows for queries to be made on all file types, allows for data relationships to be defined, and converts/projects 3D objects into a 2D framework, and vice versa, is required. It could also incorporate interpretation tools such as cross section generation or map generation tools.

In addition to an improved organization and storage system, new attributes which are linked to geological features would be useful in defining model parameters. For example, thickness of stratigraphic units (maximum and minimum), relationship to underlying and overlying units (unconformable, baselap, intrusive, conformable) as well as thinning direction (shore direction).

While there have been benefits to using the SURFE, SKUA, and SPARSE modelling methods to create 3D surfaces and models of the northern Labrador Trough, there are several challenges which must be addressed for modelling to improve in areas with complex geology. These improvements may include refinement of modelling algorithms or development of new methods to represent complex fold geometries. While these tools and related methods are in development, the hybrid approach of integrating all three methods to create a geological model, as presented here, captures the northern Labrador Trough's fault network adequately.

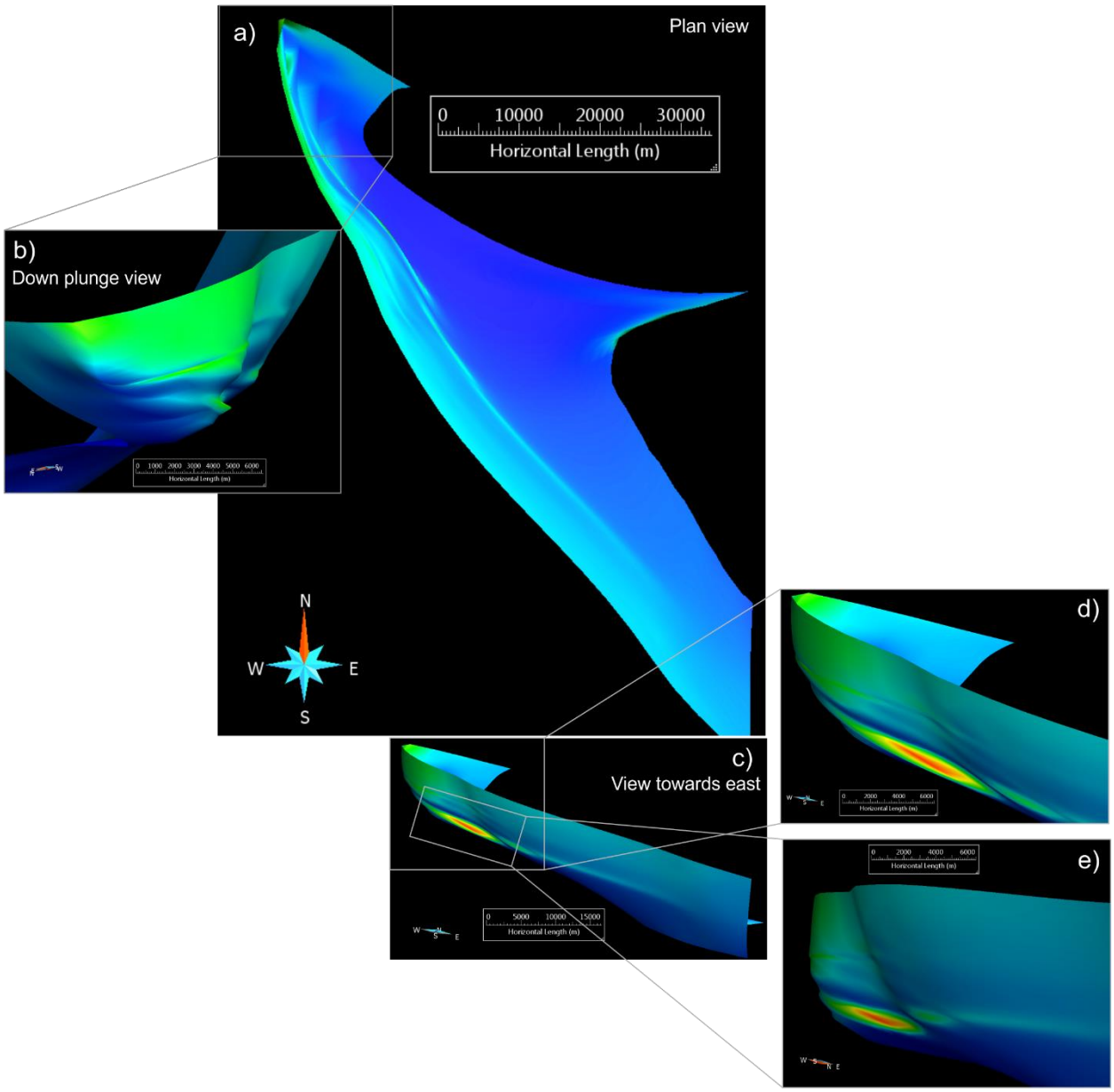

Figure 26. Example of creasing effects caused by SPARSE when modelling the Hérodier fault. Surface symbolized with first element of normal vector across fault to highlight changes in surface orientation.

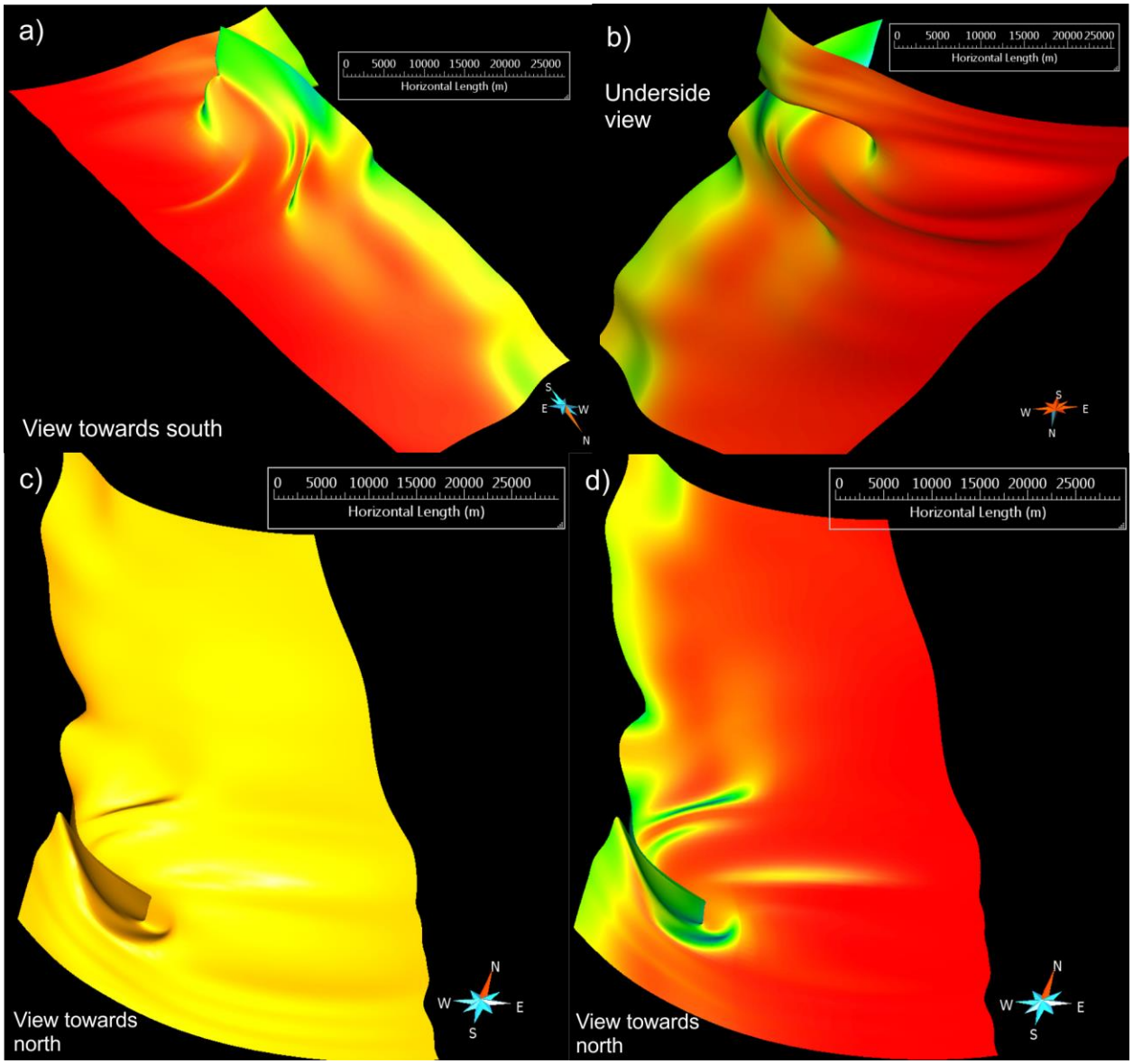

Figure 27. Example of creasing effects caused by modelling the Point Reef fault using SPARSE. Surface symbolized with first element of normal vector across fault to highlight changes in surface orientation.

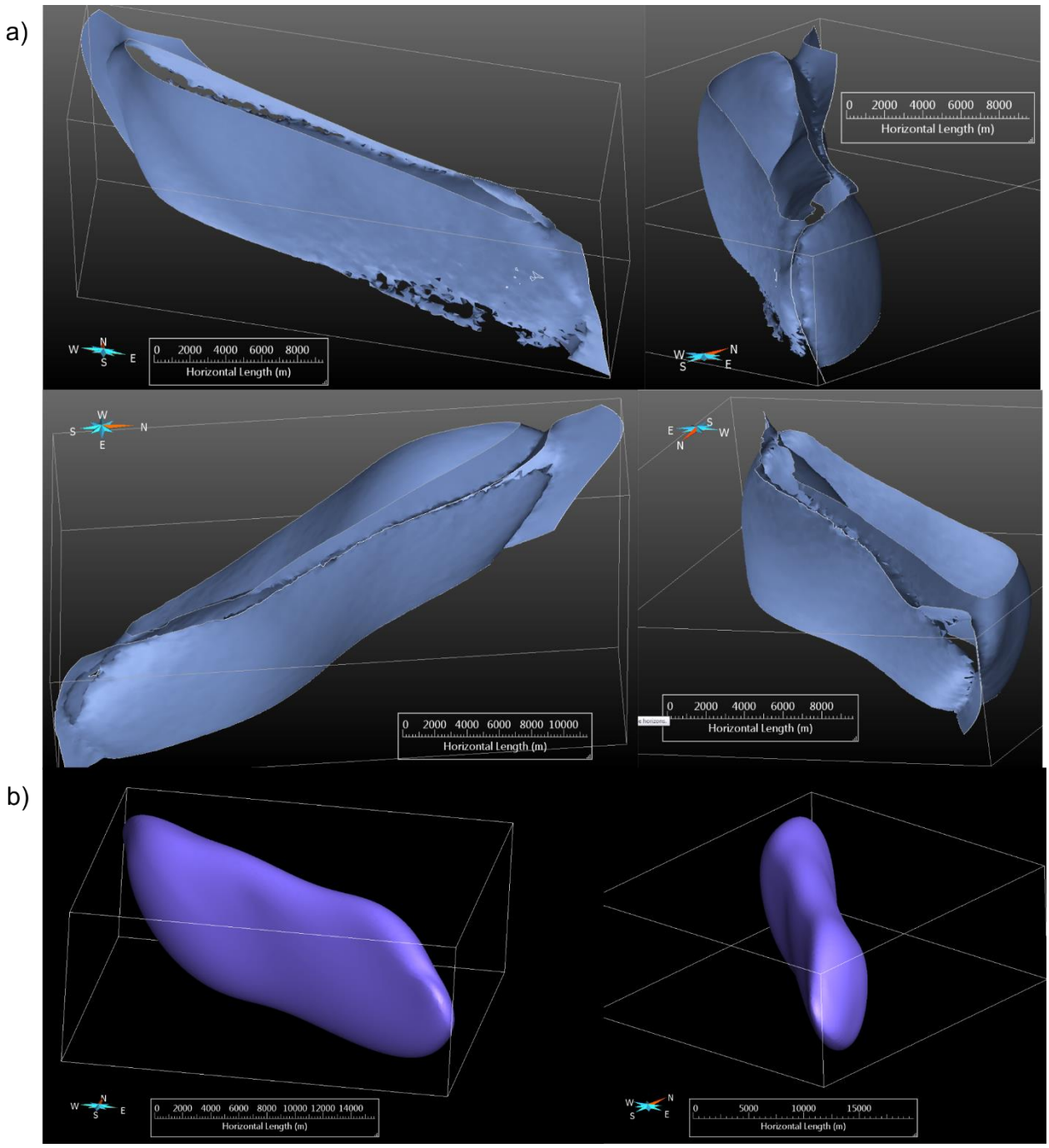

Figure 28. A) Example of failed modelling for sheath folding of the Boulder Antiform fault surface using SKUA. B) Example of Boulder Antiform created using SURFE implicit modelling.

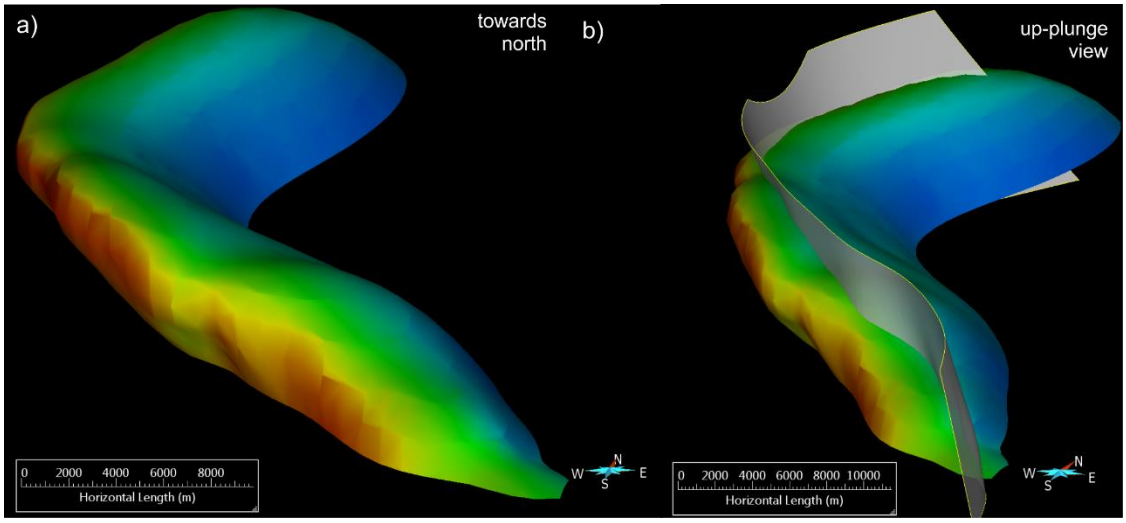

Figure 29. Example of correct geometry for overturned folds. SURFE modelled surface of the top of Cycle 1 sedimentary package in the Hellancourt Sub-Region. A) view towards the north, b) up-plunge view with modelled axial plane (white surface). Surface symbolized by first component of normal vector to highlight orientation of folded surface.

4.0.0 Discussion

Through creating a 3D model of the regional fault network in the northern Labrador Trough, including two sub-regions, new geologic insight was gained. The 2D geologic map pattern was updated, nappe culminations and specific 3D hinge trajectories were reinterpreted, updating the 3D fault-fault relationships (topology), and 3D fault geometries at depth were interpreted. During model development, several issues arose in applying currently available 3D modelling technology and methods to this type of data configuration. Namely, a sparsely sampled complex regional geologic setting. This discussion will focus on the geological insight that was gained and the modelling challenges encountered.

4.1.0 Geological insight

4.1.1 Regional model

The regional fault network model reflects the established map pattern and fault topology that Clark and Wares (2006) and MERN (*Système d'information géominière du Québec*, 2016) have proposed. In general, these two interpretations agree for regional faults; however, they show discrepancies along the western boundary, where foreland propagating faults translate relatively undeformed Kaniapiskau units westward. The Robelin, Garigue, and Forbes faults are interpreted as thrusts with listric geometry that developed during D_1. Both map patterns agree that the Garigue Fault truncates the Forbes Fault; however, Clark and Wares (2006) interprets the Robelin Fault truncating the Garigue Faults and the

Système d'information géominière du Québec (2016) interpreted these two faults to be subparallel. Additionally, the 3D topological relationships between these faults are not well defined. Based on trends in the aeromagnetic maps and spatial continuity of structural field observations, the Clark and Wares (2006) has been selected for modelling. Fault surface geometries were estimated using neighbouring S_0 and S_1 structural points, the magnetic signature on the first vertical derivative magnetic map, and Chattopadhyay et al. (2014)'s experiments. Chattopahyay et al. (2014) showed that foreland thrusts similar to those in the Labrador Trough do not develop near the orogenic front first; instead they develop distal to the orogenic front and progress away from the hinterland. For the northern Labrador Trough, this likely means that the Robelin Fault developed first, followed by the Garigue Fault and then by the Forbes Fault. This distinction is significant as topological relationships affect 3D fault geometry and fault surface relationships. They dictate how subsequent model components, such as horizons and intrusions, will interact. Currently, these fault topology relations are interpreted. Although difficult to observe, due to their scarcity and limited exposure, future work should seek to confirm these fault relationships. Future field campaigns should be guided by geophysical imagery, with targeted predictive field work to collect better fault-fault contact observations.

4.1.2 Hellancourt Sub-Region model

Fault geometry and topology is well established for the Hellancourt Sub-Region as it hosts most of the economically prospective areas in the northern Labrador Trough (Figure 5). It has benefited from several local scale studies and its tilted beds allowed stratigraphic thicknesses to be estimated. The agreement among researchers and the high resolution field data provided sufficient control to build a volumetric lithostratigraphic model. In general, the published interpretations agree and there were no conflicts in surface topology. Some generalizations in stratigraphy and local folding were required to create a sub-regional scale model; however the scale-relevant structures, such as the Hellancourt Syncline and Fauajs Antiform, were preserved.

4.1.3 Nappes Sub-Region model

Three separate interpretations have been published for the Nappes region and each was evaluated during model building. While constructing the fault network, several areas of interest emerged.

First is the Ujaralialuk Fault, a steep, late-stage, north-dipping, oblique-slip fault, with dextral motion, is proposed by this study. It is thought to juxtapose the higher metamorphic grade central nappes from the Highfall nappe. While not previously mapped by other researchers, the NW-SE fault

appears as an abrupt change in magnetic trend within the Central Nappes and Highfall nappe blocks. Placement of the fault is constrained by a linear trend on the aeromagnetic survey that appears to truncate the nappes bounding thrust faults. The 3D geometry of the fault is estimated from structural field measurements that lay on or adjacent to the lineament. Dips are extended to a depth of two kilometers where confidence in geometry decreases. Dip direction is interpreted based on the understanding that the fault developed in a collisional tectonic setting and that the older and higher grade central nappes block sits above the younger Highfall Antiform gneisses. The hypothesized fault likely developed during D_3 when significant dextral transpression affected the Archean gneiss cored nappes. The fault's oblique orientation to the orogenic front, as well as its undeformed geometry, indicate that it is the result of a late stage deformational event.

The second significant surface is an un-named thrust fault mapped by Moorhead and Hynes (1990). Moorhead and Hynes (1990) proposed an un-named refolded thrust fault that is embedded in the repeated stratigraphy of the Rachel-Laporte Supergroup at the nose of the Rénia Synform. This fault likely developed east-dipping listric geometry during early rifting, similar to those seen further west, and was refolded along with the thrust nappes (Moorhead and Hynes, 1990). This thesis proposes the name "Canoe Fault" for this T_1 thrust as its 3D geometry resembles a bent canoe (Figure 31).

Moorhead and Hynes (1990) also propose that the geometry at depth mirrors what is seen on the surface where it is folded around the Rénia Nappe 20 km below current topographic surface. While the geometry of the fault is reasonable and no alternative was presented, the depth extent is extreme (Figure 31A). The ~20 km depth is inconsistent with the amphibolite facies metamorphic grade of lithological units surrounding the fault and the fact that some early structures are still intact. If the fault truly represented a 20 km feature, the hanging wall would contain highly metamorphosed units, greater than amphibolite facies, as a result of several kilometers offset during compression. For this reason, the Canoe Fault was modelled shallower than suggested by Moorhead and Hynes (1990); its depth was constrained by earlier interpolations of the overlying Central Nappes and is ~10 km (Figure 31B). Additionally, fold interference is interpreted for the Canoe Fault and Central Nappes. The interference geometry is estimated using fold plunges reported by Moorhead (1989) and interpolations of structural data long the Central Nappes' thrust trace.

Using surfaces from a younger deformation event to inform later modelling is useful when no other constraint data exists. This is why the order in which surfaces are constructed in the workflow is significant and why late-stage, simple surfaces are constructed first and early-stage, complex surfaces

are modelled last. Without modelling the Central nappes first, the Canoe Fault's depth and geometry would not have been properly constrained.

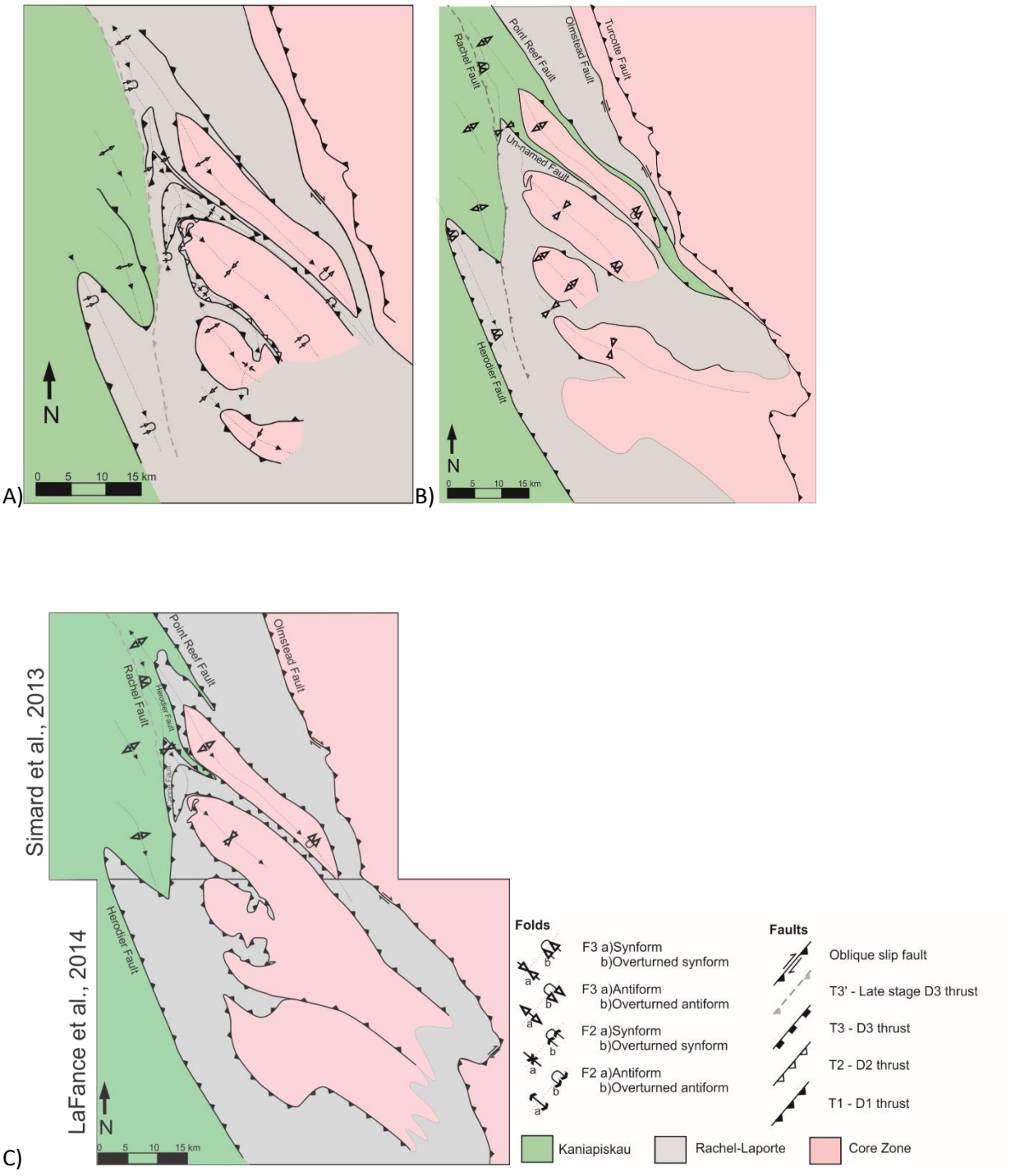

Figure 30. Generalized geological maps of the Nappes Sub-Region. Map pattern from A) Moorhead and Hynes (1990), B) Clark and Wares (2006) and C) Simard et al. (2013); and LaFrance et al., (2014).

A)

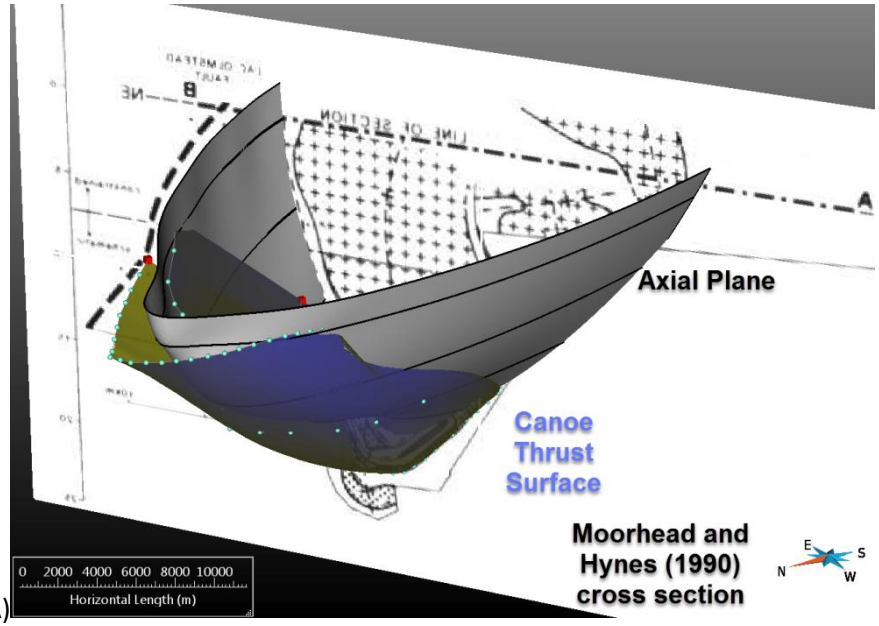

B)

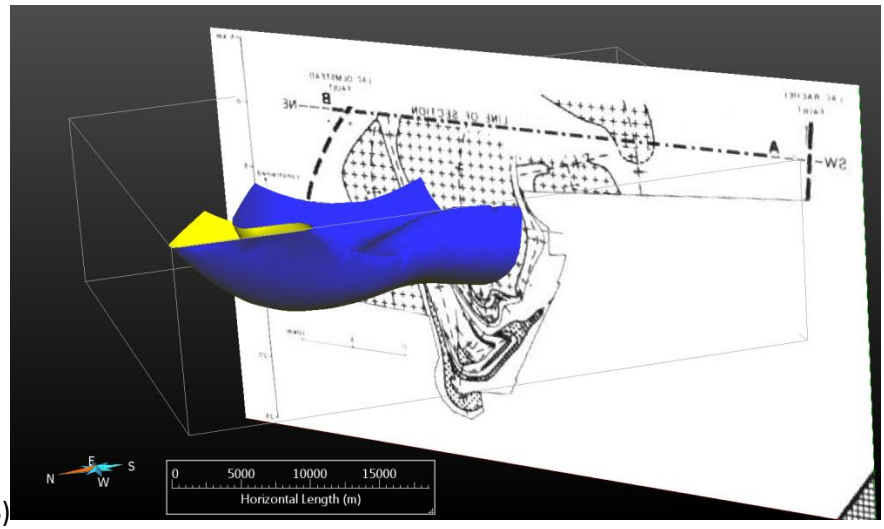

Figure 31. Example of 3D thrust fault surface representing the Canoe Fault. A) First iteration using depth from Moorhead and Hynes (1990) cross section with Sparse control nodes (green spheres and red cubes) and contoured axial planar surface (white surface with 500m contours). B) Second iteration of modelling the Canoe fault with adjusted depth constraints. Figure shows new surface in relation to Moorhead and Hynes (1990) cross section.

Among the various fault models, there is confusion about how the Hérodier Fault extends towards the north and if it joins up with the Point Reef Fault. Moorhead and Hynes (1990) have mapped the Hérodier Fault such that is truncated by the Rachel Fault. Later, Clark and Wares (2006) interpret the Hérodier Fault's northern extension to be an M-fold which is deformed around the central block of thrust nappes, eventually being truncated by the Olmstead Fault in the east. Simard et al. (2013) and

Lafrance et al. (2014) interpreted the Hérodier fault to be the southern extension of the Point Reef Fault, which deformed around the nappe structures.

The Clark and Wares (2006) interpretation also proposes that Kaniapiskau units surrounds the nappes, rather than Rachel-Laporte sediments. This is in conflict with the aeromagnetic map which shows a low and uniform package surrounding the nappes. In general, Kaniapiskau units show high variability in magnetic signatures and Rachel-Laporte units have a low and uniform aeromagnetic signature. Based on this observation, it is more likely that the nappes are hosted in the Rachel-Laporte Supergroup. Recent publications by Simard et al. (2013) and Lafrance et al. (2014) respect these magnetic susceptibility characteristics. Additionally, the Clark and Wares (2006) model tectonically isolates the Boulder nappe from the other nappe blocks by making the m-folded fault's northern limb pass between the Rénia Synform and Boulder Antiform. While patterns in the aeromagnetic maps display, structurally isolating the Boulder nappe from the other nappes seems unlikely. It and the other nappes are Archean gneiss-cored structures that show similar structural trends and aeromagnetic signatures (Figure F-1) (Clark and Wares, 2006).

Simard et al. (2013) and Lafrance et al. (2014) propose that the Hérodier is a continuation of the Point Reef Fault, which juxtaposes the Rachel-Laporte Supergroup to the Kaniapiskau Supergroup, acting as a major tectonic break. According to their interpretation, the fault surface is deformed around the nappes structures with three northward pointing fold closures. There does not appear to be any evidence to contradict this interpretation, it is topologically reasonable, and it agrees with the aeromagnetic map.

The Rachel Fault, formerly named the Lac Phillips thrust fault, is also a feature of interest. According to Moorhead and Hynes (1990), it is a NNW trending, east dipping, reverse fault that has thrust the Rachel-Laporte barckarc basin units on top of the Kaniapiskau's Hellancourt basalts. While it is likely a major break, the clockwise displacement pattern of magnetic anomalies on the aeromagnetic map indicates that there was some element of dextral motion as well. In agreement with the aeromagnetic map, Goulet (1986) interprets the fault as oblique-slip with significant right lateral movement on the order of 10 to 15 km and 7.5 to 10 km vertically. The Rachel Fault is also observed to deflect F3 axial traces in the footwall, which indicates that the fault was active after D_3 (Moorhead, 1989). The timing of formation, however, is poorly constrained. The Rachel Fault's subparallel orientation to T_1 thrusts in the west may suggest that the fault has experienced a complex and prolonged displacement history. Further field work along the Rachel Fault would provide better

constraint on displacement magnitude and timing as well as provide new insight into the tectonic history of the northern Labrador Trough.

In general, all three published models agree for the northern geometry of the fault; however, Simard et al. (2013) and Lafrance et al. (2014) have mapped the Rachel being truncated by the Point Reef/Hérodier fault in the south. Field relationships and observations reported by Moorhead (1989) as well as the north-south lineament on the aeromagnetic map make this interpretation unlikely; therefore, this current study used the Moorhead and Hynes (1990)'s interpretation for the Rachel fault.

After reviewing published fault networks, a hybrid fault scheme is proposed, which integrates the most geologically reasonable elements from each model, is proposed (Figure 22). The Hérodier Fault is interpreted as a southward continuation of the Point Reef Fault which has been deformed with and around the nappes; however, a high strain corridor must be present between the Boulder Antiform and the Rénia Synform to account for the stretched appearance between nappes in aeromagnetic map. A steeply dipping shear zone between the two nappes is suggested to account for the juxtaposition of the central nappes block and the Highfall nappe. Similarly, another shear zone is proposed north of the Boulder Antiform which has sheared the south trending closure to the Hérodier-Point Reef Fault as well as Rachel-Laporte sediments. Future field work along these features may better constrain timing of displacement and refine the current tectonic model.

To construct a 3D model of the nappes with sparse data and few published cross sections, it was useful to compare local geology to other areas with similar geologic settings. When building the Nappes and Regional models, several nappes systems were studied for comparison. A good comparative for developing the Nappe model and one used to inform the 3D interpretation are the Helvetic nappes (von Tscharner et al., 2016). The Helvetic nappes appear to be the most similar to the northern Labrador Trough based on geologic history, field observations and map patterns.

4.2.0 Modelling challenges and benefits

The issues related to current 3D modelling practices and tools have been presented in the Results sections of this thesis. This section provides discourse related to these results and groups them according to topic into data related, software related, geological interpretations related, and other.

4.2.1 Data

While constructing a fault network model in the northern Labrador Trough, several data-related issues arose beginning with data integration from numerous sources and ending with data selection.

Data acquired from compilation of regionally extensive crustal studies often are of poor quality due to the individualistic, uncoordinated and/or multi-agency approach through several survey cycles. These data are typically of heterogeneous distribution with classification incompatibilities, and may have been poorly archived. These all conspire to inhibit the 3D modelling exercise. One of the largest issues related to conducting any research at the regional scale is constructing a useful database and deriving meaning from the data. After decades of outcrop to provincial scale studies, the geoscientific community has accumulated an immense amount of data published in journal articles, maps, and cross sections regarding the Labrador Trough. Only recently has MERN begun to compile the various publications into a provincial-scale data repository. Integrating and harmonizing the various datasets in this way is a time-consuming task which may be alleviated with the use of standardized field gathering nomenclature and observation coding.

Once data has been compiled, issues arise when applying localized and clustered data points to a regional feature. At the moment, there are ways to up-scale clustered data using quantitative methods (Carmichael and Ailleres, 2016); however, local anisotropy, such as local variability in fold orientation, may mute regionally significant trends. It is, therefore, often necessary to supervise input selection methods by weighting regionally significant data or selecting only those points that the geoscientist interprets as "regionally representative" (Kaufmann and Martin, 2009). When working with complex geology, it is difficult to determine how closely to respect local anisotropy when up-scaling data. Perhaps an automated, knowledge-led method which selects structural points, based on their similarity in strike to selected surface traces as well as eigen analysis could resolve this issue.

4.2.2 Software

During modelling, it was discovered that there are limitations in the software when applied to tight folds, sheath folds, and overturned fold limbs. 3D modelling software platforms, such as GOCAD and SKUA, were developed to assist with hydrocarbon exploration. The modelling algorithms in these platforms assume lower metamorphic grade, simpler basin structures with less deformation history. Importantly, data input into these environments is dense, often continuous geophysical data from bore hole electric logs which are tied to 3D seismic surveys. Lithofacies and discontinuity geometries can be either auto-picked with trained software or interpreted by experts using a standardized workflow. The same software and modelling techniques are now being applied to regions with more complex geological settings from ancient orogenic belts that have undergone several stages of deformation and host variably complex structures (Caumon et al., 2009; de Kemp, 2015; Schetselaar et al., 2013).

Unfortunately, these regions do not have 3D seismic survey data and deep bore holes to facilitate modelling. In addition, a consistent stratigraphy with critical stratigraphic marker information is often not well established in these regions, making volumetric block modelling difficult. SURFE and Mira Geoscience's Mining Suite, which is the plug-in that contains SPARSE, have improved upon the traditional hydrocarbon exploration software by supporting more mineral exploration functionality for data handling, user interpretation and control of more complex 3D surface construction. These developments are welcome; however, they are still just adaptations built on top of a traditional hydrocarbon exploration and reservoir characterization workflow. Despite these improvements, each modelling algorithm has challenges which must be addressed to make 3D models accurately represent complex geological settings. (Software issues and concerns are summarized in Appendix I)

4.2.3 Geological Interpretations

When developing models in sparse data environments, a geoscientist is confronted with the issue of determining how geological features behave at depth. Traditionally, 3D models are constrained at depth with drill core markers and geophysical data; however, regional scale modelling is limited by sparse 3D data constraints. In such cases, a geoscientist uses software tools to interpret and extend geological features.

Geoscientist have used block diagrams and cross sections which integrate and visualize data collected in the field with interpretations (Fossen, 2016; Passchier et al., 2011; Rowland et al., 2007; Twiss and Moores, 2007) Cross sections are a standard practise for such integration, but they are time consuming to create and difficult to update when new information or insight becomes available. Several preliminary cross sections were constructed for the northern Labrador Trough using SURFE scalar field and SFI plunge vectors to constrain surface dips; however, they did not provide sufficient control to constrain model development and were, therefore, not completed across the study area. To be truly useful, dozens of cross sections at various scales and orientations would have been required. Despite this, cross sections are useful and development of a better section generating tool is warranted. Some such tools have been developed by Geosoft and Mira Geoscience; however, some refinement is still needed. Using cross sections, interpretations are validated using balancing techniques, 3D model constraints are better represented, and geology can be conceptualized before investing significant time into modelling. 2D investigations alone may not readily resolve topology or geometries adequately; however, 3D modelling brings data-model conflicts and geometrical impossibilities to the forefront,

helping to improve concept models. The exercise of 3D modelling is often valuable, just to help achieve more geologically “reasonable” solutions.

Additionally, the non-unique nature of geological interpretation presents an issue for 3D modelling as the third dimension allows for a higher degree of freedom and more solutions to fit data. With many possible solutions, a tool which generates several models, using the same constraints, would be valuable. It would allow for more geological insight to be gained and provide higher confidence in model results when model features are consistently predicted. Currently, the modelling workflow is arduous and requires a large investment of time to construct just one model solution. However, there is value in working closely with data and modelling “the manual way”. While working closely with data to construct a model, a geoscientist is able to investigate data trends and develop new theories regarding the geology.

4.2.4 Other issues

Intrusive bodies such as the Montagnais sills, which could represent a significant (~30 %) by volume of the study space, were not included in the modelling effort. As is commonly the case with other intrusive bodies in metamorphic terrains, these features can have irregular and complex shapes, deformed and cross cutting contacts with country rocks. Generally, they have more complex topology with various pulses of injections that can produce a wide range of overprinting patterns. These characteristics make regional intrusive bodies difficult to deal with in existing 3D modelling environments. While smooth and more homogenous bodies sampled with enough data could technically be modelled by SURFE, SPARSE, and SKUA, it is not usually the case to be able to constrain these features well in this type of terrain. 3D modelling of the more complex intrusive geologic features remains a significant challenge, similar to salt body modelling in the hydrocarbon domain, and should be addresses in future 3D modelling workflow developemnts.

Uncertainty modelling, which is an area of active research in 3D modelling, is much needed for exploration studies as it quantifies the likelihood of a target or geologic feature actually being where the model indicates (Bond et al., 2007; Lindsay et al., 2016, 2012; van der Meijde et al., 2015; Wellmann et al., 2010; Wellmann and Regenauer-Lieb, 2012). At the moment, uncertainty modelling is not part of the standard workflow for 3D regional modelling. Diverse data and the various ways it is integrated into the model conspire to impede geoscientists from assigning confidence measures on data. In addition each estimation step has uncertainty factors embedded in the methods and algorithms used but is rarely captured for modelling uncertainty (Lindsay et al., 2013, 2012; van der Meijde et al., 2015; Wellmann et

al., 2010). Also, with only a single model, as is the case herein, it is difficult to evaluate uncertainty. Using fitting factors and slack measures, SURFE and SPARSE are the only methods in the workflow that have some capability to influence the local uncertainty but these metrics are not actually stored in the output properties of the model. In the future, allowing the geoscientist to attribute uncertainty on the data and assess uncertainty directly in the workflow, as well as making more than one model, would improve our ability to assess and compare models. Work is currently underway to explore new methods of estimating uncertainty (Lindsay et al., 2012; Wellmann et al., 2010); however they are still in development.

6.0.0 Conclusions

3D modelling is a standard practise in hydrocarbon exploration and reservoir characterization (ie. Petrel, SKUA, EarthVision, 3D Move). These tools are now being adapted to mineral exploration (ie. GOCAD/SKUA Mining Utilities SPARSE, SURFE, Geomodeller, Leapfrog, Micromine, Vulcan, Gemcom) at mine to camp scales. As the techniques and software used in these settings are applied to larger and more complex geological environments, a customized and standard regional scale workflow is required that is unique to this domain. Through creating a 3D model of the northern Labrador Trough, some elements of the current workflow have been tested and geological insight has been gained.

Several fault topologies and geometries were tested throughout the workflow, resulting in the creation of a hybrid 3D fault network model of the northern Labrador Trough. The model incorporates the most geologically and geometrically reasonable elements of the proposed map patterns from Moorhead and Hynes (1990), Clark and Wares (2006), Simard et al. (2013), Lafrance et al. (2014) and the SIGEOM database (*Système d'information géominière du Québec*, 2016). Through visual interpretation of point structural data sets represented as 3D glyphs, and with 3D form lines some of the 2D map patterns could be adjusted as well as the 3D axis of basement-cover culminations and other regional fold hinges. A volumetric 3D model of the Hellancourt Sub-Region was created using a generalized stratigraphic column as well as a fault network model in the Nappes Sub-Region. Additionally, the lac Ujaralialuk Fault and two shear zones were proposed based on trends in the aeromagnetic map and 3D model testing. All three models generally agree with the established tectonic history from Clark and Wares (2006) and are consistent with fold and thrust belt geometry. Some minor exceptions were found while examining published map pattern and extending surfaces into the third dimension. These results provide insight for future mineral exploration in the area and tectonic reconstructions of the northern

Labrador Trough; however, further insight may be gained when stratigraphic correlations and thickness estimates are released for the Kaniapiskau and Rachel-Laporte Supergroups. Additionally, further structural observations, such as foliations, bedding, and lineations, around the eastern nappes structures would provide better control on faults in the eastern model area.

Despite on-going developments of 3D modelling technology and lack of a standard workflow unique to the complex regional domain, there are many benefits to using the existing methods presented in this thesis. Firstly, many elements of the workflow confront geologists with discrepancies in tectonic histories, understanding of structures, and topology. Secondly, 3D regional models are excellent communication tools to represent complex geology to lay-persons. They also provide opportunities to create a geospatial repository of observations and interpretation where data can be quality checked and investigated. Conceptualization and model building also reveals hidden, non-obvious topologies which would otherwise go unnoticed in 2D investigations. Finally, the 3D regional model provides a geometrical framework for other integrated studies such as geophysical inversions, exploration and resource assessment.

Despite the clear benefits to creating and using 3D regional geological models, there are several areas where further research and development is needed. First, improved tools or workflows that capture, record, organize, and store both 2D and 3D objects is required to keep track of model elements. These new practices also need to incorporate geological knowledge related to these objects and tectonic histories as well as comments on geologic reasonableness of individual modelling results. Additionally, it should be able to convert and project objects between 2D and 3D reference frames. Second, the workflow suffers from the subjective nature of geological interpretation. In the future, more rigorous, data-driven, repeatable, and quantitative approaches should be taken wherever possible; however, improvement in this area is limited by sparse 3D data that plagues regional studies. Third, the time-consuming nature of 3D modelling prevents the development and testing of multiple geological models. Improving modelling efficiency and developing simulation-type methods of modelling will hopefully allow for the creation and comparison of multiple model solutions.

References

Avramtchev, S.L., 1985. Carte géologique de Québec .

Barrett, T.J., Wares, R.P., Fox, J.S., 1988. Two-stage hydrothermal formation of a lower Proterozoic sediment-hosted massive sulphide Deposit, Northern Labrador Trough, Quebec. Can. Mineral. 26, 871–888.

Beatson, R., Cherrie, J., McLennan, T., Mitchell, T., Carr, J., Fright, W., McCallum, B., 2004. Surface reconstruction via smoothest restricted range approximation. Geom. Des. Comput. 44–52.

Bond, C.E., Gibbs, A.D., Shipton, Z.K., Jones, S., 2007. What do you think this is? "Conceptual uncertainty" In geoscience interpretation. GSA Today 17, 4–10. doi:10.1130/GSAT01711A.1

Bond, C.E., Lunn, R.J., Shipton, Z.K., Lunn, A.D., 2012. What makes an expert effective at interpreting seismic images? Geology 40, 75–78. doi:10.1130/G32375.1

Boone, E., 1987. Petrology and tectonic implication of the Hellancourt Volcanics, nothern Labrador Trough, Quebec. McGill University.

Boone, E., Hynes, A., 1990. A Structural Cross-section of the Northern Labrador Trough, New Quebec, in: Lewry, J.F., Stauffer, M.R. (Eds.), The Early Proterozoic Trans-Hudson Orogen of North America - Special Paper 37. Geological Association of Canada, pp. 387–396.

Brodaric, B., Gahegan, M., Harrap, R., 2004. The art and science of mapping: Computing geological categories from field data. Comput. Geosci. 30, 719–740. doi:10.1016/j.cageo.2004.05.001

Burns, K.L., 1975. Analysis of geological events. J. Int. Assoc. Math. Geol. 7, 295–321. doi:10.1007/BF02081703

Carmichael, T., Ailleres, L., 2016. Method and analysis for the upscaling of structural data. J. Struct. Geol. 83, 121–133. doi:10.1016/j.jsg.2015.09.002

Carr, J.C., Beatson, R.K., Cherrie, J.B., Mitchell, T.J., Fright, W.R., McCallum, B.C., B.C., Evans, T.R., 2001. Reconstruction and representation of 3D objects with radial basis functions, in: SIGGRAPH '01 Proceedings of the 28th Annual Conference on Computer Graphics and Interactive Techniques. Association for Computing Machinery, Los Angeles, pp. 67–76. doi:10.1145/383259.383266

Caumon, G., Collon-Drouaillet, P., Le Carlier der Veslud, C., Viseur, S., Sausse, J., 2009. Surface-Based 3D Modeling of Geological Structures. Math. Geosci. 41, 927–945. doi:10.1007/s11004-009-9244-2

Caumon, G., Gray, G., Antoine, C., Titeux, M., 2013. Three -Dimensional Implicit Stratigraphic Model Building from Remote Sensing Data on Tetrahedral Meshes : Theory and Application to a Regional Model of La Popa. IEEE Trans. Geosci. Remote Sens. 51, 1613–1621. doi:10.1109/TGRS.2012.2207727

Chandler, F.W., 1980. Proterozoic redbed sequences of Canada, Canadian Geological Survey Bulletin. Geological Survey of Canada. doi:10.4095/106239

Chattopadhyay, A., Jain, M., Bhattacharjee, D., 2014. Three-dimensional geometry of thrust surfaces and the origin of sinuous thrust traces in orogenic belts: Insights from scaled sandboxexperiments. J. Struct. Geol. 69, 122–137. doi:10.1016/j.jsg.2014.09.020

Chauvel, J., Dimroth, E., 1974. Facies types and depositional environment of the Sokoman Iron Formation, central Labrador Trough, Quebec, Canada. J. Sediment. Res. 44, 299–327. doi:10.1306/74D72A1D-2B21-11D7-8648000102C1865D

Clark, T., 1988. Stratigraphie, pétrographie et pétrochilllie de la forlllation de fer de Baby dans la région du lac Hérodier (Fosse du Labrador). Gouvernement du Québec.

Clark, T., 1978. Région du lac Hérodier, Nouveau-Québec. Ministére de l'Énergie et des Ressources, Québec.

Clark, T., Wares, R., 2006. Lithotectonic and Metallogenic Synthesis of the New Quebec Orogen (Labrador Trough). Ministére de l'Énergie et des Resources.

Clowes, R., Cook, F., Hajnal, Z., Hall, J., Lewry, J., Lucas, S., Wardle, R., 1999. Canada' s LITHOPROBE Project (Collaborative , multidisciplinary geoscience research leads to new understanding of continental evolution). Episodes 22, 3–20.

Conliffe, J., Wilton, D.H.C., Blamey, N.J.F., Archibald, S.M., 2013. Paleoproterozoic Mississippi Valley Type Pb-Zn mineralization in the Ramah Group, Northern Labrador: Stable isotope, fluid inclusion and quantitative fluid inclusion gas analyses. Chem. Geol. 362, 211–223. doi:10.1016/j.chemgeo.2013.08.032

Corrigan, D., 2016. Extrusion of a ribbon continent in a collisional orogen: example from the southeastern Churchill Province in Quebec and Labrador, in: Geological Association of Canada – Mineral Association of Canada Generally Assembly. Whitehorse, NT.

Corrigan, D., Brouillette, P., Morin, A., Can Rooyen, D., Wodicka, N., Houlé, M.G., Douma, S.L., Robillard, K., 2015. Report of activities for the Core Zone and bounding orogens: Tectonic framework and mineral potential. Geological Survey of Canada, Ottawa, Ontario, Canada. doi:10.4095/296141

Corriveau, L., Nadeau, O., Montreuil, J., Desrochers, J., 2014. Report of activities for the Core Zone : Strategic geomapping and geoscience to assess the mineral potential of the Labrador Trough for multiple metals IOCG and affiliated deposits. Ottawa, Ontario, Canada. doi:10.4095/295529

D'Amours, I., Intissar, R., 2013. Leve magnetique et spectrométrique aeroporte dans le secteur du Lac Romanet, Province de Churchill DP 2013-02.

D'Amours, I., Intissar, R., 2012a. Leve magnetique et spectrométrique aeroporte de la Riviere Koksoak, Province de Churchill DP 2011-07. Ministère de l'Energie et des Ressources Naturelles du Québec.

D'Amours, I., Intissar, R., 2012b. Leve magnetique et spectrométrique aeroporte dans le secteur du Lac Lemoyne, Province de Churchill DP 2011-06. Ministère de l'Energie et des Ressources Naturelles du Québec.

Dag, A., Ozdemir, A.C., 2013. A Comparative Study for 3D Surface Modeling of Coal Deposit by Spatial Interpolation Approaches. Resour. Geol. 63, 394–403. doi:10.1111/rge.12018

de Kemp, E.A., 2015. Achieving Geologically Reasonable 3D Models, in: Saying Goodbye to a 2D Earth International Confrence on 3D Geological Modelling. Margaret River, Western Australia, pp. 14–17.

de Kemp, E.A., 2000. 3-D visualization of structural field data: examples from the Archean Caopatina

Formation, Abitibi greenstone belt, Québec, Canada. Comput. Geosci. 26, 509–530. doi:10.1016/S0098-3004(99)00142-9

de Kemp, E.A., Schetselaar, E.M., Hillier, M.J., Lydon, J.W., Ransom, P.W., 2016. Assessing the workflow for regional-scale 3D geologic modeling : An example from the Sullivan time horizon , Purcell Anticlinorium East Kootenay region , southeastern Britis. Interpretation 4, SM33-SM50. doi:10.1190/INT-2015-0191.1

de Kemp, E.A., Sprague, K.B., 2003. Interpretive tools for 3-D structural geological modeling part I: Bezier-based curves, ribbons and grip frames. Geoinformatica 7, 55–71. doi:10.1023/A:1022822227691

de Kemp, E.A., Sprague, K.B., 2001. New interpretive tools for three-dimensional structural geological modelling : Bézier-based curves, ribbons, and skeletons. Curr. Res. 24. doi:10.4095/212176

de Römer, H.S., 1956. The Geology of the Eastern Border of the “Labrador Trough”, East of Thevenet Lake, New Quebec. McGill University.

Dimroth, E., 1981. Chapter 13 Labrador Geosyncline: Type Example of early Proterozoic Cratonic Reactivation. Dev. Precambrian Geol. 4, 331–352. doi:10.1016/S0166-2635(08)70018-5

Dimroth, E., 1970. Evolution of the Labrador geosyncline. Geol. Soc. Am. Bull. 81, 2717–2741. doi:10.1130/0016-7606(1970)81[2717:EOTLG]2.0.CO

Dimroth, E., Chauvel, J., 1973. Petrography of the Sokoman Iron Formation in Part of the Central Labrador Trough, Quebec, Canada. Geol. Soc. Am. Bull. 84, 111–134.

Dion, D.J., Legebvre, D.L., 1998. Donnees numeriques (profils) des leves geophysiques aeroportes du Quebec SSNRC 23J, 23O.

Dugas, J., 1970. Metallic mineralization in part of the Labrador Trough, in: Special Paper 5. Mineral Deposits Services, Quebec, p. 23.

Fahrig, W., 1965. Lac Herodier, Quebec, Map 1146A. Ottawa, Ontario, Canada. doi:10.4095/107520

Feng, L., Bartholomew, M.J., Choi, E., 2015. Spatial arrangement of decollements as a control on the development of thrust faults. J. Struct. Geol. 75, 49–59. doi:10.1016/j.jsg.2015.03.002

Findlay, J., 1996. Petrology, geochemistry and evolution of the Labrador Trough Basaltic Suite, Labrador and New Quebec. University of Ottawa (Canada).

Fossen, H., 2016. Structural geology, 2 nd. ed. Cambridge University Press, Leiden.

Goulet, N., 1987. Étude tectonique de la partie nord de la fosse du Labrador Rapport intérimaire, Série des manuscrits bruts. Québec City, Québec, Canada.

Goulet, N., 1986. Étude tectonique et stratigraphique de la partie nord de la Fosse du Labrador: région de la baie aux Feuilles et du lae Bérard. Ministère de l’Énergie et des Ressources, Québec, Québec City, Québec, Canada.

Goutier, J., Wares, R., 1991. Géologie du secteur de l’indice aurifère Dessureault, Fosse du Labrador - MB 91-10. Québec City, Québec, Canada.

Gross, G.A., 1972. Primary features in cherty iron-formations. Sediment. Geol. 7, 241–261. doi:10.1016/0037-0738(72)90024-3

Hall, J., Louden, K.E., Funck, T., Deemer, S., 2002. Geophysical characteristics of the continental crust along the Lithoprobe Eastern Canadian Shield On-shore Off-shore Transect (ECSOOT): a review. Can. J. Earth Sci. 39, 569–587. doi:10.1139/e02-005

Hammouche, H., Legouix, C., Goutier, J., Dion, C., 2012. Géologie de la région du lac Zeni.

Hillier, M.J., de Kemp, E.A., Schetselaar, E.M., 2015. Implicit 3D modelling of geological surfaces with the generalized radial basis functions (GRBF) algorithm, in: Paradis, S. (Ed.), Targeted Geoscience Initiative 4: Sediment-Hosted Zn-Pb Deposits: Processes and Implications for Exploration. Geological Survey of Canada, Ottawa, Canada, pp. 253–266. doi:10.4095/296328

Hillier, M.J., de Kemp, E.A., Schetselaar, E.M., 2013. 3D form line construction by structural fi eld interpolation (SFI) of geologic strike and dip observations. J. Struct. Geol. 51, 167–179. doi:10.1016/j.jsg.2013.01.012

Hillier, M.J., Schetselaar, E.M., de Kemp, E.A., Perron, G., 2014. Three dimensional modelling of geological surfaces using generalized interpolation with radial basis functions. Math. Geol. 46, 931–953.

Hoffman, P.F., 1990. Dynamics of the tectonic assembly of Northeast Laurentia in geon 18 (1.9-1.8 Ga). Geosci. Canada 17, 222–226.

Hoffman, P.F., 1988. United Plates of America, the birth of a craton: Early Proterozoic assembly and growth of Laurentia. Annu. Rev. Earth Planet. Sci. 16, 543–603.

Houlé, M.G., Bédard, M.-P., McNicoll, V.J., Corrigan, D., Huot, F., 2016. Report of activities for the Core Zone: investigations of the mafic and ultramafic intrusive rocks of the Montagnais Sills, northern Labrador Trough, Nunavik, Quebec. Ottawa, Ontario, Canada. doi:10.4095/297548

Hynes, A., 1978. Early recumbent folds in the northeastern part of the northern Labrador Trough. Can. J. Earth Sci. 15, 245–252.

James, D.T., Dunning, G.R., 2000. U–Pb geochronological constraints for Paleoproterozoic evolution of the Core Zone, southeastern Churchill Province, northeastern Laurentia. Precambrian Res. 103, 31–54. doi:10.1016/S0301-9268(00)00074-7

Kaufmann, O., Martin, T., 2009. 3D geological modelling from boreholes, cross-sections and geological maps, application over former natural gas storages in coal mines. Comput. Geosci. 35, 70–82. doi:10.1016/S0098-3004(08)00227-6

Koivisto, E., Malehmir, A., Hellqvist, N., Voipio, T., Wijns, C., 2015. Building a 3D model of lithological contacts and near-mine structures in the Kevitsa mining and exploration site, Northern Finland: Constraints from 2D and 3D reflection seismic data. Geophys. Prospect. 63, 754–773. doi:10.1111/1365-2478.12252

Lafrance, I., Bandyayera, D., Simard, M., 2012. Geologie - Ile Koksoak. System d'information geominiere du Quebec, Québec City, Québec, Canada.

Lafrance, I., Simard, M., Bandyayera, D., 2014. Géologie de la région du lac Saffray (SNRC 24G, 24F), RG; 2014-02. Géologie Québec, Ressources naturelles Québec, Québec City, Québec, Canada.

Laurent, G., Caumon, G., Jessell, M., 2015. Interactive editing of 3D geological structures and tectonic history sketching via a rigid element method. Comput. Geosci. 74, 71–86. doi:10.1016/j.cageo.2014.10.011

Lindsay, M., Aitken, A., Ford, A., Dentith, M., Hollis, J., Tyler, I., 2016. Reducing subjectivity in multi-commodity mineral prospectivity analyses: Modelling the west Kimberley, Australia. Ore Geol. Rev. 76, 395–413. doi:10.1016/j.oregeorev.2015.03.022

Lindsay, M.D., Aillères, L., Jessell, M.W., Kemp, E.A. De, Betts, P.G., 2012. Locating and quantifying geological uncertainty in three-dimensional models : Analysis of the Gippsland Basin , southeastern Australia. Tectonophysics 456–547, 10–27. doi:10.1016/j.tecto.2012.04.007

Lindsay, M.D., Jessell, M.W., Ailleres, L., Perrouty, S., de Kemp, E., Betts, P.G., 2013. Geodiversity: Exploration of 3D geological model space. Tectonophysics 594, 27–37. doi:10.1016/j.tecto.2013.03.013

Lorensen, W.E., Cline, H.E., 1987. Marching Cubes: A High Resolution 3D Surface Construction Algorithm, in: SIGGRAPH '87 Proceedings of the 14th Annual Conference on Computer Graphics and Interactive Techniques. Association for Computing Machinery, pp. 145–152. doi:10.1145/37401.37422

Machado, N., Clark, T., David, J., Goulet, N., 1997. UPb ages for magmatism and deformation in the New Quebec Orogen. Can. J. Earth Sci. 34, 716–723. doi:10.1139/e17-058

Mallet, J.-L., 2002. Geomodeling. Oxford University Press, New York.

Maxelon, M., Renard, P., Courrioux, G., Brandli, M., Mancktelow, N., 2009. A workflow to facilitate three-dimensional geometrical modelling of complex poly-deformed geological units. Comput. Geosci. 35, 644–658. doi:10.1016/j.cageo.2008.06.005

Montsion, R., de Kemp, E.A., Lydon, J.W., Ransom, P.W., Joseph, J., 2015. 3D Stratigraphic , Structural and Metal Zonation Modelling of the Sullivan Mine , Kimberley , B, in: Paradis, S. (Ed.), Targeted Geoscience Initiative 4: Sediment-Hosted Zn-Pb Deposits: Processes and Implications for Exploration Open File 7838. Geological Association of Canada, Ottawa, ON, pp. 236–252. doi:10.4095/296328

Moorhead, J., 1989. Stratigraphy, Structure and Metamorphism of the Renia Basement Gneiss and the Adjacent Cover Succession in the Western hinterland Zone of the Northern Labrador Trough, West of Kuujjuaq, Northern Quebec. McGill University.

Moorhead, J., Hynes, A., 1990. Nappes in the internal zone of the northern Labrador Trough. Geosci. Canada 17, 241–244.

Neal, H.E., 2000. Iron deposits of the Labrador Trough. Explor. Min. Geol. 9, 113–121. doi:10.2113/0090113

Passchier, C., Trouw, R., Coelho, S., de Kemp, E., Schmitt, R., 2011. Key-ring structure gradients and sheath folds in the Goantagab Domain of NW Namibia. J. Struct. Geol. 33, 280–291.

doi:10.1016/j.jsg.2010.12.005

Perreault, S., Hynes, A., 1990. Tectonic evolution of the Kuujjuaq Terrane, New Quebec Orogen. Geosci. Canada 17, 238–240.

Philippon, M., Le Carlier de Veslud, C., Gueydan, F., Brun, J.-P., Caumon, G., 2015. 3D geometrical modelling of post-foliation deformations in metamorphic terrains (Syros, Cyclades, Greece). J. Struct. Geol. 78, 134–148. doi:10.1016/j.jsg.2015.07.002

Poblet, J., Lisle, R.J., 2011. Kinematic evolution and structural styles of fold-and-thrust belts Kinematic evolution and structural styles of fold-and-thrust belts. Geol. Soc. London, Spec. Publ. 349, 1–24. doi:10.1144/SP349.1

Poirier, G.G., 1989. Structure and metamorphism of the eastern boundary of the Labrador Trough near Kuujjuaq, Quebec and its tectonic implications. Dep. Geol. Sci. McGill University.

Poirier, G.G., Perreault, S., Hynes, A., 1990. Nature of the eastern boundary of the Labrador Trough near Kuujjuaq, Quebec, in: Lewry, J.F., Stauffer, M.R. (Eds.), The Early Proterozoic Trans-Hudson Orogen of North America. Geological Association of Canada, pp. 387–412.

Putz, M., Stüwe, K., Jessell, M., Calcagno, P., 2006. Three-dimensional model and late stage warping of the Plattengneis Shear Zone in the Eastern Alps. Tectonophysics 412, 87–103. doi:10.1016/j.tecto.2005.10.003

Rohon, M.L., Vialette, Y., Clark, T., Roger, G., Ohnenstetter, D., Vidal, P., 1993. Aphebian mafic-ultramafic magmatism in the Labrador Trough (New Quebec). Can. J. Earth Sci. 30, 1582–1593. doi:10.1139/e93-136

Rowland, S.M., Duebendorfer, E.M., Schiefelbein, I.M., 2007. Structural analysis and synthesis a laboratory course in structural geology, 3rd ed, Structural analysis & synthesis. Blackwell Publishing, Malden, MA.

Sanborn-Barrie, M., 2016. Refining lithological and structural understanding of the southern Core Zone, northern Quebec and Labrador in support of mineral resource assessment, Geological Survey of Canada Open File Report. Geological Survey of Canada, Ottawa, Ontario, Canada. doi:10.4095/297560

Schetselaar, E.M., 2013. Mapping the 3D lithofacies architecture of a VMS ore system on a curvilinear-faulted grid: A case study from the Flin Flon mining camp, Canada. Ore Geol. Rev. 53, 261–275. doi:10.1016/j.oregeorev.2013.01.012

Schetselaar, E.M., de Kemp, E.A., Hillier, M.J., Perron, G., 2013. 3D modelling for mineral exploration: confronting the challenges of hard rock settings by optimal extraction and use of geological constraints., in: 12th SGA Biennial Meeting. Uppsala, Sweden, pp. 46–49.

Simard, M., Lafrance, I., Hammouche, H., 2013. Géologie de la région de Kuujjuaq et de la baie d'Ungava (SRNC 24J, 24K) RG 2013-04. Ministère de l'Energie et des Ressources Naturelles du Québec, Québec City, Québec, Canada.

Simard, M., Lafrance, I., Hammouche, H., Legouix, C., 2014a. Geolgoie – Lac Ballantyne CG-24K11-2014-01. Ministère de l'Energie et des Ressources Naturelles du Québec, Québec City, Québec, Canada.

Simard, M., Lafrance, I., Hammouche, H., Legouix, C., 2014b. Geolgoie – Lac de Freneuse CG-24K06-2014-01. Ministère de l'Energie et des Ressources Naturelles du Québec, Québec City, Québec, Canada.

Simard, M., Lafrance, I., Hammouche, H., Legouix, C., 2014c. Geolgoie – Lac Thevenet. Ministère de l'Energie et des Ressources Naturelles du Québec, Québec City, Québec, Canada.

Skulski, T., Wares, R.P., Smith, A.D., 1993. Early Proterozoic (1.88-1.87 Ga) tholeiitic magmatism in the New Quebec Orogen. Can. J. Earth Sci. 30, 1505–1520. doi:10.1139/e93-129

Sprague, K.B., de Kemp, E.A., 2005. Interpretive tools for 3-D structural geological modelling part II: Surface design from sparse spatial data. Geoinformatica 9, 5–32. doi:10.1007/s10707-004-5620-8

St-Onge, M.R., Scott, D.J., Wodicka, N., Lucas, S.B., 1998. Crustal architecture of the Trans-Hudson Orogen in northern Quebec and southern Baffin Island: plate margin configuration between 2.04-1.76 Ga. in Eastern Canadian Shield Onshore-Offshore transect (ESCOOT), Report of the 1998 Transect Meeting. LITHOPROBE, Merrickville, pp. 151–166.

Stockwell, C.H., 1963. Third report on structural provinces, orogenies and time classification of rocks of the Canadian Precambrian Shield.

Système d'information géominière du Québec, 2016. . Ministère de l'Énergie et des Ressources naturelles, Québec City, Québec, Canada.

Taylor, F.C., 1979. Reconnaissance geology of a part of the precambrian shield, northeastern quebec, northern labrador and northwest territories. Geological Survey of Canada, Ottawa, Ontario, Canada.

Telmat, H., Mareschal, J.C., Gariepy, C., 1999. The gravity field over the Ungava Bay region from satellite altimetry and new land-based data: implications for the geology of the area. Can. J. Earth Sci. 36, 75–89.

Thiele, S.T., Jessell, M.W., Lindsay, M., Ogarko, V., Wellmann, J.F., Pakyuz-Charrier, E., 2016. The topology of geology 2: Topological analysis. J. Struct. Geol. 91, 74–87. doi:10.1016/j.jsg.2016.08.010

Twiss, R.J., Moores, E.M., 2007. Structural geology, 2nd ed. New York, NY : W.H. Freeman, c2007., New York, NY.

van der Meijde, M., Fadel, I., Ditmar, P., Hamayun, M., 2015. Uncertainties in crustal thickness models for data sparse environments : A review for South America and Africa. J. Geodyn. 84, 1–18. doi:10.1016/j.jog.2014.09.013

von Tscharner, M., Schmalholz, S.M., Epard, J.L., 2016. 3-D numerical models of viscous flow applied to fold nappes and the Rawil depression in the Helvetic nappe system (western Switzerland). J. Struct. Geol. 86, 32–46. doi:10.1016/j.jsg.2016.02.007

Wardle, R.J., Bailey, D.G., 1981. Early Proterozoic Sequences in Labrador, in: Campbell, F.H.. (Ed.), Proterozoic Basins of Canada. Geological Survey of Canada, pp. 331–359.

Wardle, R.J., James, D.T., Scott, D.J., Hall, J., 2002. The southeastern Churchill Province: synthesis of a

Paleoproterozoic transpressional orogen. Can. J. Earth Sci. 39, 639–663. doi:10.1139/e02-004

Wardle, R.J., Ryan, B., Nunn, G.A.G.A.G., 1990. Labrador Segment of the Tans-Hudson Orogen: Crustal Development Through Oblique Convergence and Collision, in: Lewry, J.F., Stauffer, M.R. (Eds.), The Early Proterozoic Trans-Hudson Orogen of North America: Geological Association of Canada, Special Paper 37. Geological Association of Canada, pp. 353–369.

Wares, R., Berger, J., St. Seymour, K., 1988. Synthèse métallogénique des indices de sulfure au nord du 57e parallèle (Étape I), Fosse du Labrador. Ministère de l'Énergie et des Ressources, Québec, Québec City, Québec, Canada.

Wares, R.P., Goutier, J., 1990. Deformational style in the foreland of the northern New Quebec Orogen. Geosci. Canada 17, 244–249.

Weber, W., Lewry, J.F., Stauffer, M.R., 1990. The Churchill-Superior Boundary Zone, Southeast Margin of the Trans-Hudson Orogen: A Review, in: Lewry, J.F., Stauffer, M.R. (Eds.), The Early Proterozoic Trans-Hudson Orogen of North America: Geological Association of Canada, Special Paper 37. Geological Association of Canada, pp. 41–55.

Wellmann, J.F., Horowitz, F.G., Schill, E., Regenauer-Lieb, K., 2010. Towards incorporating uncertainty of structural data in 3D geological inversion. Tectonophysics 490, 141–151. doi:10.1016/j.tecto.2010.04.022

Wellmann, J.F., Regenauer-Lieb, K., 2012. Uncertainties have a meaning: Information entropy as a quality measure for 3-D geological models. Tectonophysics 526–529, 207–216. doi:10.1016/j.tecto.2011.05.001

Wex, S., Passchier, C.W., de Kemp, E.A., Ilhan, S., 2014. 3D visualization of sheath folds in Ancient Roman marble wall coverings from Ephesos, Turkey. J. Struct. Geol. 67, 129–139. doi:10.1016/j.jsg.2014.07.005

Woodcock, N.H., 1977. Specification of fabric shapes using an eigenvalue method, in: Geological Society of America Bulletin. pp. 1231–1236.

Appendix A – Previous work

The Labrador trough was first described by Father Babel, a Jesuit Priest, who observed iron-rich rocks during his travels from 1866 to 1870 (Conliffe et al., 2013). In 1892, Dr. A. P. Low of the Geological Survey of Canada investigated this discovery, describing iron ore in the Dyke Lake and Koksoak River areas (Neal, 2000). These investigations spiked public interest and initiated a season of intense exploration. In 1929, Dr. W. James and Dr. J. Gill discovered the first of many high-grade iron ore deposits near Knob Lake; however, exploration was halted as a result of the 1930s market crash (Neal, 2000). In 1936, private companies began to explore the Labrador Trough for base metals and, specifically, for iron. Mining companies that worked in the area include the Iron Ore Company of Canada, Hollinger North Shore Exploration Company, and Fenimore Iron Mines (de Römer, 1956; Telmat et al., 1999).

After several years of industry-led exploration, government agencies such as the Geological Survey of Canada (GSC) and the Québec Ministry of Natural Resources (QMNR) began reconnaissance-scale mapping campaigns to assess mineral potential and improve understanding in the Labrador Trough. The first, regional geological map (Map 1146A) was released in 1965 by W. F. Fahrig from the Geological Survey of Canada following field work in 1955 (Fahrig, 1965). The first work released by the QMNR was a compilation of metallic mineralization composed by J. Dugas in 1970 which built upon Fahrig's work (Dugas, 1970). The next major publication was T. Clark's maps of regional metallogenic potential, published by QMNR in 1978 (Clark, 1978). In 1979, Taylor (1979) released large scale reconnaissance maps of the northern Labrador Trough and Core Zone. Following this, Avramtchev (1985) released a geographically-extensive compilation of the region.

During the 1990s, there was active exploration for Kimberlite pipes which provided an opportunity to re-evaluate current geological understanding and data. Exploration efforts were further invigorated with the discovery of precious metal concentrations in the Labrador Trough. In 1986, La Fosse Platinum Group announced anomalous platinum group element (PGE) concentrations near Shefferville, Québec (Findlay, 1996). This has sparked ongoing exploration for PGEs, gold, silver and rare earth elements (REEs) by several companies including Midland, Rio Silver and Rockland Minerals Corp as well as base metals such as copper and nickel.

The recent activity in northern Québec has refocused the GSC, Ministère de l'Energie et des Ressources Naturelles du Québec (MERN) and the Newfoundland and Labrador Department of Natural Resources

on regional mapping projects in the Labrador Trough. The MERN has released several regional compilation maps (Hammouche et al., 2012; Lafrance et al., 2014, Simard et al., 2013, 2014a, 2014b, 2014c), mineral potential maps, geophysical surveys (D'Amours and Intissar, 2013, 2012a, 2012b; Dion and Legebvre, 1998), drilling surveys and a database of field observations (SIGEOM). The GSC has several tectonic, geochronological, geochemical, structural and 3D modelling studies underway as part of its second Geo-mapping for Energy and Minerals (GEM) initiative which seeks to better understand the complex geological history of the Canadian Arctic (Corrigan, 2016; Corrigan et al., 2015; Corriveau et al., 2014; Houlé et al., 2016; Sanborn-Barrie, 2016). This thesis is part of the GEM2 initiative.

Beyond map and data releases, both surveys have published valuable reports and open files which have greatly shaped current understanding of how the Labrador Trough formed and how it has evolved over the last billion years.

Appendix B – Resource Potential

This Paleoproterozoic fold and thrust belt is noteworthy to Canadian and global geology as it hosts a number of base and precious metal deposits. Based on past and current exploration, the Labrador Trough has economic potential for iron, copper, nickel, platinum group elements (PGE), zinc, and cobalt (Figure B - 1). Recently, exploration efforts in the Labrador Trough have been reinvigorated. New discoveries of precious and base metal deposits are drawing national attention to this highly deformed region.

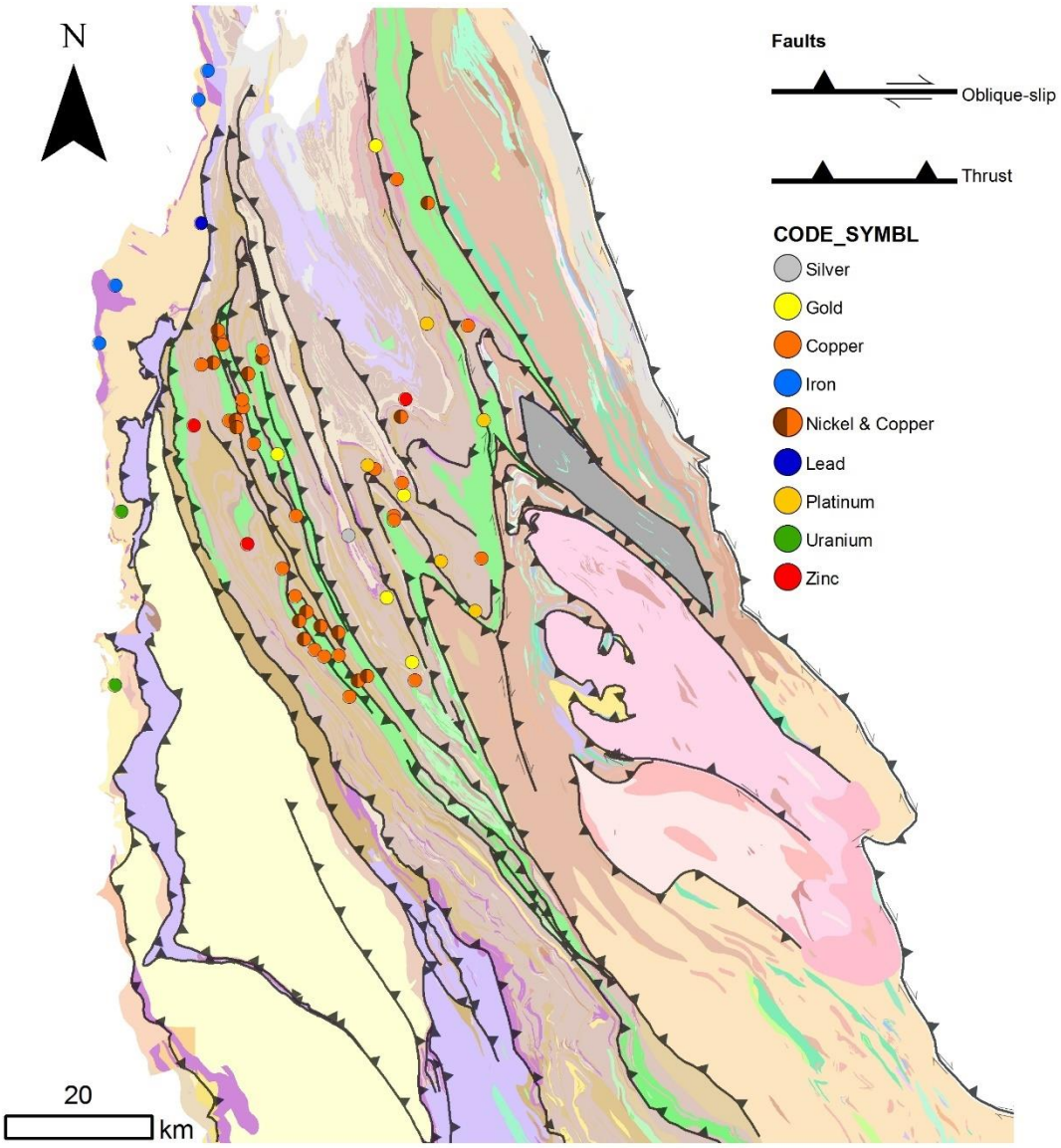

Figure B - 1. Mineral occurrence points superimposed on bedrock geology map for the northern Labrador Trough. Highlights areas of economic significance. Many mineralized zones along contact of gabbro (green) and Kaniapiskau sedimentary units (Mineral occurrence points and geological units from SIGEOM geodatabase. Fault interpreted by Montsion in this study).

Iron

Throughout the orogen, nearly half of the known iron deposits developed syngenetic or diagenetically while the other half developed epigenetically. The most notable of all iron deposits in the region is the Lake Superior type Sokoman Iron Formation, a laterally extensive chert marker bed that can be traced across much of the Labrador Trough (Chauvel and Dimroth, 1974; Dimroth and Chauvel, 1973). It is bounded by Cycle 2 quartz arenites of the Wishart Formation and the shales and turbidities of the Menihek Formation, placing it near the center of Cycle 2 (Clark and Wares, 2006). This deposit records an environmental transition from shallow water, high energy to deep water, low energy. Subsequent weathering of this iron formation during the Cretaceous, in the Shefferville area, formed a residual deposit with economic potential, making it the richest deposit of its type in Canada. Its formation is thought to be the result of phreatic water percolating down to roughly 150 m, along transverse fractures and inclined porous beds. The water dissolved/leached silica and oxidized iron, which produced fine-grained hematite and goethite iron ore (Clark and Wares, 2006; Gross, 1972).

Other iron deposits discovered in the Labrador Trough are Algoma-type deposits of interbedded chert and iron-rich minerals, which are associated with volcanic rocks (Clark and Wares, 2006). Although the source of iron is currently under debate, a common opinion is that iron in the Labrador Trough has a volcanic-hydrothermal origin (Gross, 1972).

Uranium

In the 1970's search for uranium, it was discovered that the majority of deposits were related to early rifting and are hosted in the Paleoproterozoic sedimentary outliers west of the orogen. These deposits are located in argillaceous sediments near the Archean-Proterozoic contact in the Cambrian Zone. During rifting, uranium was extracted from enriched Archean granitic and metamorphic rocks and transported in oxidizing surface waters to the sedimentary units. It is thought that deposition occurred in low energy, shallow water such as playa lakes or deltas where reduction occurred. Today, we find these uranium accumulations as insoluble U^{4+}, in the form of pitchblende (Clark and Wares, 2006).

Copper

Throughout the orogen, there are only a handful of copper deposits. These deposits are diagenetic and are hosted by early Cycle 1 sandstones and conglomerates. The most notable deposits are found along the Argencourt Fault and subsidiary shear zones where the Portage and Lace Lake formations are in contact. Hydrothermal fluid moved through the fault zone and precipitated copper in the oxidized

environment. Additionally, accumulations of stratiform copper in the Wheeler and Howse zones' Dunphy dolomite and siltstone are also important. These stratiform deposits accumulated during a period of quiescence when energy was low and cyanobacteria flourished. Copper accumulated in the primary porosity space, called fenestrae or birds eyes. The source for copper in the region is thought to be the Chakonipau redbeds (Clark and Wares, 2006).

Gold

Two gold rich zones have been discovered in the Labrador Trough. The first is hosted in an Archean iron formation near Schefferville, Québec. At this location, gold has accumulated between boudins that can reach up to several meters in thickness and decimeters in length (Clark and Wares, 2006). The second zone lies within the study area of this thesis and is located just west of Kuujjjuaq. In this zone, gold has been discovered in epigenetic quartz veins with in an iron formation of the Paleoproterozoic Middle Baby Formation. This accumulation flanks a regional anticline, proximal to a reactivated thrust fault (Clark and Wares, 2006; Wares and Goutier, 1990)(Wares and Goutier, 1990; Clark and Wares, 2006). A gold rich zone has also been located west of Kuujjuaq, Québec in epigenetic quartz veins.

Cu-Zn-Co-Ag-Au and Zn-Pb-Cu-Ag-Au

The Cu-Zn-Co-Ag-Au present in the Labrador Trough are located in the Gerido Zone and are hosted by iron-rich sedimentary units of the upper Baby Formation, directly below the Hellancourt basalts (Barrett et al., 1988; Wares et al., 1988). This deposit area is within the Hellancourt Sub-area and exploration for this deposit type may benefit from the model product of this thesis. Additionally, some of these deposits are also found in association with gabbro sills which intrude the Cycle 2 sedimentary sequence (Clark and Wares, 2006). The Zn-Pb-Cu-Ag-Au deposits are hosted in the graphitic mudstones of the upper Menihek Formation where it is found in association with iron formation marker beds of the Baby Formation (Clark and Wares, 2006). Both deposit types are thought to have an exhalative origin similar to iron formations elsewhere (Clark and Wares, 2006).

Nb-Ta-REE (Rare Earth Elements)

Nc-Ta-REE deposits in the Labrador Trough are hosted by carbonatite within the Le Moyne complex, a volcanic-intrusive body located in the Gerido Zone. These deposits have a magmatic origin (Clark and Wares, 2006). While there are only two known deposits at present, there is growing interest within industry for a new Canadian source of REEs.

Cu-Ni±PGE (Platinum group elements)

Cu-Ni±PGE deposits are common throughout the Labrador Trough. These deposits have a magmatic origin and some are found in association with epigenetic sulphides. The four main environments of accumulation are picritic basalts, aphyric gabbro sills, glomeroporphyritic gabbro sills and gabbro sills with pegmatite (Clark and Wares, 2006).

Appendix C – Expanded Geological Context

The Southeastern Churchill Province (SECP) makes up a significant portion of the northeastern Canadian Shield, extending across northern Québec and Labrador. While previously thought to be the southerly extension of the Churchill Province (Stockwell, 1963), St-Onge et al., (1998) found that it is cut off from the greater Churchill Province by an easterly extension of the Labrador Trough. The province consists of, from west to east, the Paleoproterozoic Labrador Trough, the Archean Core Zone and the Paleoproterozoic Torngat Orogen. This study focuses on the Labrador Trough, a fold and thrust belt that hosts the western extent of the Archean Core Zone and Paleoproterozoic Labrador trough. Within the Labrador Trough, there are three further sub-divisions: the Kaniapiskau Zone, the Rachel-Laporte Zone and the Core Zone.

The Labrador Trough has been the subject of much study since its discovery in the 1800s and has historically included all the Paleoproterozoic metasedimentary and metavolcanic units found between the Superior Craton and the western Core Zone. It has been given many names such as “Labrador Geosyncline” (de Römer, 1956), “the Trough” and the “New Québec Orogen” (Hoffman, 1988; Rohon et al., 1993; Skulski et al., 1993). Hereafter, the “Labrador Trough” will refer to the Paleoproterozoic metasedimentary and metavolcanic units of the Kaniapiskau Supergroup and the Rachel-Laporte Zone.

Labrador Trough

The Labrador Trough is 800 km long and 100 km wide, reaching from a disconfomable contact with the underlying Superior Craton’s Ashuanipi complex in the west and the Lac Olmstead Fault in the east. It was named as a reference to its basinal setting of deformation, but it is in fact orogen flattened by erosion and is situated more within Québec rather than Labrador. Its geographic extent has been subdivided into northern, central and southern regions by Dimroth et al. (1970). The study area sits within the northern region.

The Labrador Trough is a Paleoproterozoic, west-verging fold and thrust belt made up of early thin-skinned imbricate thrusts and later out-of-sequence thrusts which divide the major lithotectonic blocks of the orogen. The major out-of-sequence thrusts are thought to stem from a master décollement which marks the unconformable contact. However results from this study suggest that a master décollement was present along the Superior-Trough contact during D_1, which accounted for large displacement of Paleoproterozoic sediments westward. The décollement was likely deformed during later stages of deformation, similar décollement geometries reported by Feng et al. (2015).

The Trough is composed of two major lithotectonic supergroups, the Kaniapiskau and Rachel-Laporte, which will be described in detail later in this appendix.

Core Zone

The Core Zone is a 200 km expanse of tonalitic to granitic gneiss complexes, which is bounded by the Lac Olmstead Fault in the west, which marks the boundary of the Labrador Trough, the Torngat Orogen in the east, the Grenville front in the south, and the Ungava Bay in the north. The exact nature and geometry of the northern termination is currently unknown because it sits below the Ungava Bay in northern Québec. The age range for the mid- to lower-crust gneiss complexes of the Core Zone is 2.7 to 2.6 Ga, with some dates of 3.0 Ga in the northeast, indicating that most of the region is Archean (Lafrance et al., 2014; Simard et al., 2013; Wardle et al., 2002). In addition to the Archean complexes, some Paleoproterozic metasedimentary units have been infolded with the gneisses and both have been intruded by Hudsonian age plutons such as the De Pas Batholith (Dimroth, 1981; Wardle et al., 2002).

It was previously hypothesized that the Core Zone was an extension of the Rae Province (Hoffman, 1990; Wardle et al., 1990); however, work by St-Onge et al. (1998) has shown that the Rae has been cut off from the Southeastern Churchill Province by the Trans-Hudson Orogen. It is now thought that the Core Zone is either a detached block of the Superior Craton, as it shows an affinity to the neighboring Archean craton, or a composite block of Archean crust assembled during the Paleoproterozoic (James and Dunning, 2000; Machado et al., 1997; Wardle et al., 2002). Its geochemistry, geochronology and petrography all resemble the Superior Craton; however, the presence of blocks with variable metamorphic grades adjacent to one another suggests that the formation history may be more compelx than previously thought. Recent work by Corrigan et al. (2016) has identified several unique Archean blocks which were juxtaposed, making up a composite, complex block between the two Paleoproterozoic orogens. Further work by the Geologic Survey of Canada is being conducted and will be published in the coming year. To date, several activity reports and conference presentations communicate their findings (Corrigan et al., 2015; Houlé et al., 2016; Sanborn-Barrie, 2016).

Tectonic history and structures

Within the Labrador Trough, two phases of rifting and three phases of deformation are observed. The early stages of the Labrador Trough consisted of ensialic rifting along the Superior Craton margin and deposition of immature sediments (Cycle 1) (Dimroth, 1970). It is likely that the Core Zone became a raft of the Superior Craton during this event and widespread mafic and ultramafic magnetism began;

however, rifting failed before a true ocean basin could form (Findlay, 1996). The three phases of deformation record the collision between the Nain and Superior Cratons during the Hudsonian Orogen, an event which resulted in 50% shortening; however Dimroth (1981)reports up to five generations of overprinting structures (Dimroth, 1981). In general, deformation began as east-west convergence with shortening in the east/west direction (D_1). As orogenesis progressed, deformation and metamorphism intensified with a minor dextral shear component (D_2) and finally deformation became dominated by dextral shear (D_3) (Clark and Wares, 2006).

D_1

The first deformational phase within the Labrador Trough was a westward translation of the Paleoproterozoic supracrustal units onto the Superior Craton, producing a strong bedding-parallel foliation and schistosity (S_1) (Moorhead, 1989; Poirier, 1989; Poirier et al., 1990), NNW trending thrusts with listric geometry, a décollement between cover rocks and the Superior basement, W-vergent, outcrop-scale, rare fault-associated folds (Boone, 1987; Goulet, 1987, 1986; Wares et al., 1988), a fault-associated stretching lineation (L_1) (Hoffman, 1988) and Archean cored, imbricate thrust nappes (Poirier, 1989). The expression of these structures is not uniform across the orogen. Instead, they are preserved in the west where later deformation events have not overprinted structures as strongly; however, the S_1 schistosity is more strongly developed in the hinterland (Moorhead, 1989). Moving eastward, D1 structures become obscured by increasingly intense deformation associated with the Lac Tudor shear zone and nappe structures.

D_2

In the west, the D_2 phase is expressed by outcrop to regional scale, tight, upright to recumbent folds with axial planes trending to the NE. An associated S_2 foliation is rare and generally only observed in metapelitic units (Poirier et al., 1990). Additionally, Moorhead (1989) reports E to NE trending, shallowly plunging open folds that deform the basement and cover rocks in the Labrador Trough into large-scale folds. These observations suggest that the nappes along the eastern margin of the Labrador Trough may have developed during this phase of deformation. This interpretation is supported by Moorhead (1989)'s field observations that D_1 and nappes fold morphologies greatly differ, that S_1 is deformed by the nappes, and the presence of interference patterns between F_1 folds in the interior of the nappes. The involvement of the basement during folding suggests that the décollement was segmented or deformed during this phase. Further investigation is needed to validate this interpretation.

In the east, D_2 produced E to NE trending, upright, open cross-folds and an associated rare, weak axial planar cleavage (Machado et al., 1997). A strong stretching lineation L_2 developed parallel to fold axes near major fold closures in the western Core Zone and Rachel-Laporte Zone (Moorhead, 1989).

Some authors also hypothesize that the D_2 structures observed in the Labrador Trough may represent a southern extension of Cape Smith's E trending D_2 deformation (Moorhead, 1989; Wardle et al., 2002). Since the two orogenic belts have a closely linked history (St-Onge et al., 1998; Wardle et al., 2002), this hypothesis is likely.

D_3

From west to east, the intensity of metamorphism and deformation increases. In the west, low grade metamorphism and outcrop-scale open folds transition into intensely folded amphibolite to granulite grade rocks in the east (Dimroth, 1981). Across the Labrador Trough, D_3 is expressed by numerous outcrop- to regional-scale folds and an associated crenulation cleavage (S_3). Fold geometry and orientation is variable at the regional scale. In the northern region of the study area, folds have steep, upright axial planes and plunge to the NE. In the south, folds are overturned and axial planes trend SE (Poirier et al., 1990). This is further complicated by interference with the competent, basement-cored thrust nappes in the east of the study area. Folds proximal to the nappes are NNW trending, SW-vergent and tight. Some folds are upright, but many are overturned to the west (Moorhead and Hynes, 1990). Interference between F_2 and F_3 in the western autochthonous zone has caused local reversals in fold plunges and variable interference patterns.

In the metasedimentary units infolded with Archean gneisses of the western Core Zone, there are tight, shallow plunging folds with steeply dipping axial planes. A strong axial planar cleavage developed in association with the tight folds and acted as a plane for bedding transposition. These folds produced a mushroom interference pattern with the F_1 isoclinal recumbent folds (Hynes, 1978). This deformational event was coeval with peak metamorphism in the region (Hynes, 1978).

Post D_3

Following the intense deformation of the Hudsonian Orogeny, late sage, NNW-SSE trending strike slip faults developed (Poirier et al., 1990) This post deformational event may have resulted in the formation of the dextral Rachel Faults; however there was significant displacement associated, indicating that it formed during peak deformation.

Stratigraphy

The Labrador Trough is a Paleoproterozoic metasedimentary and metavolcanic package which consists of the Kaniapiskau and Rachel-Laporte supergroups. The majority of work done in the area has been completed in the Kaniapiskau Supergroup, which constitutes the main body of the Labrador Trough (Chandler, 1980; Clark and Wares, 2006; Houlé et al., 2016; Rohon et al., 1993; Wardle and Bailey, 1981; Weber et al., 1990). A regional model of stratigraphy for the Kaniapiskau Supergroup has been established based on limited geochronological work (Clark, 1988; Clark and Wares, 2006; Dimroth, 1981); however, there has been limited published work for the Rachel-Laporte Supergroup.

Kaniapiskau Supergroup

The Kaniapiskau Supergroup comprises the bulk of supracrustal rocks in the Labrador Trough. It consists of metasedimentary and metavolcanic units, which lay disconformably on the Superior Craton to the Rachel Fault. These units have been well researched as they host many of the base and precious metal deposits, which made the Labrador Trough famous. The full stratigraphic assemblage is presented in Figure C-1.

Three cycles of sedimentation and several intrusive bodies make up the Kaniapiskau Supergroup. The first crustal forming event, termed “Cycle 1”, was the deposition of an intracratonic rift basin sequence at 2.2 Ga (Clark and Wares, 2006; Wardle et al., 2002). The Seward Group’s immature continental rift sequence of sandstones and conglomerates were deposited discordantly over the Superior Craton’s Ashuanipi complex along the western margin of the orogen. This sequence was intruded by gabbro sills at 2.914 Ga (Clark and Wares, 2006).

Between 2.17 – 2.14 Ga, passive margin sediments and MORB-type, axial mafic volcanic rocks began to accumulate. After a period of stability, a platform developed around 2.06 Ga, allowing dolomite, chert and other marine sedimentary units of the Chakonipau, Portage, Dunphy and Milamar formations to accumulate. Deposition continued under these conditions until regression shut off the system between 2.14 to 1.94 Ga (Clark and Wares, 2006). In the northern region of the Trough, the lower members of this sequence are generally missing from the stratigraphic pile because, during the early stages of basin formation deposition was restricted to the central Trough here the basin was deepest (Findlay, 1996). As rifting continued, the basin opened and Pistolet and Swampy Bay sediments were deposited across the Trough. According to Dimroth (1981), the maximum thickness of Cycle 1 is 10 km at the center of the Trough and thins towards the east.

Following rifting, Cycle 2 deposition began at 1.88 Ga with a transgressive sequence of platform sediments and turbidites which continued until the Hudsonian Orogen changed the tectonic regime at 1.87 Ga (Clark and Wares, 2006; Dimroth, 1981). This cycle deposited the Ferriman, Doublet, Koksoak and Le Moyne groups. The name Montagnais Sills, former “Montagnais Group”, has been used to refer to a sequence of tholeiitic mafic and ultramafic intrusions in Cycle 1 and 2 sediments.

During the late stages of deformation, a new cycle of sedimentation began. Cycle 3 is a syn-orogenic molasse sequence accumulated as material from the young Labrador Trough was eroded and deposited in a nearby basin. This immature sedimentary material discordantly overlays the deformed Cycle 2 platform sequence (Clark and Wares, 2006).

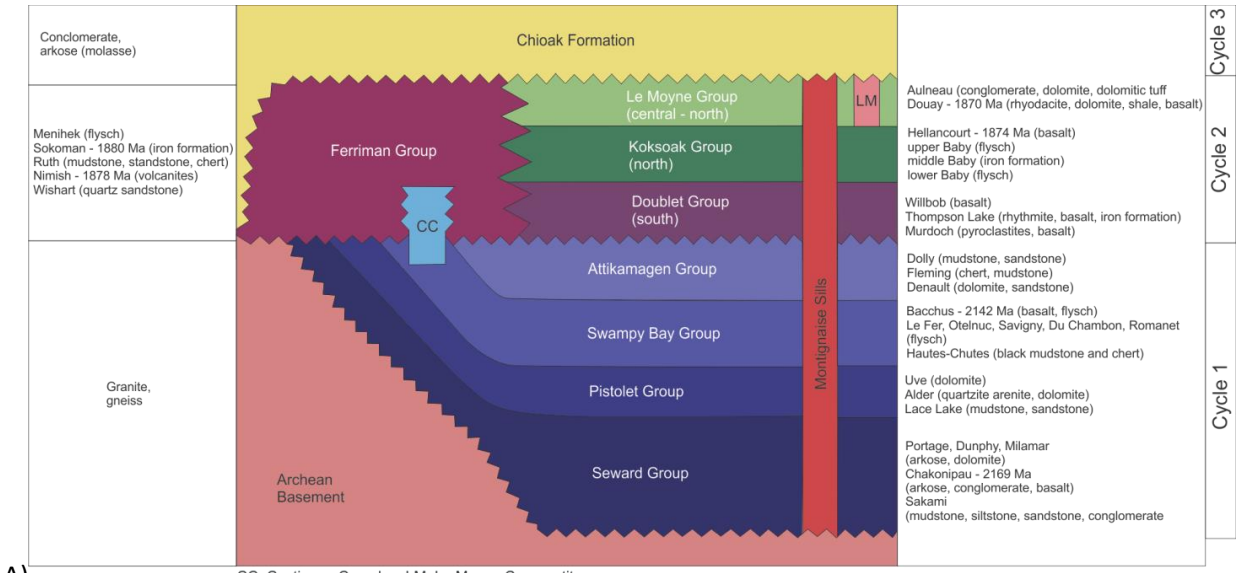

A)

CC: Castignon Complex, LM: Le Moyne Carnonatite

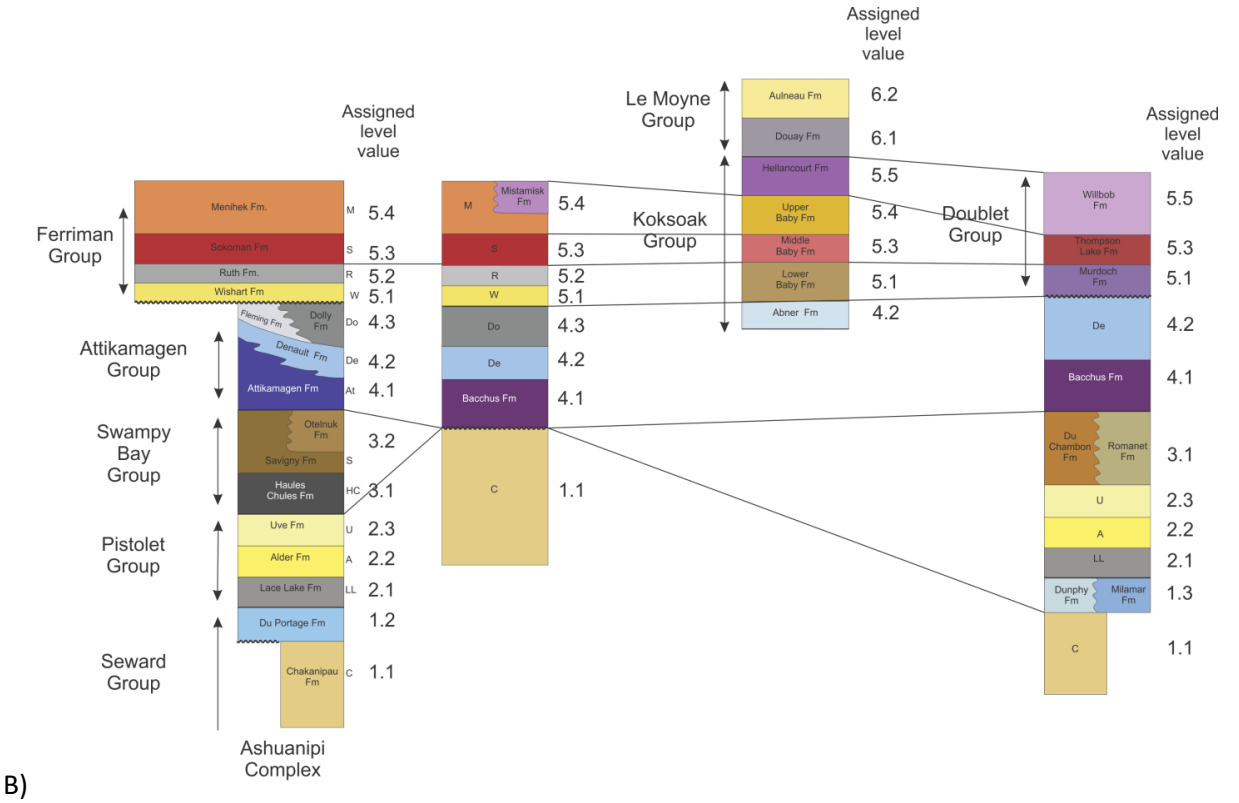

B)

Figure C. - 1 Kaniapiskau Supergroup simplified stratigraphy after A) Clark and Wares (2006). B) Stratigraphic correlations across the Labrador Trough modified from Wardle and Bailey (1981).

Rachel-Laporte Supergroup

The Rachel -Laporte domain of the Labrador Trough is an allochtonous block of back-arc basin sediments and volcanics which are thought to be coeval with the Kaniapiskau Supergroup. While the depositional setting differs from the passive margin Kaniapiskau sediments, there appears to be several similarities in the stratigraphic sequences of the Ferriman Group of the Kaniapiskau Supergroup and the Freneuse Group of the Rachel-Laporte Supergroup.

The back-arc basin units of the Rachel–Laporte domain are currently being investigated as new chronological and petrographic data become available. Until recently, the Rachel-Laporte domain was thought to contain heavily metamorphosed, late stage metasedimentary units of the Kaniapiskau Supergroup. In light of new field observations, it was proposed that the Rachel-Laporte units represent a backarch basin that is coeval with the Kaniapiskau platform sediments (Corrigan et al., 2015). Although formations have not been defined in the literature, generalized groups were defined published by Simard et al. (2013) (see Figure C-2).

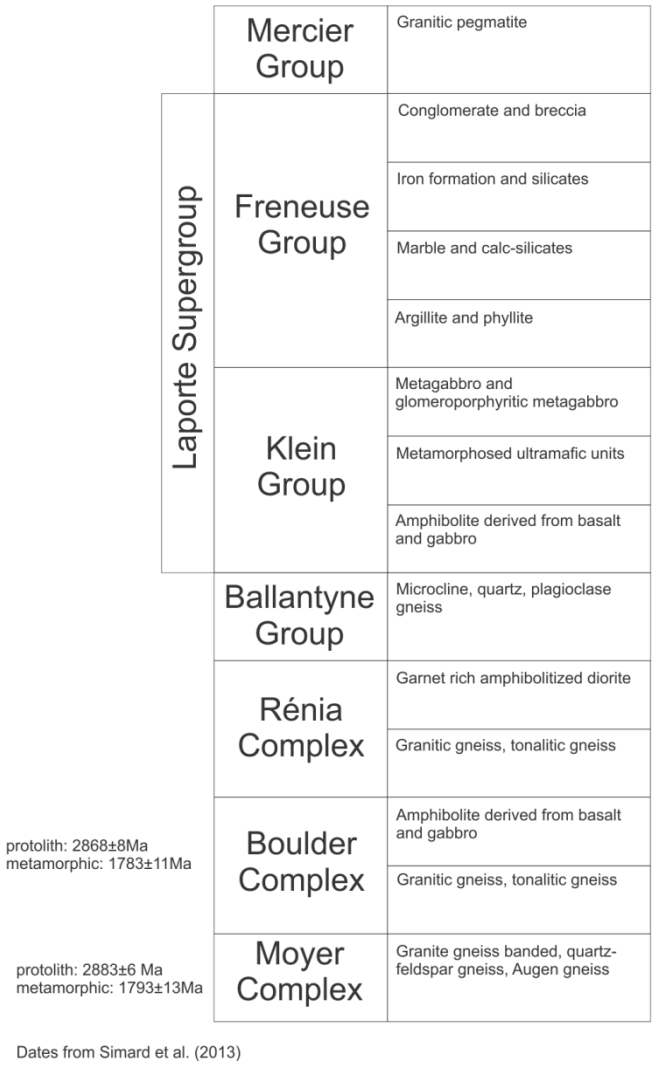

Figure C – 2. Generalized stratigraphy of the Rachel-Laporte Zone after Simard et al. (2013).

Appendix D – Constraint Sources

Information regarding the type of constraints used to construct 3D models and their properties.

Observational Constraints

Table D - 1. Description of observational constraint properties

Constraint type	Method	Total Population (N)	Quality	Uncertainty	Availability	Other important features	Sources
On-Contact	Observed at outcrop	N/A	Moderate	Moderate	Rare to measure in field		Map traces from SIGEOM database and digitized from scanned maps (see references in table below)
Inequality	Indicated by occurrence of neighbouring features or lithologies (overlying or underlying)	N/A	High	Low	Common and easy to find from lithostratigraphic classifications		SIGEOM database as lithological unit polygons
Gradient	Strike and dip of planar features measured in the field	7197	Low	Low	Dependent on outcrop exposure and metamorphic grade	• Younging direction (tops) is rare in metamorphosed terranes (n=362) • Relation to deformational event (generation information) is uncommon as measurements are not often assigned to events in the field (n=5012).	SIGEOM database and digitized from scanned maps (see references in table below)
Tangent	Lineations measured in field	557	High	Low	Dependent on outcrop exposure and metamorphic grade		SIGEOM database and digitized from scanned maps (see references in table below)

Derived Constraints

Table D - 2. Description of derived constraint properties

Constraint type	Method	Total Population (N)	Quality	Uncertainty	Availability	Other important features	Sources
On-Contact	Estimated from map pattern or interpreted between outcrop		Moderate	Moderate	Commonly interpreted		Digitized from scanned maps (see references in table below) or interpreted during model building
Inequality	Indicated by occurrence of neighbouring features or lithologies		High	Low	Generally not common practice but easily acquired if needed		Digitized from scanned maps (see references in table below) or interpreted during model building
Gradient	Strike and dip of planar points which have been up scaled (quantitatively and qualitatively) or calculated using steronets. Some points interpreted	Regional faults: 32	Moderate	Moderate	Common practise for regional studies	• Tops interpreted • Generation information interpreted	Derived points generalize observational gradient points or interpreted during model building
Tangent	Calculated with steronets or SFI. Some points interpreted		Moderate	Moderate	Dependent on outcrop exposure and metamorphic grade		Derived points generalize observational gradient points or interpreted during model building

Constraint type: Type of input used to constrain the model

Method: A general sense of where constraint points come from

Quality: Refers to how clean or consistent the constraint population is. High quality constraints are generally incorporated into the model with minimal difficulty or need for organization. Low quality constraints require organization and up-scaling to be useful for modelling.

Uncertainty: General estimation of uncertainty for each data source

Planar structural points

Planar points from the SIGEOM database (*Système d'information géominière du Québec*, 2016), Corrigan et al. (2015) field work database and digitized scanned maps were harmonized and merged to create the 7,520 points used in this thesis. Map sources and associated references are listed below.

Table D - 3. Sources for planar points in structural database

Map Code	Reference
13-1968_e_1969_mn011	Taylor, F.C., Bell, C.K., Reinhardt, E.W., and Skinner, R., *Northeastern Québec and Northern Labrador* [map], Map 13-1963, Paper 68-43, Scale 1:500,000: Geological Survey of Canada, Department of Energy, Mines and Resources, 1969
36-1962_e_1963_mn011	Stevenson, I.M., Fahrig, W.F., Currie, K.L., Schiller, E.A., Roach, T., *Geology-Géologie Leaf River, New Québec* [map], Map 36-1962, Paper 62-24, Scale 1:506,880: Geological Survey of Canada, 1962
a_1229a_e_1969_mn011	Stevenson, I.M., Taylor, F.C., Skinner, R., Bostock, H.H., Williams, M.G., Mirynech, E., *Geology-Géologie Leaf River, Québec* [map], Map 1229A, GSC Memoir 356, Scale 1:1,000,000: Geological Survey of Canada, 1968
gscprmap_55-371	Fahrig, W.F., *Preliminary Map 55-37 Lac Herodier (East Half), New Québec* [Map], Scale 1:235,440: Geological Survey of Canada, 1956
gscprmap_55_11	Fahrig, W.F., *Preliminary Map 55-1, Lac Herodier, New Québec* [Map], Scale 1:253,443: Geological Survey of Canada, 1953
MB8805P001	Wares et al., 1988
MB8938P001	Wares, R., Goutier., *Métallogénie des indices de sulfures au nord du 57e parallèle, Fosse du Labrador* [Map], Scale, 1:10,000: Scale 1:10,000: Ministère de l'Énergie et des Ressources, Service géologique de Québec, 1989
MB9025P001	Wares, R., and Goutier, J., 1990, *Synthèse métallogénique des indices de sulfures au nord du 57e parallèle , Fosse du Labrador*, Special Paper MB 90-25, Ministère de l'Énergie et des Ressources, Service géologique de Québec
MB9110P001	Goutier and Wares, 1991
RG104C001	Bergeron, R., 1955, *Gerido Lake Area, New-Québec Territory, Map 1473, Map of Geological Report No.104* [Map], Scale 1:63,360: Ministère des Richesses Naturelles, Québec, 1955
RG104C002	Sauvé, P., and Bergeron, R., *Thévenet Lake Area, New-Québec Territory, Map 1499, Map of Geological Report No.104* [Map], Scale 1:63,360: Ministère des Richesses Naturelles, Québec, 1955
RG111(A)C001	Bérard, J., *Feuilles Lake Area, New-Québec Territory*, Map 1471, Map of Geological Report No. 111 [Map], Scale: 1:63,360: Ministère des Richesses Naturelles, Québec, 1958
RG111C002	Bérard, J., *Berard Lake Area, New-Québec Territory, Map 1472, Map of Geological Report No. 111* [Map], Scale 1:63,360: Ministère des Richesses Naturelles, Québec, 1957
RG195C003	Dressler, B., *Fosse du Labrador, Feuille Lac la Lande, Nouveau-Québec* [Map], Scale 1:50,000: Ministère des Richesses Naturelles, Québec, 1979
RG195C004	Dressler, B., *Fosse du Labrador, Feuille Lac Jogues, Nouvea-Québec, Map 1917 [Map]*, Scale 1:50,000: Ministère des Richesses Naturelles, Québec, 1979

Linear structural points

Linear points from the SIGEOM database (*Système d'information géominière du Québec*, 2016), Corrigan et al. (2015) field work database and digitized scanned maps were harmonized and merged to create the 338 points used in this thesis. Map sources and associated references are listed below.

Table D - 4. Sources for linear points in structural database

Map Code	Reference
MB8627P003	Goulet, N., *Baie Profonde 24K/12O*, accompanying map of MB 86-27 [Map]: Ministère des Richesses Naturelles, Québec, 1986
MB8627P005	Goulet, 1986
MB9025P0011	Wares, R., and Goutier, J., *Géologie détaillée de l'indice Venditelli,* accompanying map of MB 90-25 [Map], Scale 1:10,000: Ministère des Richesses Naturelles, Québec, 1990
RG104C001	Bergeron, R., 1955, *Gerido Lake Area, New-Québec Territory, Map 1473, Map of Geological Report No.104* [Map], Scale 1:63,360: Ministère des Richesses Naturelles, Québec, 1955
RG104C002	Sauvé, P., and Bergeron, R., *Thévenet Lake Area, New-Québec Territory, Map 1499, Map of Geological Report No.104* [Map], Scale 1:63,360: Ministère des Richesses Naturelles, Québec, 1955
RG111(A)C001	Bérard, J., *Feuilles Lake Area, New-Québec Territory*, Map 1471, Map of Geological Report No. 111 [Map], Scale: 1:63,360: Ministère des Richesses Naturelles, Québec, 1958
RG111(A)C002	Bérard, J., *Berard Lake Area, New-Québec Territory*, Map 1472, Map of Geological Report No. 111 [Map], Scale: 1:63,360: Ministère des Richesses Naturelles, Québec, 1958

Appendix E – Fault Descriptions

Below is table of the faults investigated during this thesis. It is important to note that not all faults were modelled as some did not have regional significance.

Figure E-1. Plan view of labelled regionally significant modelled fault traces map for the northern Labrador Trough.

Below is table of the faults investigated during this thesis.

Table E - 1. Fault descriptions

Fault	Deformation event	Details
Forbes Thrust	D1	East dipping thrust fault. Fault is the furthest west and may represent the orogenic front.
Garigue Thrust	D1	Thrust fault that cuts or over-rides the Forbes fault
Robelin Thrust	D1	Thrust fault that cuts or over-rides the Forbes and Garigue fault in the north of the study area. Marks the boundary between the allochthonous and autochthnonous blocks.
Archaic Thrust	D1	Thrust fault that is parallel to the Robelin fault and is cut by the Hérodier fault in the south. Generally parallel to bedding and S1.
Canoe Thrust	D1	Cuts Rachel-Laporte Sueprgroup units. Deformed around the Rénia Synform.
Hérodier Thrust	D1 or D2	Marks major tectonic boundary, acting as the major slip plane which transports the Rachel-Laporte Supergroup onto the parathochthonous Kaniapiskau Supergroup. Fault is folded by D_3 transpression
Lac Barrie Fault	D1 or D2	SW dipping fault, likely a thrust fault connected as part of an M-fold geometry with the Hérodier fault
Boulder Fault	D2	Contact between the Archean gneiss of the Boulder Antiform and the Rachel-Laporte Supergroup
CentralNappes Fault	D2	Contact between the Archean gneiss of the central block of thrust nappes and the Rachel-Laporte Supergroup. Must be younger than Canoe Fault as the Canoe fault deforms around it.
Highfall fault	D2	Contact between the Archean gneiss of the Highfall Antiform and the Rachel-Laporte Supergroup
Point Reef Thrust	D2 or D3	Tightly folded and poly-deformed fault. Likely the northern extension of the Hérodier fault. Has been sheared around the Boulder Antiform. Marks the contact between the Kaniapiskau Supergroup in the west and the Rachel-Laporte Supergroup in the east.
Lac Olmstead	D2 or D3	Fairly undeformed fault; marks the boundary between the Core Zone and Labrador Trough.
Lac Ujaralialuk Thrust	D3	Late stage, north-dipping fault which juxtaposes the central block of thrust nappes and the Highfall Antiform
Lac Rachel Thrust	D3’	Late stage oblique slip fault. 15 km right-lateral offset and 10 km vertical offset (Simard et al., 2013)

Appendix F – Geochronology sample map

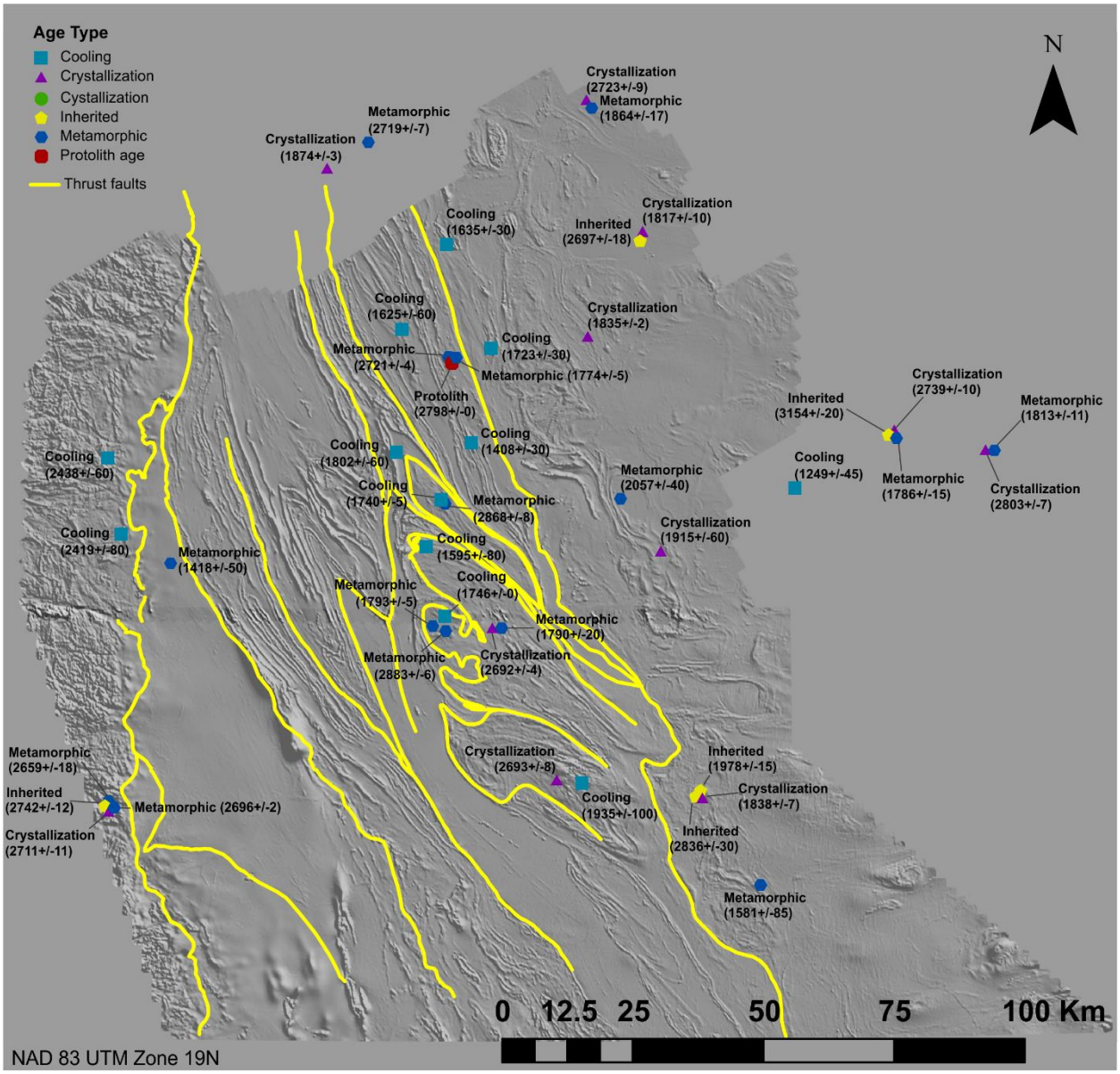

Figure F - 1. Geochronology map of the northern Labrador Trough. Dates from SIGEOM database (*Système d'information géominière du Québec*, 2016)**, Simard et al. (2013), and Lafrance et al. (2014). Yellow lines represent fault traces. Background of hillshaded magnetic first vertical derivative map (hillshade with 45° azimuth and 45° shade angle; 75 m x 75 m cell size from magnetic survey with 300 m line spacing).**

Appendix G – Schmidt equal area stereonets

Axial plane calculations

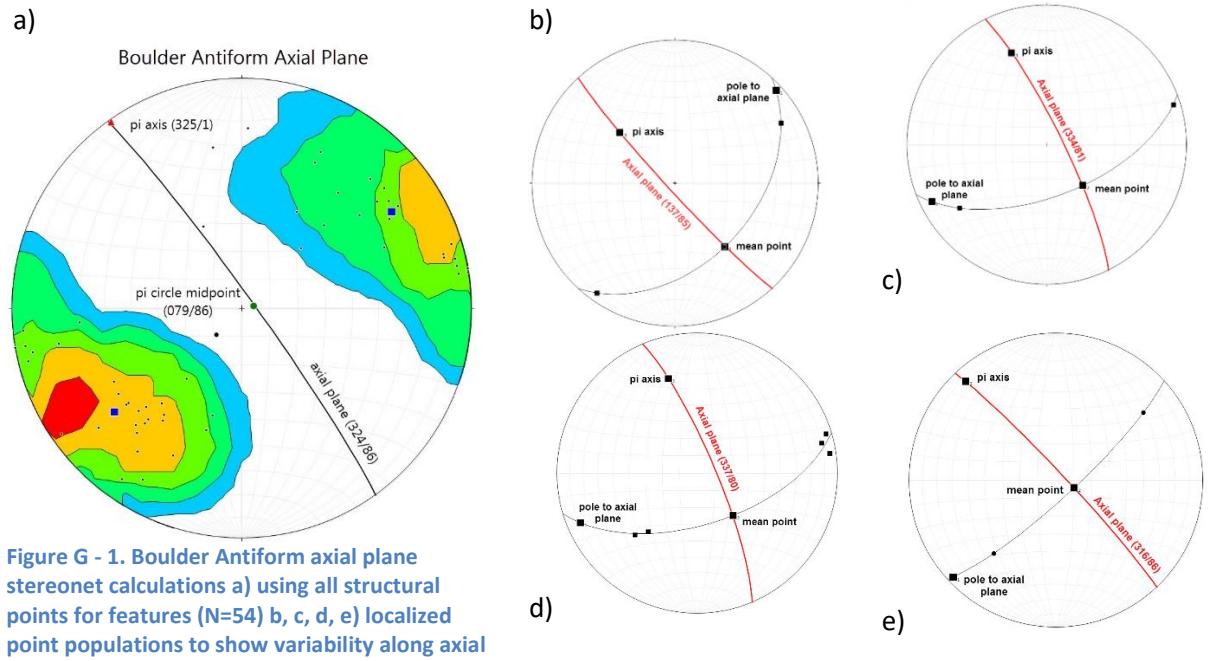

Figure G - 1. Boulder Antiform axial plane stereonet calculations a) using all structural points for features (N=54) b, c, d, e) localized point populations to show variability along axial plane b) N=2, c) N=2, d) N=5, e) N=2.

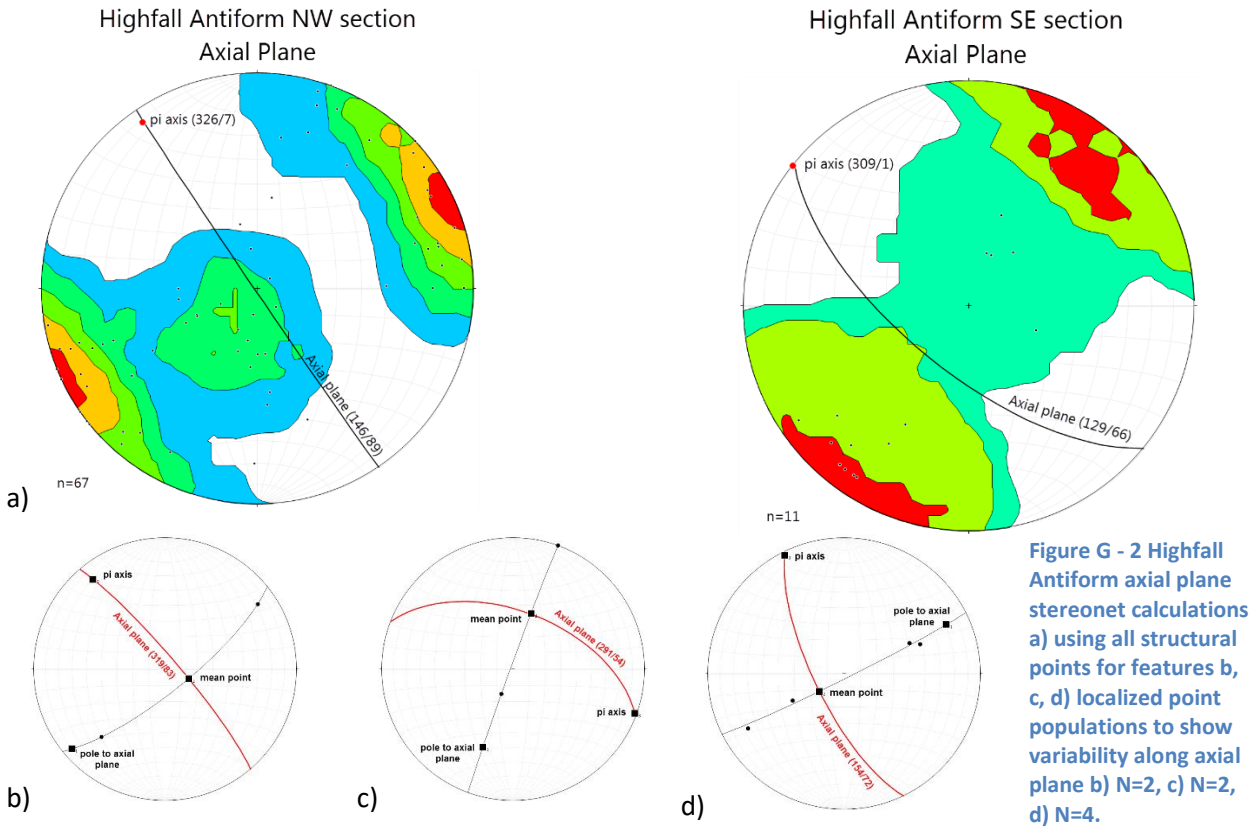

Figure G - 2 Highfall Antiform axial plane stereonet calculations a) using all structural points for features b, c, d) localized point populations to show variability along axial plane b) N=2, c) N=2, d) N=4.

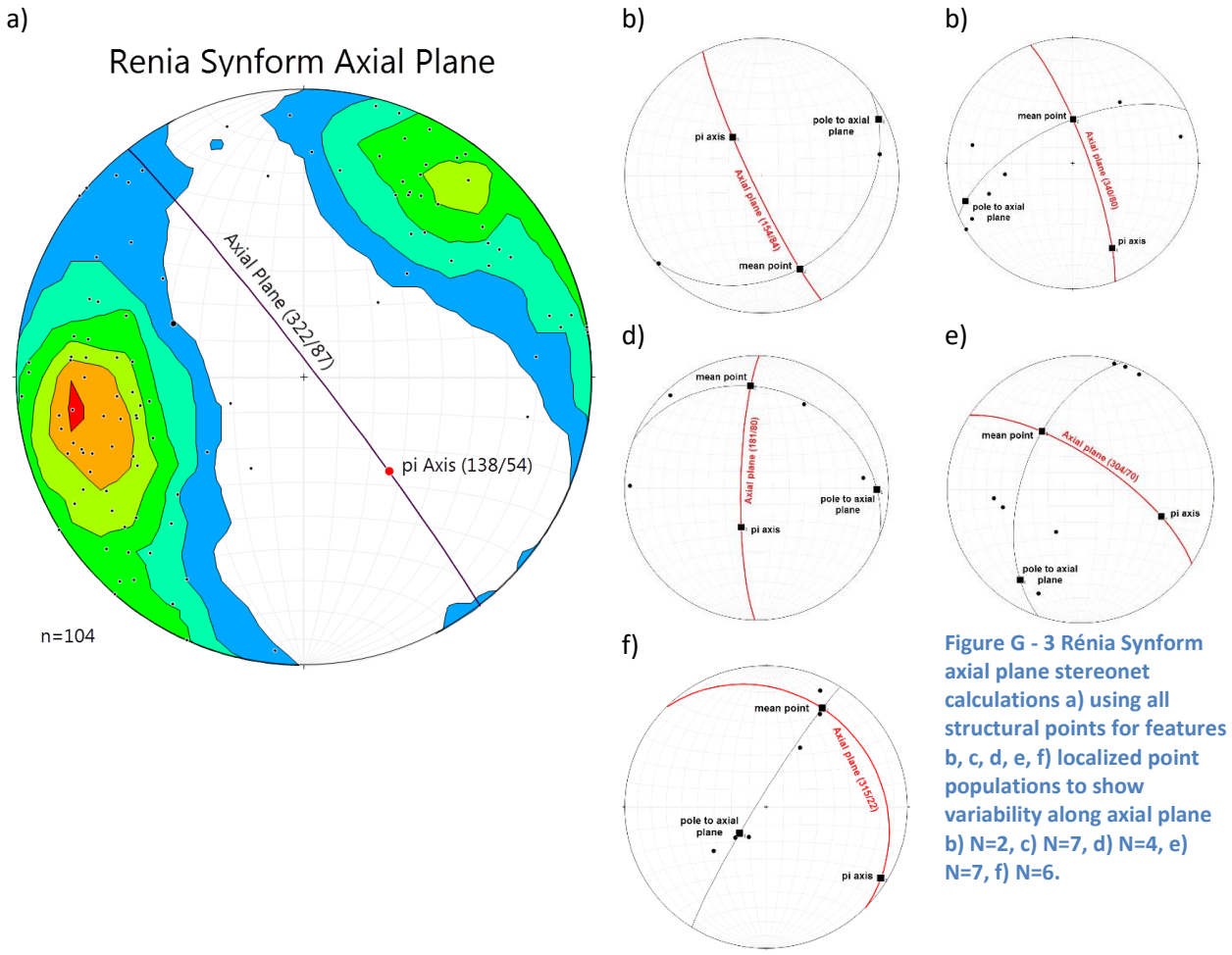

Figure G - 3 Rénia Synform axial plane stereonet calculations a) using all structural points for features b, c, d, e, f) localized point populations to show variability along axial plane b) N=2, c) N=7, d) N=4, e) N=7, f) N=6.

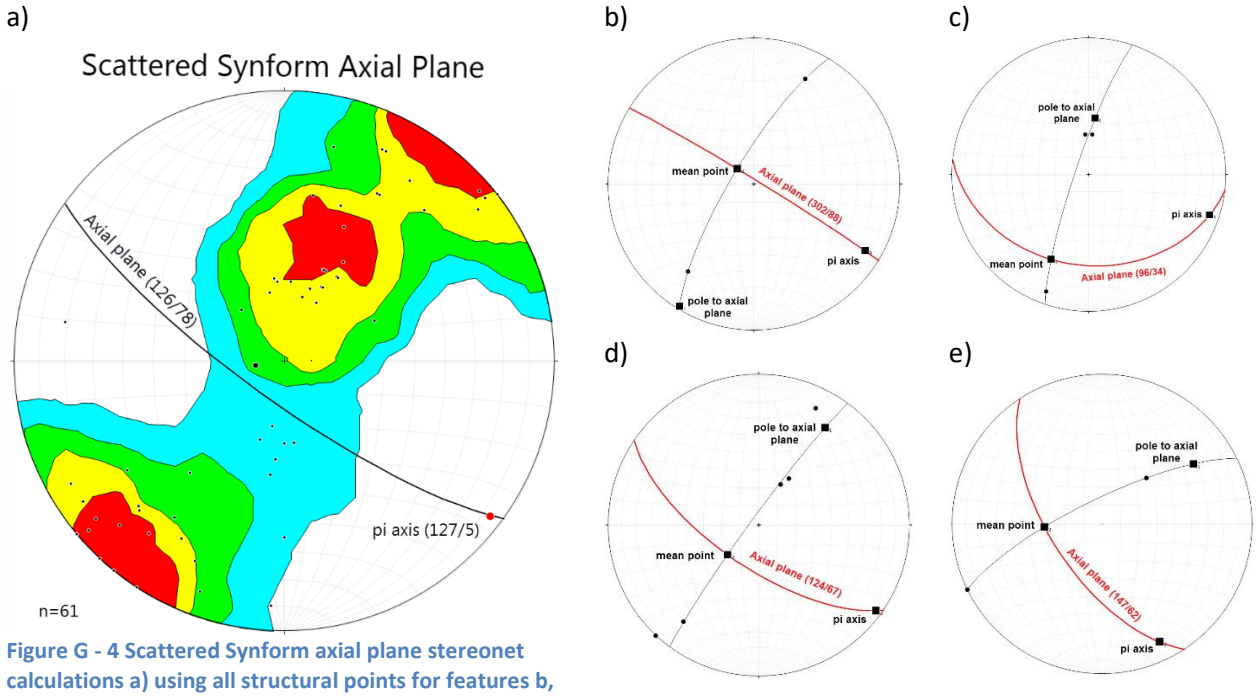

Figure G - 4 Scattered Synform axial plane stereonet calculations a) using all structural points for features b, c, d, e) localized point populations to show variability along axial plane b) N=2, c) N=3, d) N=5, e) N=2.

Appendix H – Data codes

Table H - 1 Codes for data sources

Code	Source	Reference
1	SIGEOM	(*Système d'information géominière du Québec,* 2016)
2	Scanned maps	See Appendix D
4	Interpreted by this thesis	
5	Clark and Wares (2006)	Clark and Wares (2006)
6	Simard et al. (2013)/Lafrance et al. (2014)	Simard et al. (2013) and Lafrance et al. (2014)
7	Moorhead and Hynes (1990)	Moorhead and Hynes (1990)
8	Wares and Goutier (1990)	Wares and Goutier (1990)
9	Calculated with steronets	
10	Corrigan et al. (2015)	Corrigan et al. (2015)
11	SIGEOM 2015 Field observations	(*Système d'information géominière du Québec,* 2016)

Appendix I – Technical concerns

SURFE

SURFE has an excellent feature, called Global Plunge Model, which align fold hinge lines to be subparallel with one another. This is very useful when trying to keep fault parallel, however, in poly-deformed regions like the northern Labrador Trough, fold orientation is variable. To model the trajectory of regional fold hinges, which have variable trends and plunges, there needs to be a way to incorporate and set tolerance for local anisotropy. See Figure I-1 for example of how the Global Plunge Model method was used in the Hellancourt sub-region model.

In addition to having control over local anisotropy, SURFE would benefit from incorporating axial plane measurements or surfaces to gain better control on fold geometry. See Figure I-2 for example of how folds often have geometries that would benefit from axial plane constraints.

Finally, SURFE would benefit from using a slack or wobble attribute that in individualized for every data point in the selected set of constraints.

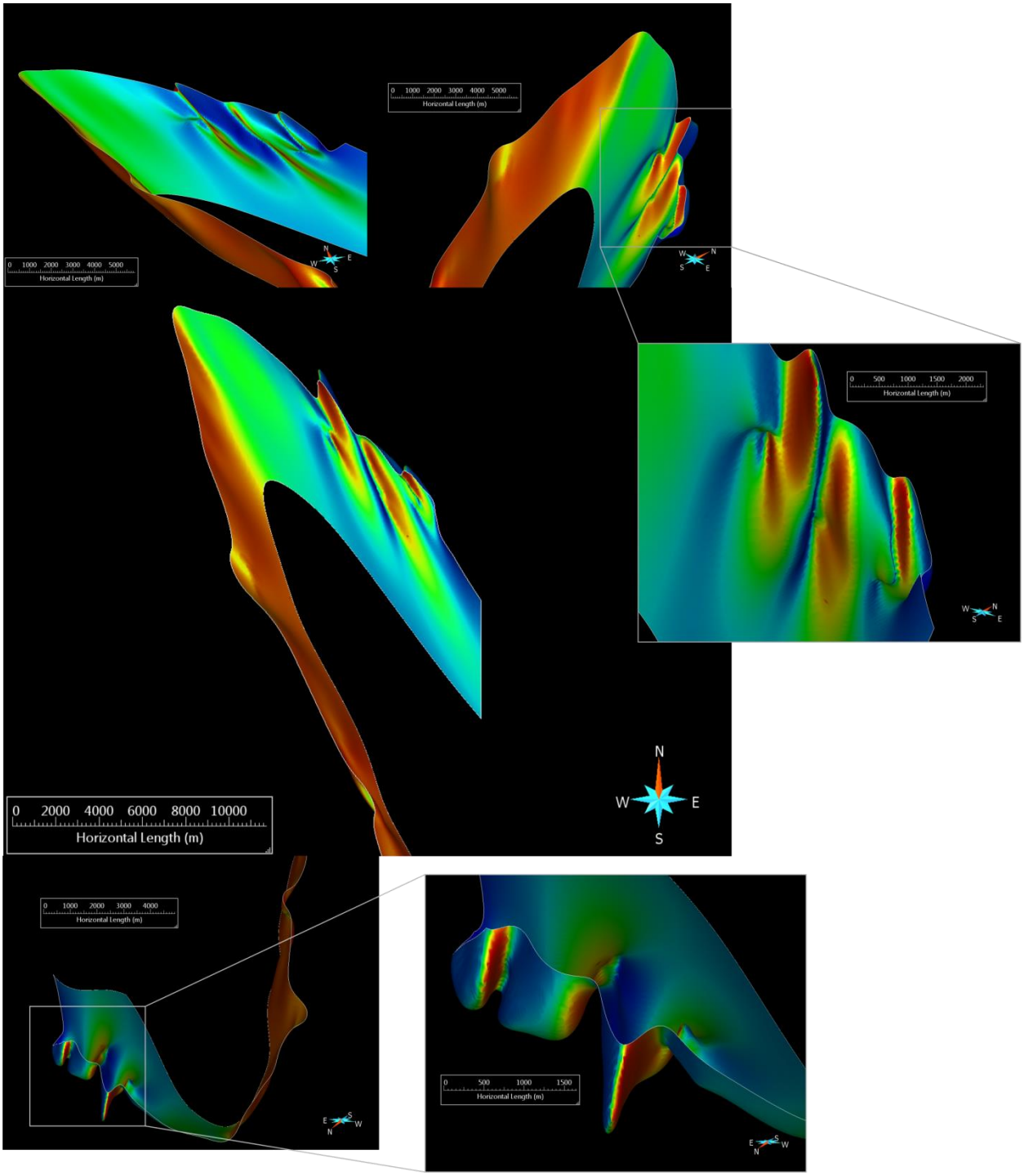

Figure I - 1 Example of Global Plunge Model results from SURFE for the base of the Baby Iron Formation. Symbolized for the first component of surface vector to highlight limbs of folds.

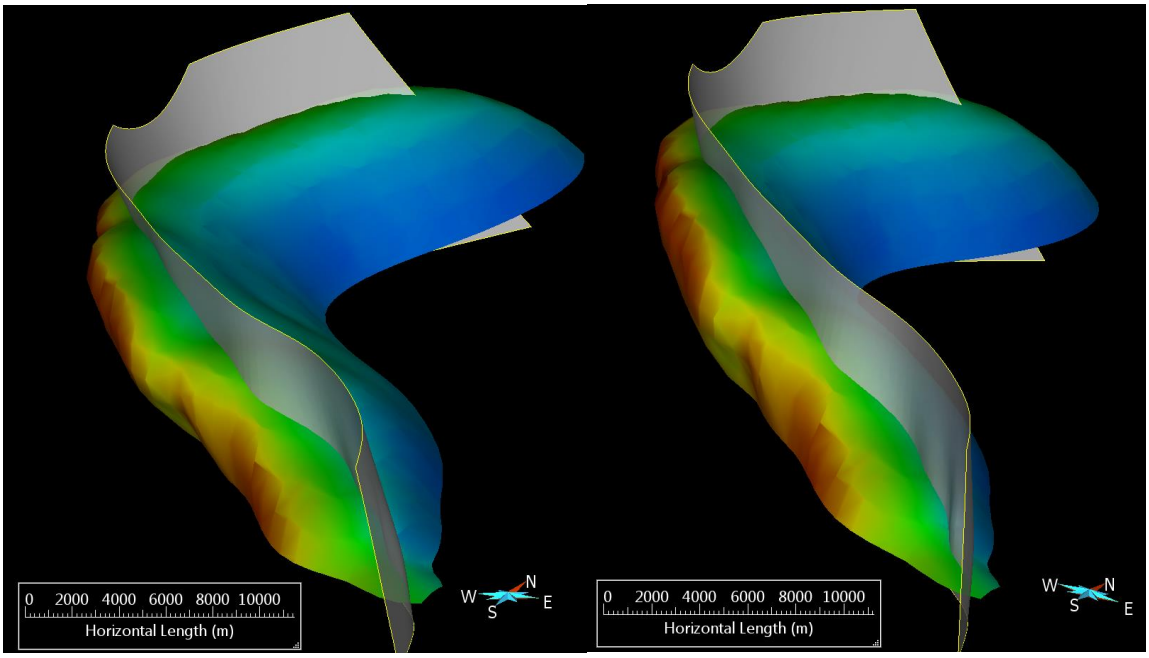

Figure I - 2 Example of overturned surface. Top of Cycle 1 stratigraphy in the Hellancourt sub-region model and white axial surface. Stratigraphic surface symbolized with first component of surface's normal vector.

SKUA

During development of the Hellancourt Sub-Region model, it was determined that a rectangular volume of interest (VOI) must be defined rather than one that is irregular. Using an irregular VOI produces an unstable 3D grid and the UVT transform produces a geologically invalid model; however, using a rectangular VOI, SKUA is able to construct a geologically valid model using the same inputs. Figure I-3 demonstrates this issue for the Hellancourt Sub-Region model. This is significant as the deformed coordinate system will prevent future geophysical inversions from being reliable; however, to use a rectangular VOI, the model extent must be reduced.

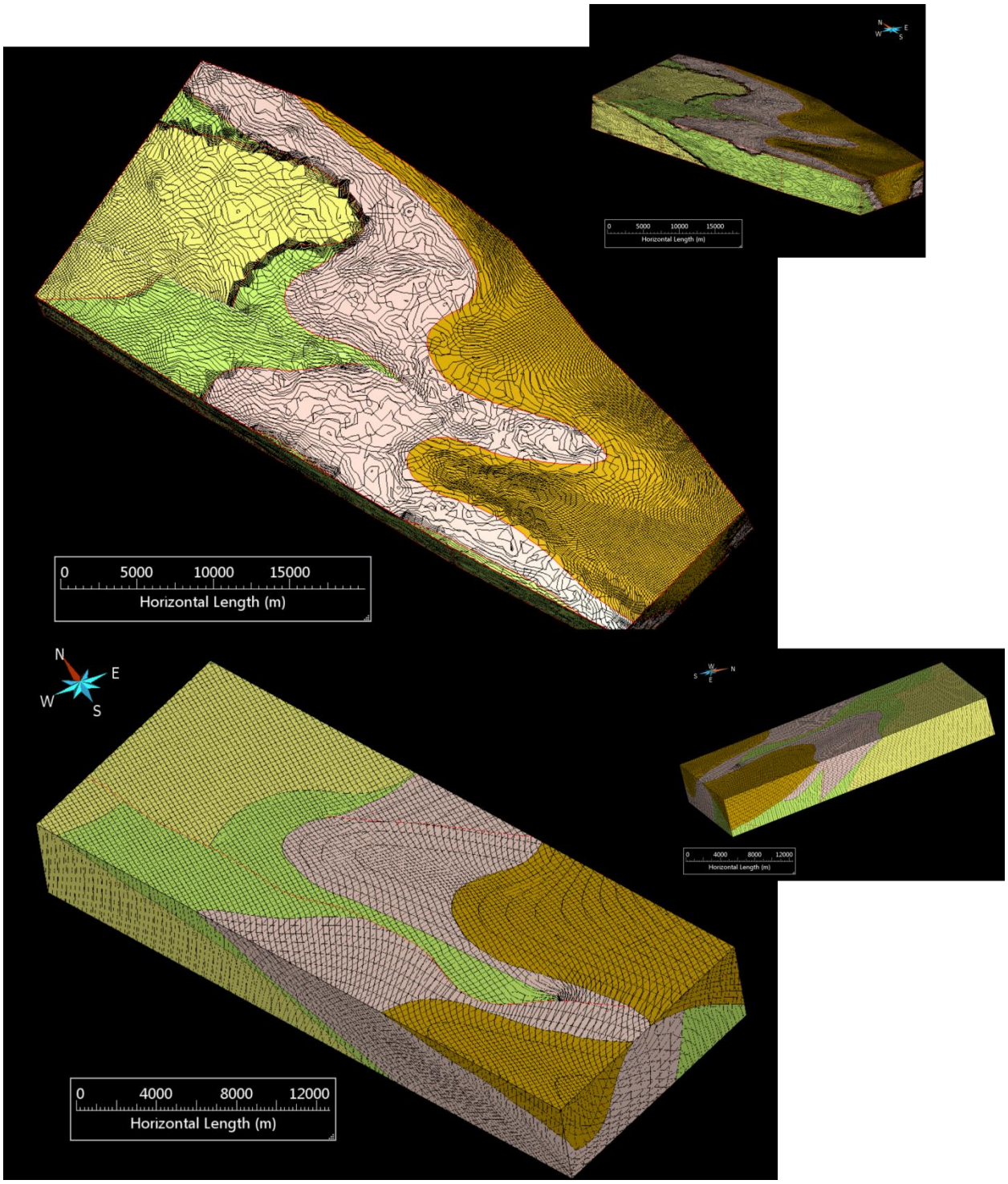

Figure I - 3 Example of using irregular (top) and rectangular (bottom) volume of interests (VOIs) in SKUA's Structure and Stratigraphy workflow. Geologically invalid grids are produced when irregular VOIs are used.

Appendix K – Harmonized data codes

Harmonized attribute codes for structural points in ArcMap

Table K - 1 Harmonized attribute codes for planar structural points in ArcMap

Type	Sub_Type	Code	Desc_
Planar	Brittle Deformation	DFAULT	Dextral fault
Planar	Brittle Deformation	FAULT	local fault orientation
Planar	Brittle Deformation	JOINT	Included joint face
Planar	Brittle Deformation	NFAULT	Normal fault
Planar	Brittle Deformation	RDFAULT	Reverse dextral fault
Planar	Brittle Deformation	RFAULT	Reverse fault
Planar	Brittle Deformation	RSFAULT	Reverse sinistral fault
Planar	Brittle Deformation	SINFAULT	Sinistral fault
Planar	Brittle Deformation	VEIN	Vein
Planar	Depositional	CON	Contact
Planar	Depositional	IBED	Inclined bedding unknown tops
Planar	Depositional	OBED	Inclined overturned bedding
Planar	Depositional	UBED	Inclined upright bedding
Planar	Ductile Deformation	FOLDAXIS	Local fold axial surface orientation
Planar	Igneous	DYKE	Dyke
Planar	Igneous	IBAND	Primary mineral foliation (magmatic)
Planar	Igneous	IBAND	Primary igneous banding
Planar	Metamorphic	CLV	Cleavage
Planar	Metamorphic	COMLAY	Compositional layering
Planar	Metamorphic	GNLAY	Gneissosic layering
Planar	Metamorphic	K1	Delta-type porphyroclasts
Planar	Metamorphic	K2	Pressure shadows, on opposed sides of a*
Planar	Metamorphic	K3	Fold asymmetry
Planar	Metamorphic	K4	Shear bands
Planar	Metamorphic	K5	C/S fabric
Planar	Metamorphic	K6	Sigma-type porphyroclasts
Planar	Metamorphic	KBAND	Kink bands
Planar	Metamorphic	MBAND	Migmatic Banding
Planar	Metamorphic	MFOL	Mineral foliation, tectono-metamorphic
Planar	Metamorphic	MYBAND	Mylonitic foliation or banding
Planar	Metamorphic	S1	Penetrative foliation first generation
Planar	Metamorphic	S2	Penetrative foliation second generation
Planar	Metamorphic	S3	Penetrative foliation third generation
Planar	Metamorphic	S9	Foliation generation unknown
Planar	Metamorphic	SHST	Schistosity
Planar	Metamorphic	TBAND	Tectonic banding

Appendix L – Structural points field definitions

Field definitions for structural points in ArcMap attribute tables.

Table L - 1 Attribute field definitions for planar structural points in ArcMap for shapefiles created during this study

Field name	Type	Length	Precision	Description
FID	esriFieldTypeOID			
Shape	esriGeometryPoint			
UniqueID	Text	50		Unique identifier for each point
Source	Text	15		Generalized source of data (ex. maps or outcrop)
Source_ID	Text	20		Specific source of data
Rule	Text	4		Rule of measurement
Type	Text	10		Type of structure
Sub_Type	Text	25		Sub type of structure
Code	Text	10		Code for structure
Desc_	Text	50		Description of code
Generation	Long		9	Generation of structure
StrikeTrnd	Long		9	Strike or trend of the structure
DipPlunge	Long		9	Dip or plunge
Overturned	Long		9	Overturned
X	Double		0	X
Y	Double		0	Y
Z	Long		9	Elevation
ShearSense	Text	10		Shear sense
UTMZone	Text	10		UTM zone
Map_Sheet	Text	10		NTS map sheet
Domain	Text	20		Geological domain
Zone	Text	30		Lithotectonic zone
SymbolCode	Text	10		Code for geologic symbol
Author	Text	20		Person, project or organization that produced this data
Notes	Text	254		Notes

Table L - 2 Attribute field definitions for linear structural points in ArcMap

Field name	Type	Length	Precision	Description
FID	esriFieldTypeOID			
Shape	esriGeometryPoint			
UniqueID	Text	50		Unique identifier for each point
Source	Text	15		Generalized source of data
Source_ID	Text	20		Specific source of data
Associated	Text	20		Associated features to point
Rule	Text	4		Rule of measurement
Accuracy	Long		9	Accuracy of data
Type	Text	10		Type of structure
Sub_Type	Text	25		Sub type of structure
Code	Text	10		Code for structure
Desc	Text	50		Description of code
Generation	Long		9	Generation of structure
StrikeTrnd	Long		9	Strike or trend of the structure
DipPlunge	Long		9	Dip or plunge
Overturned	Long		9	Overturned
Degree	Long		9	Degree of metamorphism
X	Double		0	X
Y	Double		0	Y
Z	Long		9	Elevation
Fold_Style	Text	25		Shape of fold
Zone	Text	10		UTM zone
Map_Sheet	Text	10		NTS map sheet
Domain	Text	20		Geological domain
SIGEOM	Text	10		SIGEOM structural symbol code
SymbolCode	Text	10		Code for geologic symbol
Author	Text	20		Person, project or organization that produced this data
Notes	Text	254		Notes

Appendix M – File structure

Bullet points representing the file structure for data exports and organization.

- 2D (*two-dimensional files/objects*)
    - Hellancourt_SubRegion
        - Working (*Objects that have been created or modified during the project; Organized by topic*)
            - Litho (*Objects related to lithological units used to create the Hellancourt Sub-Region model*)
                - Cycle1
                - Cycle2
                - HellancourtFm
                - Intrusions
                    - LowerIntrusive
                    - UpperIntrusive
                - IronFm
    - Local_Models (*Local-scale models that were not completed*)
        - LacenCrochet
            - Litho (*Objects related to lithological units*)
        - LacStPierre
            - Litho (*Objects related to lithological units*)
        - SuperiorContact
        - Venditelli
            - Faults
            - Folds
        - Willibob
            - Faults
            - Folds
                - Old (*Old files or versions*)
            - Litho (*Objects related to lithological units*)
    - Nappes_SubRegion
        - Faults
            - Ujaralialuk
        - Folds
    - Regional_Model
        - Original
            - CrossSections (*Georeferenced and ungeoreferenced cross sections)*
                - Georeferenced
                - Old (*Old files or versions*)
            - DEM (*Digital Elevation Model*)
                - 0.75ArcSec

        - 3ArcSec
        - DEM_Hillshade
    - Faults
    - Geophysics
        - D315551
        - Geophysics_Geodatabase
        - Gravity
        - Magnetics
        - Rediometrics
    - Layers_Symbology (*ArcMap layer files used to save shapefile symbology*)
    - Maps
    - Remote_Imagery
        - GeoBase_Orthoimage_index
        - Imagrey_LabradorTrough.gdb
        - Landsat7_Orthoimages
        - Multispectral
        - Pamchromatic2
        - Panchromatic_DIMAPformat
        - Spot4
        - Spot5
    - Stereonets
    - Structures
        - FieldObs
            - Corrigan2015 (*Data collected during GSC 2015 field campaign new Kuujjuaq*)
            - Lineation
            - Planar
        - Folds
    - Topo
        - Cities
        - NTS
        - Water
- Projects
    - Old *(old files or versions)*
- Working
    - CrossSections (*Cross sections that were created during the project)*
        - Old *(old files or versions)*
    - Database
    - DEM
        - Old *(old files or versions)*
    - Faults

        - Old *(old files or versions)*
            - Turcotte
    - GeoChronology
    - Geodatabase
        - Old *(old files or versions)*
    - Layers_Symbology (*ArcMap layer files used to save shapefile symbology*)
    - Litho
        - Old (*Old files or versions)*
        - Sokoman_IronFm
    - Maps (*Maps that were created during the project)*
    - Metamorphic
    - QualityControl
        - PointDensity
    - Structures
        - FieldObs (*Field observations*)
        - Folds
        - Formlines
    - TectonicZones
        - Old (*Old files or versions)*
    - Topo
- 3D (*3D projects, models, or objects I created or that were created for Kuujjuaq*)
    - Hellancourt_SubRegion
        - Faults (*One folder for each fault*)
            - All
                - Old (*Old files or versions)*
            - Baby
            - Faujas
            - Herodier
            - IronFault
            - Old (*Old files or versions)*
            - Rachel
            - Thevenet
                - Old (*Old files or versions)*
        - Folds
            - Old (*Old files or versions)*
        - Formlines
        - Horizons (*One folder for each horizon; Horizon = a single surface*)
            - Base_HellancourtFm
                - Old (*Old files or versions)*
            - Base_IronFm
                - Old (*Old files or versions)*

- Cycle2
  - Old (*Old files or versions)*
- LowerIntrusion
  - Old (*Old files or versions)*
- Top_Cycle1
  - Old (*Old files or versions)*
- UpperIntrusion
  - Old (*Old files or versions)*

- Lithologies (*Lithologies = a lithological unit*)
  - Original
  - Working
    - HellancourtFm
- Projects
  - Old (*Old files or versions)*

- Local_Models
  - LacenCrochet
  - LacStPierre
  - Venditelli
    - Faults
      - Colourmaps
  - Willibob
    - Faults
      - Colourmaps
    - Folds
    - Litho
- Nappes_SubRegion
  - Faults
    - Canoe
      - Old (*Old files or versions)*
    - Nappes
      - Boulder
      - Central
        - Old (*Old files or versions)*
  - FieldObs
  - Folds
  - Horizons
  - Projects
    - Old (*Old files or versions)*
- Regional_Model
  - CrossSections
    - Old (*Old files or versions)*

- DEM
- Faults
    - All
        - Colourmaps
        - LookUpTable
    - Archiac
    - Baby
    - Faujas
    - FerrumRiver
        - Old (*Old files or versions)*
    - Forbes
        - Old (*Old files or versions)*
    - Gabriel
        - Old (*Old files or versions)*
    - Garigue
        - Old (*Old files or versions)*
    - Gerido
    - Herodier
        - Old (*Old files or versions)*
    - Highfall
        - Old (*Old files or versions)*
    - Olmstead
        - Old (*Old files or versions)*
    - Other
        - Old (*Old files or versions)*
    - Pingiajjulik
        - Old (*Old files or versions)*
    - PointReef
        - Old (*Old files or versions)*
    - Rachel
        - Old (*Old files or versions)*
    - Robelin
        - Old (*Old files or versions)*
    - Ujaralialuk
- Horizons
    - Old (*One folder for each horizon*)
        - Base_IronFm
- Lithologies
    - Old
- Other (*Faults that were un-named and were not used in the final model*)
- Projects

                - Old (*Old files or versions)*
            - Structures
                - FieldObs
                    - Old (*Old files or versions)*
                        - Lineations
                        - Planar
                - Folds
            - TectonicZones
                - Old (*Old files or versions)*
            - Topo
                - Colourmap
                - Curves
                - LookUpTable
                - Mixed
                - Voxet
- Source (*grouped by name of source; generally personal communications*)
- Deliverables (*documents, reports, and posters created for the project*)
    - ASCERC2016
    - GACMAC_2016
    - GACMAC_2017
    - Methodology_Workflow
    - MontsionMSc_2017
    - PDAC2016
    - PDAC2017
    - SURFE_Notes
- Images
- Resources
    - Codes (*tables of codes created for the project*)
    - CrossSections
    - DigSym_XLS
        - Old (*Old files or versions)*
    - Fonts
    - Other (*other documents that do not fit elsewhere*)
    - Publications (*publications collected for use in the project*)
    - Scripts (scripts used during the project)
    - Styles